Electronic Theses and Dissertations

Theses, Dissertations, and Major Papers

1-17-2020

Nonlinear Phenomena during the Electrochemical Oxidation of Sulfur Compounds

Michelle Dao
University of Windsor

Follow this and additional works at: https://scholar.uwindsor.ca/etd

Nonlinear Phenomena during the Electrochemical Oxidation of Sulfur Compounds

By

Michelle Dao

A Thesis
Submitted to the Faculty of Graduate Studies
through the Department of Chemistry and Biochemistry
in Partial Fulfillment of the Requirements for
the Degree of Master of Science
at the University of Windsor

Windsor, Ontario, Canada

2020

Nonlinear phenomena during the Electrochemical Oxidation of Sulfur Compounds

by

Michelle Dao

APPROVED BY:

_____

A. Fisk
Great Lakes Institute for Environmental Research

_____

D. Marquardt
Department of Chemistry & Biochemistry

_____

J. Wang, Advisor
Department of Chemistry & Biochemistry

January 17, 2020

DECLARATION OF CO-AUTHORSHIP / PREVIOUS PUBLICATION

I.   Co-Authorship

I hereby declare that this thesis incorporates material that is result of joint research, as follows:

Chapters 2 and 3 of the thesis was co-authored and under the supervision of Dr. Jichang Wang. In all cases, the key ideas, primary contributions, experimental designs, data analysis, interpretation, and writing were performed by the author. Dr. Jichang Wang provided contributions through feedback, revisions, and discussion to the manuscripts.

I am aware of the University of Windsor Senate Policy on Authorship and I certify that I have properly acknowledged the contribution of other researchers to my thesis, and have obtained written permission from each of the co-author(s) to include the above material(s) in my thesis.

I certify that, with the above qualification, this thesis, and the research to which it refers, is the product of my own work.

II.   Previous Publication

This thesis includes 2 original papers that have been previously published/submitted for publication in peer reviewed journals, as follows:

Thesis Chapter	Publication title/full citation	Publication status*
Chapter 2	Bifurcations Induced by the Size of Glassy Carbon Electrodes during the Electrochemical Oxidation of Bisulfite. 2019. M. Dao and J. Wang. Journal of the Electroanalytical Chemistry.	*Submitted*
Chapter 3	Electrochemical Oxidation of Sodium Bisulfite in Neutral Media. 2019. M. Dao and J. Wang.	*To Be Submitted*

I certify that I have obtained a written permission from the copyright owner(s) to include the above published material(s) in my thesis. I certify that the above material describes work completed during my registration as a graduate student at the University of Windsor.

III.   General

I declare that, to the best of my knowledge, my thesis does not infringe upon anyone's copyright nor violate any proprietary rights and that any ideas, techniques, quotations, or any other material from the work of other people included in my thesis, published or otherwise, are fully acknowledged in accordance with the standard referencing practices. Furthermore, to the extent that I have included copyrighted material that surpasses the bounds of fair dealing within the meaning of the Canada Copyright Act, I certify that I have obtained a written permission from the copyright owner(s) to include such material(s) in my thesis.

I declare that this is a true copy of my thesis, including any final revisions, as approved by my thesis committee and the Graduate Studies office, and that this thesis has not been submitted for a higher degree to any other University or Institution.

ABSTRACT

Sulfur compounds have important applications in biological function and industry, such as DNA sequencing and energy production. From the perspective of fundamental research on macroscopic reaction kinetics, sulfur compounds have also a great deal of interest due to its ability to exhibit unique dynamical behaviors. This thesis focuses on uncovering nonlinear dynamics/phenomena during the electrochemical oxidation of two distinct sulfur compounds, bisulfite and L-cysteine. Chapter 2 demonstrated that the dominant S(IV) electroactive species in acidic media, dissolved sulfur dioxide, could exhibit a surface area-dependence of the onset of potential and current oscillations. Furthermore, electrochemical impedance spectroscopy was able to identify the oscillator as the HN-NDR type. The electro-oxidation of bisulfite in neutral media resulted in significantly different dynamical behaviors and was the focus in Chapter 3. In KCl electrolytes, sustained oscillations arose despite not exhibiting a NDR in the j-E curve. The competition between the oxidation of bisulfite and chloride ions were proposed to be the major driving force behind the observed oscillatory behavior. Preliminary characterization using impedance spectroscopy suggested that the instabilities may be of a possible new type of electrochemical oscillator. Lastly, the electrochemical oxidation of L-cysteine at a Pt electrode was explored in acidic, neutral, and alkaline conditions, where a well-defined negative branch was observed in the polarization curve and was able to exhibit bistability. Moreover, in a sufficiently high solution pH, the deprotonation of the -NH$_2$, -SH and -COOH groups caused the emergence of current oscillations within a narrow range of parameters. In addition, This thesis also demonstrated the formation of sulfur elements as well as cysteine polymers, suggesting the great relevance of this nonlinear kinetics research to the field of material sciences, where the fabrication of various materials, such as different allotropes of sulfur, and cystine, may be feasible.

DEDICATION

I would like to dedicate this thesis to my loving parents.

ACKNOWLEDGEMENTS

I would like to firstly thank Dr. Wang for giving me the opportunity to pursue my graduate studies under your supervision. I am very grateful for your guidance and support over the years, especially for always being available to discuss any concerns, ideas, or questions that I had. I will always be indebted for the important lessons, skills, and knowledge I have acquired during my Masters degree. It has helped me become more confident as a researcher. To my fellow lab members, Alex and Xin, I am thankful for the help and encouragement you have provided me. You have truly made coming in every day memorable. As for Dr. Jeffrey Bell, thank you for your mentorship and advice, it is appreciated.

I would also like to thank Dr. Drew Marquardt and Dr. Aaron Fisk to take their time to be on my committee and for your valuable input and suggestions.

Additionally, I want to thank Sharon for helping me run many SEM experiments, and Janeen for MS experiments.

To Marlene, thank you for your help by making sure I met many deadlines, and making sure my whole Masters went smoothly.

Lastly, I would like to thank my parents, and my brother for the continuous love and support, I could have not done this without you. To my boyfriend, Mitchell, thank you for uplifting my spirits during the difficult and stressful times while studying and doing research. I am grateful for your endless support and your understanding for the past year – it truly means the world to me. Finally, to my friends, thank you for always being in my corner.

TABLE OF CONTENTS

LIST OF TABLES

LIST OF FIGURES

LIST OF APPENDICES

LIST OF ABBREVIATIONS/SYMBOLS

CE	Counter Electrode
C-PDR	Capacitance Mediated Positive Differential Resistance
CV	Cyclic Voltammetry
EIS	Electrochemical Impedance Spectroscopy
EDS	Energy Dispersive X-Ray Spectroscopy
GCE	Glassy Carbon Electrode
HN-NDR	Hidden N-shaped Negative Differential Resistance
LSV	Linear Sweep Voltammetry
NDR	Negative Differential Resistance
N-NDR	N-shaped Negative Differential Resistance
S-NDR	S-shaped Negative Differential Resistance
SEM	Scanning Electron Microscopy
SN	Saddle-Node
RDE	Rotating Disk Electrode
RPM	Rotations Per Minute

CHAPTER 1 - INTRODUCTION

1.1 Nonlinear Dynamics and Self-organization

A fundamental feature of nature is its ability to exhibit complex behaviors that are governed by nonlinear equations. Many living and physical processes can be viewed as dynamical systems, in which the future configuration(s) of an entity may be defined by the past and present states, assuming that the rules or laws concerning the transformation of the states does not change over time.[1,2] In simpler terms, dynamical systems deals with its evolution or change as a function of time.

Nonlinear dynamics plays a vital role in a large array of systems belonging to different disciplines, and its existence can be found not only in laboratory settings, but also in day-to-day life. Such examples can include the firing of neurons,[3] predator-prey interactions,[4] self-assembly of nanoparticles,[5] and can even extend to economic models of production and consumption.[6]

Self-organization refers to the unexpected formation of pattern and structure through local interactions between individual constituents of a system. Under appropriate conditions, the development of order is spontaneous, as it does not require input from external sources. The global coherence can manifest in many forms in both time and/or space. A well-known example of spatiotemporal dynamical self-organization is the Turing pattern, which are macroscopic stationary patterns originating from symmetry-breaking phenomena (Figure 1.1).[7] More commonly, the emergence of self-organization appears as sustained periodic or complex (e.g., aperiodic, quasi-periodic) temporal oscillations.
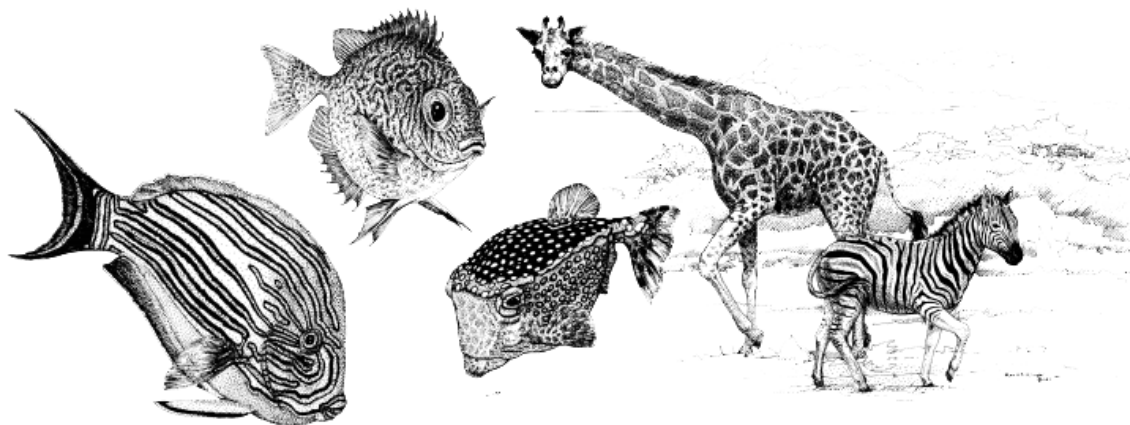
Figure 1.1. Examples of stationary Turing patterns observed in skin pigmentation on various species of fish and in coat patterns of zebras and giraffes.[8]

The first reports of nonlinear phenomena in chemical systems date back to 1828, when Fechner observed periodic current oscillations during the anodic dissolution of nickel in nitric acid.[9] Since the initial discovery, years of investigations uncovered that overwhelming amounts of processes in the areas of electrodissolution,[10–19] electrodeposition,[20–25] and electrocatalysis could exhibit nonlinear instabilities.[26-40] The field of electrochemistry has attracted great interest to researchers studying nonlinear dynamics as it is capable of providing endless opportunities to investigate its underlying mechanisms.[40] Experimental and numerical data obtained from experiments are used to develop theoretical models as an attempt to describe the origins of pattern formation. These understandings of fundamental principles on a mathematical level derived from electrochemical concepts and techniques allowed nonlinear dynamists to apply to other analogous phenomena observed in other systems.

1.2 Conditions of Non-linear Systems

The spontaneous onset of self-organization and other non-linear phenomena can only occur when the system maintains far from thermodynamic equilibrium. In thermodynamics, the state of equilibrium refers to the absence of dissipation of energy in a given system.[41] Therefore, a constant

perturbation from an external source is required to prevent the system from approaching equilibrium. The thermodynamic requirement for the creation of order can be explained with the second law of thermodynamics, which states that the total entropy of an isolated system or universe can only increase or remain constant ($\Delta S_{total} \geq 0$). The creation of order involves a decrease of entropy, so there must be a parallel dissipative process that results in an overall increase of entropy in order to compensate.[42,43] The recognition for the need of energy dissipation led to the term dissipative structures, coined by Prigogine for the complex structures created by the irreversible processes between a system and its surroundings.[44] Based on this definition, any forms of nonlinear phenomena (such as spatiotemporal and temporal patterns) are therefore, dissipative structures.

The overall two kinetic requirements are: (a) the differential equations used to describe the dynamics are nonlinear (i.e., autocatalysis and/or autoinhibition) and (b) the presence of feedback loops in the mechanism to destabilize the system.[42] Oscillatory behavior becomes possible when two variables assumes the roles of a fast positive feedback and a slow negative feedback. Typically, self-regulation through feedback loops are related to activator-inhibitor interactions, such as autocatalysis (positive feedback) and autoinhibition (negative feedback).[45] It is worthy to note that it is important to identify the appropriate feedback loops in order to gain significant understanding of the oscillatory mechanism.

1.3 Stability Analysis

Stability analysis of a state is commonly used to determine the dynamical evolution of a system. A steady state means that the characteristics of a state do not change with respect to time. A steady state is not to be confused with the term stable state, as this refers to the system's resistance to small internal or external perturbations. The perturbations may result in small arbitrary deviations from the initial conditions of a system, but the system will return to its original state. Contrarily, an unstable state is unable to resist any size of perturbations and the system continues

to deviate from its initial state and will leave to another state within close proximities. The notion of stable and unstable states can be explained with the analogy of a ball sitting at the top of a hill and at the bottom of a basin (Figure 1.2). When the ball is positioned at the top of the hill, the ball is unstable because any fluctuations in either direction will result in a displacement of the ball, and it will continue to deviate from its initial position. However, at the bottom of the basin, the ball is in a stable state since small fluctuations are damped.[42]
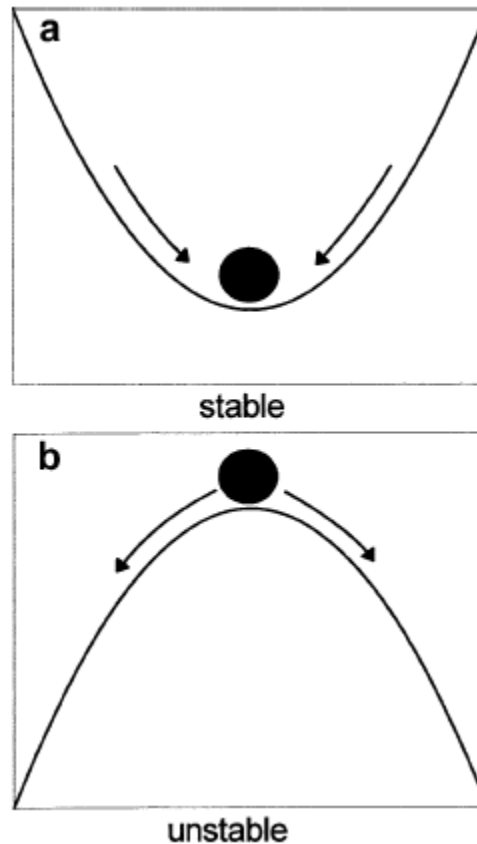
stable

unstable

Figure 1.2. The analogy of the position of a ball at the bottom and at the top of a hill to represent (a) stable states and (b) unstable states.[42]

Having introduced the appropriate terminology, it is important to note that steady states can be stable or unstable. A stable steady state, also known as a point attractor, is depicted as a fixed point in a phase space, which is a graphical representation of all possible future and present

states (or positions) and the trajectories of a system.[2] The surrounding trajectories of a point attractor leads to the fixed (equilibrium) point, otherwise it is an unstable steady state, or a point repeller.[42]

A particular type of stability, called the asymptotic stability, refers to the ability of a system to return to its exact initial conditions after experiencing a perturbation. This is due to the asymptotical perturbation decay to zero as a function of time. In order for a system to be globally stable, the system will always return back to a single point (or initial conditions) regardless of the starting point and the perturbation applied. For a system that is locally stable, the system is able to "switch" to a nearest stable state upon the application of larger than a threshold perturbation.[42]

Another type of local stability is the Lyapunov (or Liapunov) stability, developed by a Russian mathematician named Lynapunov in 1892. Here, instead of the system switching to concurrent stable state, the system stays near the equilibrium point as $t \rightarrow \infty$. However, if the distance between Lyanpunov state and the original stable state shrinks to zero, then it now turns into the case of asymptotic stability.[42]

More commonly, a system will have one stable steady state, much like a ball positioned at the bottom of a basin. However, it is also possible for more complex systems to exhibit bistability and multistability, if the system exists in two or more steady states within a range of parameters. This concept can be imagined using the same example with the ball at the bottom of a basin, except there is another basin within the same geographical landscape. Now, the ball can exist in either stable steady state locations. A common manifestation of multistability is the phenomenon of hysteresis, a response lag which results in two possible values for one variable or control parameter. Similarly, when there are two oscillatory states within the same control parameter range, that is referred to as birhythmicity.[47]

1.4 Bifurcations

The emergence of oscillations and waveforms in any given system are associated with a loss of stability. The transition of the dynamic state of a system, for example, from a stationary state to an oscillatory state, can be explained by using the bifurcation theory. A bifurcation occurs when changes made to the control parameter exceeds the critical threshold that ultimately results in a qualitative change in the behavior of a generally nonlinear system.[48] The control parameters that are accountable for the transformation of the dynamic states are called bifurcation parameters (μ). Typical electrochemical bifurcation parameters can include the initial concentration of an electroactive species, applied potential, applied current, temperature, pH, etc.[40] When the system is driven close to the bifurcation point, perturbations are magnified due to the presence of nonlinear feedback loops that leads to the changes of stability of the dynamical state.

The bifurcation theory can predict on a mathematical basis if a bifurcation can occur in a given system.[40] The derived properties and characteristics of a bifurcation derived from a particular system may be applied to other resembling systems that exhibit similar dynamic changes. According to literature, there are three main types of bifurcations: (1) saddle-node, (2) Hopf, and (3) homoclinic. Saddle-node and Hopf bifurcations are local in nature, so its stationary state can be assessed by linearizing differential equations, in which nonlinear terms can be ignored.[40] To solve a linearized equation means to calculate the eigenvalues and eigenvectors that are associated with the Jacobian matrix. If the eigenvalues are negative, that means the stationary state is stable, otherwise it is unstable. However, homoclinic types are global bifurcations, so a more complex approach must be adopted.[40,42]

1.4.1   Saddle-Node Bifurcation

A saddle-node bifurcation occurs when a pair of hyperbolic stationary states, typically one stable and one unstable, suddenly emerge or coalesce and annihilate each other when the control parameter is varied from the critical point.[49] In a mathematical standpoint, the saddle-node bifurcation occurs when one of the eigenvalues of the Jacobian matrix crosses zero.[50,51] The name "saddle-node" comes from the configuration of the trajectories surrounding the steady states, which one resembles a node around the stable state, and a saddle around the unstable one.[43]
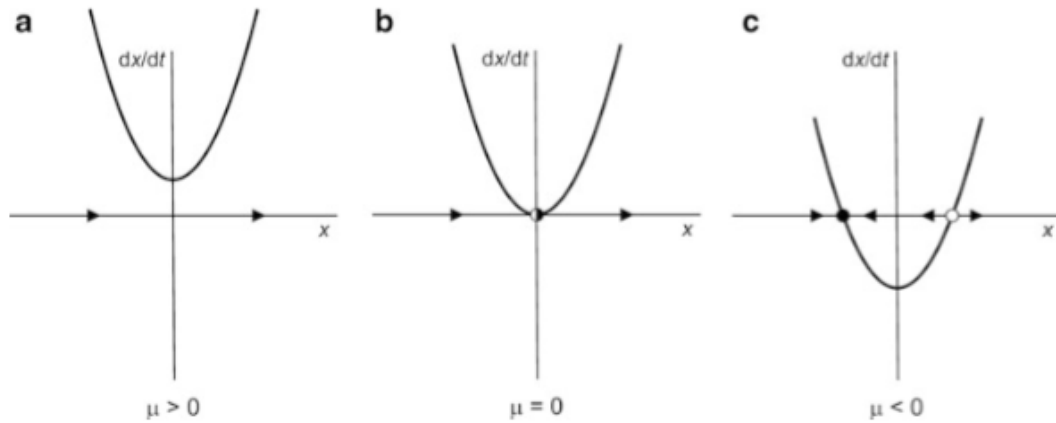
Figure 1.3. Generic diagram of a saddle-node bifurcation for a one-dimensional system, which shows the creation/annihilation of a pair of stable steady states as a function of the bifurcation parameter, μ.[42]

Figure 1.3 shows a typical bifurcation diagram of a saddle-node bifurcation in a one-dimensional system, where μ is the bifurcation parameter and x is the dynamic variable. To recall, a fixed point along the x axis represents a steady state ($\frac{dx}{dt} = 0$). Depending on the direction of the bifurcation parameter (μ) change, the creation, coalescence or destruction of the two steady states will take place.
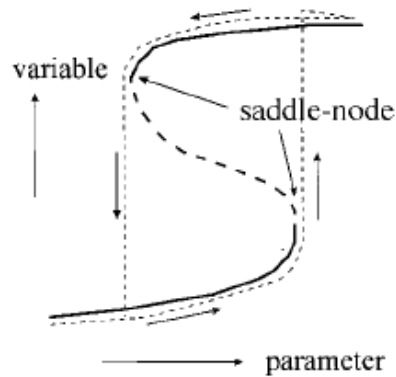
Figure 1.4. Generic diagram of a saddle-node bifurcation for a multi-dimensional system. The solid line represents the steady stable states, whereas the dashed line is the unstable region. The dotted lines and the arrows show the direction of the variable response when periodic changes are made to the parameters.[40]

Saddle-node bifurcations usually come in pairs in systems containing more than one variable (two-dimensional system), which is depicted in Figure 1.4, where two stable steady states can exist between the two bifurcations.[40] Here, the phenomenon of hysteresis is illustrated when the changes to the control parameters are applied in a cyclic fashion.

1.4.2   Hopf Bifurcation

Undoubtedly, most of the oscillatory behavior in a two-dimensional system is developed through the Hopf bifurcation, where a real pair of complex eigenvalues converges through zero.[51] In general, the Hopf bifurcation occurs when a stationary state loses its stability, and the neighbouring trajectories surround the point attractor or point repeller in a closed periodic orbit in a phase space, called a limit cycle.[52] In fact, a limit cycle can be viewed as an isolated trajectory, containing inner and outer components, as seen in Figure 1.5(a) and Figure 1.5(b). Similar to a steady state, a limit cycle can be stable, or unstable, depending on the direction of its neighbouring trajectories. If they spiral towards the closed orbit as time → ∞, the limit cycle is stable, otherwise

8

it is unstable (Figure 1.5(c) and Figure 1.5(d)).
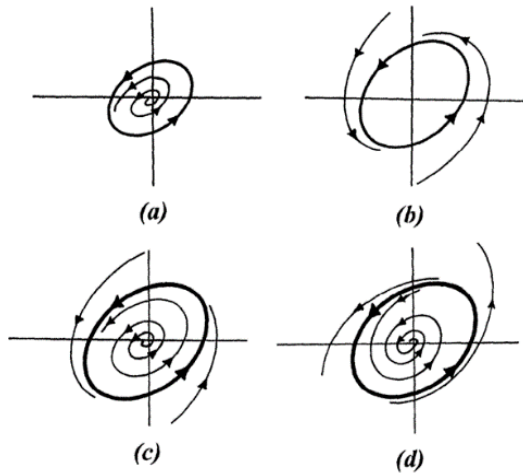
Figure 1.5. Periodic orbits and limit cycles: (a) inner limit cycle, (b) outer limit cycle, (c) stable limit cycle, and (d) unstable limit cycle. [52]

How the limit cycle evolves will determine the stability of the oscillatory state, and this criterion becomes the basis for the sub-classification of the Hopf bifurcation. The bifurcation diagrams of the supercritical and the subcritical types can be seen in Figure 1.6, where the amplitude of the oscillations are represented as the distance between the two stable branches.
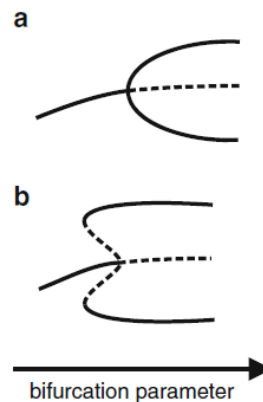
Figure 1.6. A generic bifurcation diagram of a (a) supercritical Hopf bifurcation and (b) a subcritical Hopf bifurcation. [42]

9

1.4.2.1 Supercritical Hopf Bifurcation

A supercritical Hopf bifurcation will cause the emergence of stable oscillations, where a limit cycle grows from the point attractor as a response to the change of the control parameter (Figure 1.7(a)). At the bifurcation point, the radius of the limit cycle, or the amplitude of the oscillations is virtually zero, and will increase linearly with $\sqrt{\mu-\mu_c}$. However, if the control parameter was decreased back to the bifurcation point, the qualitative change of the system's behavior (disappearance of oscillations) would occur at the same value and thus, no hysteresis would be observed.[40,42]

1.4.2.2 Subcritical Hopf Bifurcation

In contrast to the supercritical type, there is no gradual onset of the amplitude of the oscillations. Instead, the point attractor suddenly jumps into a limit cycle, which leads to non-zero amplitude oscillations. Before the bifurcation point, the stable steady state co-exists with an inner unstable limit cycle, and an outer stable one, see Figure 1.7(b). As the bifurcation parameter approaches the critical value, the unstable limit cycle shrinks and eventually becomes engulfed by the steady stable state. Thus, when $\mu = \mu_c$, the steady stable state then becomes unstable, also known as the point repeller. However, the outer limit cycle is still stable, so the oscillations are able to continue to develop in the system. Since there are two attractors (stable steady state and the outer limit cycle) prior to the bifurcation point, the system cannot revert back to its original characteristics at the same parameter value. Therefore, the system is able to exhibit bistability near the bifurcation point.
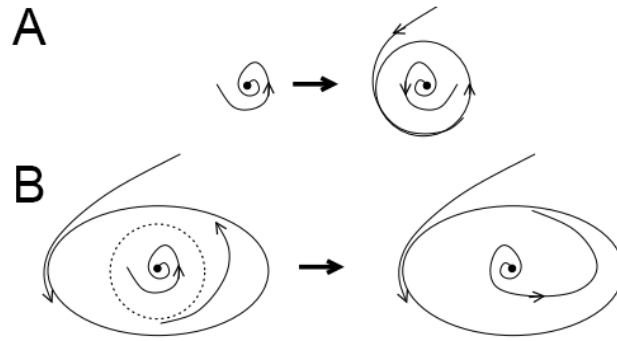
Figure 1.7. The phase space representation of the growth and evolution of a limit cycle in (a) supercritical Hopf bifurcations, and (b) subcritical Hopf bifurcations.[53]

1.4.3   *Homoclinic Bifurcation*

The homoclinic bifurcation occurs when a stable limit cycle born from a Hopf bifurcation, and a saddle steady state connects to form oscillations of infinite periods when $\mu = \mu_c$.[42] The coalescence process as a function of the bifurcation parameter in the phase space is shown in Figure 1.8(a). As μ approaches the critical value, the period of the oscillatory state increases logarithmically. However, when the bifurcation parameter is driven past μ_c, a sudden disappearance of the oscillations takes place. The typical bifurcation diagram of the homoclinic bifurcation is depicted in Figure 1.8(b). To recall, linear stability analysis cannot be performed for homoclinic bifurcations since they are global in nature.
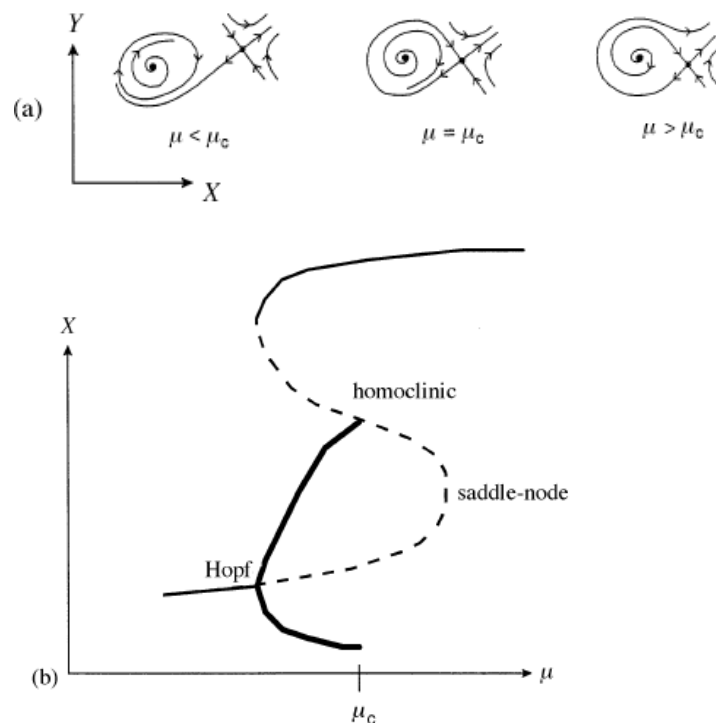
Figure 1.8. (a) Phase space representation of a limit cycle in a homoclinic bifurcation. (b) Generic bifurcation diagram of a homoclinic bifurcation. [40]

1.4.4 Application of Electrochemical Impedance Spectroscopy to Bifurcation Theory in Electrochemical Systems

Electrochemical Impedance Spectroscopy (EIS) is a powerful analytical technique that is commonly used in the field of electrochemistry to characterize heterogeneous charge-transfer processes, such as corrosion and passivation processes.[15,54–57]

Typically, an AC potential is applied to the electrode in the form of low-amplitude sinusoidal perturbations within a fixed range of frequencies. The excitation signal is expressed as:

$$E_t = E_0 \sin(\omega t)$$

where E_t is the potential at a particular time, E_0 is the perturbation amplitude, and ω is the angular frequency ($\omega = 2\pi f$). The instrument then measures the current response (output signal) while

taking the phase shift (ϕ) into consideration:

$$I_t = I_0 \sin(\omega t + \phi)$$

Therefore, the impedance of the system can be expressed as $Z = \frac{E_t}{I_t}$. Impedance is very similar to

resistance, and thus retains the same units of ohm (Ω). However, the major difference lies with the

dependence on frequency for impedance. Typically, the impedance spectra can be represented in

the Nyquist plot that contains a real and imaginary parts, where the x axis is real impedance (Z'),

which is $\frac{\Delta E}{\Delta I} \cos\phi$, and y is the imaginary impedance Z", $\frac{\Delta E}{\Delta I} \sin\phi$.[58]

The impedance response is typically from the working electrode-electrolyte interface, as

other counterparts of the electrochemical cell produces negligible impedances. One of them is the

uncompensated solution resistance, designated as R_s, and can be described as an ohmic resistor

connected in an electric circuit. The current that passes through the circuit can be passed through

the double layer capacitance C_d (non-faradaic), or a result of the faradaic processes (oxidation or

reduction) that produce a faradaic impedance (Z_f).[59]

In nonlinear electrochemical systems, EIS can be used to analyze or detect local

bifurcations (i.e., saddle-node and Hopf). The impedance spectrum represents the linearized

response over a frequency range, and thus, can make assessments of the stability of the system.[40]

If the system intersects on the complex impedance plane at a finite frequency, this refers to the

presence of a Hopf bifurcation, if it is at a zero frequency, then it is a saddle-node bifurcation.

More recently, Strasser, Eiswirth and Koper developed the classification scheme of

electrochemical oscillators on the basis of the mechanistic roles of the double layer potential and

chemical species, and as well as the behavior of the obtained impedance spectrum.[60] The three

primary identified classes are the N-NDR, HN-NDR, and S-NDR oscillators, where the presence

of the negative differential resistance (NDR) is the common feature among the three.

1.5 Classification of Electrochemical Oscillators

1.5.1 Negative Differential Resistance

Undoubtedly, the most common prerequisite of electrochemical oscillations is Negative Differential Resistance (NDR).[42,46,61,62] A NDR is characterized as the negative slope of a I-E dependence curve obtained at sufficiently slow scan rates. However, the presence of a negative slope alone is not an objective confirmation that the system is able to exhibit oscillatory behavior. In fact, there are many sources that cause a decrease in the current response but do not necessary produce dynamical instabilities. Some of the proposed processes that result in a NDR and the emergence of oscillations are highlighted below based on the factors affecting the current response.

$$I = nFAk(E)c(0)$$

The faradic current is given by the number of electrons involved in the electron transfer process (n); Faraday's constant (F); the surface area of the working electrode (A), the potential-dependent heterogeneous rate constant ($k(E)$), and the surface concentration of the electroactive species $c(0)$.[40,42,61]

1. A negative dA/dE slope is typically caused by the potential-dependent adsorption of an inhibitor or the passivation of the electrode surface. In both cases, the number of active sites available for the electrocatalytic reaction is reduced, which gives rise to the negative current response.

2. A negative k(E)/dE slope corresponds to the potential-dependent desorption of a catalyst that facilitates the electro-oxidation or electro-reduction reaction. The potential-dependent adsorption of an non-ideal inhibitor (that does not completely block the surface) is another example that falls into this category, as it decreases the rate of electron-transfer.

3. A negative kc(0)/dE slope can be explained by the Frumkin effect, where the
   concentration of the chemical species at the double layer is different than in the bulk
   when the concentration of the electrolyte is low.

1.5.1.1 N-shaped Negative Differential Resistance

The N-shaped Negative Differential Resistance (N-NDR) or Class III oscillators are widespread in electrochemical systems, such as the reduction of In^{3+} at the hanging mercury drop electrode in the presence of SCN^-,[63] the reduction of H_2O_2 at Pt,[64] and the electrodissolution of Fe in H_2SO_4 to name a few.[65] N-NDR oscillators will produce a linear sweep voltammogram (LSV) that resembles the letter "N" due to the presence of a negative impedance branch (Figure 1.9(a)), [46,62] which is also demonstrated in a complex impedance spectrum, Figure 1.9(c).[60] Here, the system intersects with the real axis at a negative impedance.

The oscillations belonging to the N-NDR class can only occur in the current at constant applied potentials on the negative branch with the presence of an ohmic external resistance (Figure 1.9(b)).[60,66] Otherwise, the current response remains in a stable steady state and oscillations do not emerge. However, there is an upper and lower limit of the resistance; so an appropriate resistance size must be introduced in the electrochemical circuit. Under galvanostatic control, the system is capable to exhibit bistability but not potential oscillations.[42,46,66]

With respect to the mechanism, the autocatalytic variable that is involved in the fast positive feedback loop is the electrode potential, while the concentration of the electroactive species provides the slow feedback loop and is the inhibitory variable.[60]
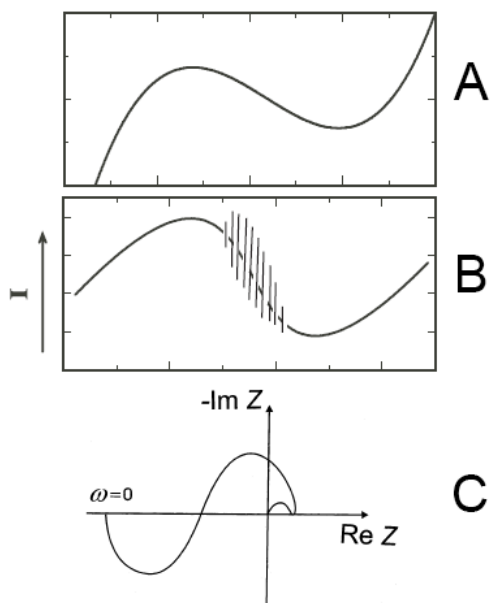
Figure 1.9. (a) A typical LSV in the absence of an external resistor, (b) LSV in the presence of a sufficiently large external resistor and (c) Nyquist plot of an N-NDR electrochemical oscillator.[46,60]

1.5.1.2 Hidden N-shaped Negative Differential Resistance

Over the years, many researchers have reported simple and complex electrochemical oscillations that belong to the Hidden N-shaped Negative Differential Resistance (HN-NDR) or Class IV type. These systems include but are not limited to the oxidation of ethylene glycol,[67] formic acid,[68] sulfite,[69] and methanol on Pt surfaces.[32] Arguably, the most well-known example would be the oxidation of formic acid on Pt electrodes. These HN-NDR oscillators contain a negative impedance that is undetectable in the stationary polarization curve, as it is hidden or masked by a characteristic positive slope (Figure 1.10(a)).[60,62] The concealed negative impedance can however be uncovered through impedance investigations at applied potentials along the positive branch.[62] Figure 1.10(c) shows a typical Nyquist plot of a HN-NDR electrochemical oscillator, where the system crosses the positive and negative imaginary axis and terminates at a positive real impedance. Negative impedance responses occur at a wide range of relatively high and intermediate frequencies, while the positive impedance at a zero-frequency indeed is reflective

of the positive slope observed in the LSV. It has been proposed that the coupling of fast negative impedance processes and a slow positive impedance process is required for the emergence of HN-NDR oscillations.[61]

One of the marked contrasts between the HN-NDR and the classical N-NDR system is the ability to exhibit both potentiostatic and galvanostatic oscillations, whereas the latter can only oscillate in the current.[46] For oscillations at potentiostatic conditions, the presence of a sufficiently high resistor must be inserted in the circuit in order to destabilize the system (Figure 1.10(b)).[66] However, the emergence of galvanostatic oscillations does not necessarily require any external resistor inserted, and are also typically found on the positive slope of the I-E curve.[42]

On a mechanistic basis, the essential variables remain the same for HN-NDR and the N-NDR oscillators, in which the double layer potential is the autocatalytic variable, and the chemical species acts as the inhibitory variable.[60]
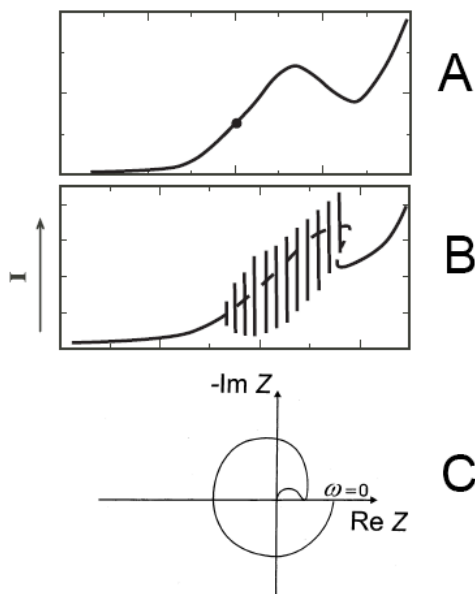
Figure 1.10. (a) A typical LSV in the absence of an external resistor, (b) LSV in the presence of a sufficiently large external resistor and (c) Nyquist plot of an HN-NDR electrochemical oscillator.[46,60]

1.5.1.3 S-shaped Negative Differential Resistance

The third NDR type is the S-shaped Negative Differential Resistance (S-NDR), where the double layer potential is the slow essential variable, and the chemical species participates in the fast positive feedback.[60,70] These oscillations only arise in very specific or rare conditions, for example, when the surface area and the capacitance is effectively large.[71,72] For this class, the source of instability is usually the potential-dependent electrode surface coverage of adsorbates with high interactions within the layer which experiences a phase transition between an ordered and disordered state.[42,60]

The typical I-E dependence curve manifests itself as a S shape profile. At potentiostatic conditions, the system exhibits bistability without the presence of an ohmic resistance (Figure 1.11(a)).[60] However, with the insertion of sufficiently large resistors, the system is able to oscillate in the current (Figure 1.11(b)). In contrast to N-NDR types, potential oscillations under galvanostatic control could be observed. Some examples of oscillations belonging to the S-NDR class are the electrodeposition of Zn,[73] and electro-oxidation of H_2/CO in polymer electrolyte membrane fuel cells.[72]

The impedance spectra obtained from EIS experiments of a S-NDR oscillator shows the system to cross the real impedance axis at a finite perturbation frequency, and conclude at negative real impedance values, Figure 1.11(c).
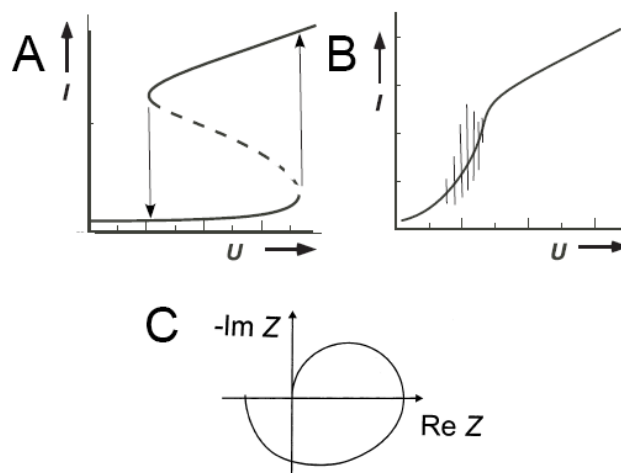
Figure 1.11. (a) A typical LSV in the absence of an external resistor, (b) LSV in the presence of a sufficiently large external resistor and (c) Nyquist plot of an S-NDR oscillator.[46,60]

1.5.2 Convection Mass Transportation

Instabilities, such as oscillations in the response current or potential in electrochemical reactions, can arise through non-NDR mechanisms, one being convection mass transfer induced by hydrogen or oxygen gas evolution (depending on whether it is an oxidation or reduction reaction).[74] Thus, the oscillations typically occur at higher anodic or cathodic potentials, past the limiting current plateau during the slow voltage scanning. At the minimum peak of the current oscillations, the O_2 or H_2 formation represses the electro-oxidation or electro-reduction of some species due to the growth and detachment of bubbles that generates a forced convection of the electroactive species. At maximum peaks, the electrochemical oxidation or reduction reaction of interest is the predominant process.[74]

One method to determine whether the oscillatory behavior is caused by convection mass transportation is through the application of some form of agitation with a force larger or equal to the bubble evolution. Under such circumstances, the electroactive ions will be continually replenished at the working electrode, and the oxidation of hydroxide ions is negligible. Therefore,

19

the current response will be in steady stable state and no oscillations would occur. Some systems that were found to exhibit this behavior by Li and co-workers are the electro-reduction of $Fe(CN)_6^{3-}$ and $S_2O_8^{2-}$ in NaOH on Pt electrodes.[74]

1.5.3   *Capacitance Mediated Positive Differential Resistance*

In recent studies, it has been proposed by Krischer and co-workers that the electroformation and electrodissolution of a current-inhibiting layer, such as a salt or an oxide, at the working electrode plays an important role in the emergence of electrochemical oscillations.[71] In contrast to NDR types, oscillations belonging to the Capacitance Mediated Positive Differential Resistance (C-PDR) description occur at positive impedances for all frequency ranges, and are observed on the current plateau of a stationary I-E dependence curve in the absence of an ohmic resistor.

The surface film acts as a charge storage, where the capacitance is a function of the layer thickness and time. Thus, for C-PDR oscillators, the capacitance and the potential drop across the passive layer become the two essential variables involved in the feedback mechanisms. This model is especially relevant for many electrodissolution processes of certain metals and semi-conductors, such as InP,[75] GaP,[76] Cu,[13] and Si.[15,77–79] A highly cited example is the anodic dissolution of Fe in H_2SO_4,[80–82] where under a certain range of applied potentials, an iron sulfate film is produced.

1.6   *Oscillatory Electro-oxidation of Sulfur Compounds*

Sulfur-containing compounds have been attractive to many topics of research, but especially in the study of nonlinear kinetics due to its ability to exhibit unique and exotic reaction behaviors, such as self-organization phenomena. This stems from the multiple oxidation states in which sulfur can exist in (-2, 0, +2, +4, and +6).

Current and/or potential oscillations have been reported in redox reactions of many sulfur compounds. For example, Gao et. al described the emergence of oscillations under galvanostatic

20

and potentiostatic control during the electro-oxidation of thiosulfate on Au electrodes.[83] Here, two distinct regions on the positive branch of the stationary polarization curve were found to exhibit simple, and complex oscillations. Through impedance spectroscopy investigations, it was revealed that the oscillations were of the HN-NDR nature. Another oscillatory system that falls under the same category is the electro-oxidation of hydroxymethanesulfinate on Pt and Au.[84] On Au electrodes, the dissolution of the surface that causes pitting seen through scanning electron microscopy (SEM) images was suggested to be most likely the dominant factor that causes the dynamical instabilities. Wang and his co-workers reported the HN-NDR oscillator in the electro-oxidation of thiourea on a Pt electrode, and the influence of temperature on the reaction kinetics.[85] Complex oscillations were able to appear at lower reaction temperatures, and the frequency of the oscillations increased with increasing temperature.

The electro-oxidation of sulfide on Pt electrodes in the presence of an external ohmic resistor was shown to oscillate in the current. In fact, these oscillations were determined to belong to both N-NDR and HN-NDR types, depending on the applied potential.[86] A similar study was performed by Miller and Chen on a microstructured Ti/Ta_2O_5-IrO_2 electrode.[87] The current oscillations during the electro-oxidation of sulfite on Pt electrodes were of the N-NDR oscillator, where the reaction behavior exhibited great dependence on the pH of the solution.[88]

1.7   *References*

(1)   Kuznetsov, Y. A. Introduction to Dynamical Systems. In *Elements of Applied Bifurcation Theory*. Applied Mathematical Sciences Volume 112; Springer: New York, N.Y., 2004; pp 1-37.

(2)   Kuznetsov, Y. A. *Elements of Applied Bifurcation Theory Third Edition*; Springer: New York, N.Y., 2013.

(3)   Goldbeter, A. *Biochemical Oscillations and Cellular Rhythms: The Molecular Bases of Periodic and Chaotic Behaviour*; Cambridge University Press: Cambridge, U.K., 1997.

(4)   Solé, R.; Bascompte, J. *Self-Organization in Complex Ecosystems*; Princeton University Press: Princeton, N.J., 2012.

(5)   Burnside, S. D.; Shklover, V.; Barbé, C.; Comte, P.; Arendse, F.; Brooks, K.; Grätzel, M. Self-Organization of TiO_2 Nanoparticles in Thin Films. *Chem. Matter* **1998**, *10*, 2419–2425.

(6)   U. Witt. Self-Organization and Economics - What Is New? *Struct. Chang. Econ. Dyn.* **1997**, *8*, 489–507.

(7)   Castets, V.; Dulos, E.; Boissonade, J.; De Kepper, P. Experimental Evidence of a Sustained Standing Turing-Type Nonequilibrium Chemical Pattern. *Phys. Rev. Lett*. **1990**, *64*, 2953–2956.

(8)   Yates, F. E. What is Self-Organization?
http://assets.press.princeton.edu/chapters/s7104.pdf.

(9)   Fechner, M. G. Ueber Umkehrungen Der Polaritat Der Einfachen Kette. *Schweingg. J* **1828**, *53*, 61–76.

(10)   Hankins, M. J.; Gaspar, V.; Kiss, I. Z. Abrupt and Gradual Onset of Synchronized Oscillations Due to Dynamical Quorum Sensing in the Single-Cathode Multi-Anode Nickel Electrode. *Chaos* **2019**, *29*, 033114.

(11)   Li, L.; Chen, S.-H.; Yang, X.-G.; Wang, C.; Guo, W.-J. Pitting Corrosion Induced Current Oscillations during Electrodissolution of Al in HClO$_4$ Solutions. *J. Electroanal. Chem.* **2004**, *572*, 41–49.

(12)   Sazou, D. Current Oscillations and Mass-Transport Control during Electrodissolution of Iron in Phosphoric Acid Solutions. *Electrochim. Acta* **1997**, *42*, 627–637.

(13)   Lee, H. P.; Nobe, K.; Pearlstein, A. J. Film Formation and Current Oscillations in the Electrodissolution of Cu in Acidic Chloride Media I. Experimental Studies. *J. Electrochem. Soc*. **1985**, *132*, 1031–1037.

(14)   Zheng, J.; Huang, W.; Chen, S.; Niu, Z.; Li, Z. New Oscillatory Phenomena during Gold Electrodissolution in Sulfuric Acid Containing Br- or in Concentrated HCl. *Electrochem. commun*. **2006**, *8*, 600–604.

(15)   Koster, D.; Patzauer, M.; Salman, M. M.; Battistel, A.; Krischer, K.; La Mantia, F. Measurement and Analysis of Dynamic Impedance Spectra Acquired during the Oscillatory Electrodissolution of P-Type Silicon in Fluoride-Containing Electrolytes. *ChemElectroChem* **2018**, *5*, 1548–1551.

(16)   dos Santos, C. G. P.; Machado, E. G.; Kiss, I. Z.; Nagao, R. Investigation of the Oscillatory Electrodissolution of the Nickel-Iron Alloy. *J. Phys. Chem*. C **2019**, *123*, 24087–24094.

(17)   Bassett, M. R.; Hudson, J. L. The Oscillatory Electrodissolution of Copper in Acidic Chloride Solution I. 0.1 M Chloride. *J. Electrochem. Soc*. **1990**, *137*, 922–932.

(18)   Potkonjak, N. I.; Nikolic, Z.; Anic, S. R.; Minic, D. M. Electrochemical Oscillations during Copper Electrodissolution/Passivation in Trifluoroacetic Acid Induced by Current Interrupt Method. *Corros. Sci.* **2014**, *83*, 355–358.

(19)   Otterstedt, R. D.; Jaeger, N. I.; Plath, P. J. Various Wave Phenomena during the Oscillatory Electrodissolution of Cobalt. *Int. J. Bifurc. Chaos* **1994**, *4*, 1265–1273.

(20)   Lopez-Sauri, D. A.; Veleva, L.; Perez-Angel, G. Potentiostatic Current and Galvanostatic Potential Oscillations during Electrodeposition of Cadmium. *Phys. Chem. Chem. Phys.* **2015**, *17*, 22266–22271.

(21)   Suter, R. M.; Wong, P. Nonlinear Oscillations in Electrochemical Growth of Zn Dendrites. *Phys. Rev. B* **1989**, *39*, 4536–4540.

(22)   Nakanishi, S.; Fukami, F.; Tada, T.; Nakato, Y. Metal Latticeworks Formed by Self-Organization in Oscillatory Electrodeposition. *J. Am. Chem. Soc*. **2004**, *126*, 9556–9557.

(23)   Saliba, R.; Mingotaud, C.; Argoul, F.; Ravaine, S. Spontaneous Oscillations in Gold Electrodeposition. *Electrochem. commun*. **2002**, *4*, 629–632.

(24)   Nakanishi, S.; Sakai, S.; Nishimura, K.; Nakato, Y. Layer-by-Layer Electrodeposition of Copper in the Presence of o-Phenanthroline, Caused by a New Type of Hidden NDR Oscillation with the Effective Electrode Surface Area as the Key Variable. *J. Phys. Chem. B* **2005**, *109*, 18846–18851.

(25)   Krastev, I.; M. T. M. Koper. Pattern Formation during the Electrodeposition of a Silver-Antimony Alloy. *Phys. A Stat. Mech. its Appl*. **1995**, *213*, 199–208.

(26)   Oliveira, C. P.; Lussari, N. V.; Sitta, E.; Varela, H. Oscillatory Electro-Oxidation of Glycerol on Platinum. *Electrochim. Acta* **2012**, *85*, 674–679.

(27)   Seidel, Y. E.; Jusys, Z.; Lindström, R. W.; Stenfeldt, M.; Kasemo, B.; Krischer, K. Oscillatory Behaviour in Galvanostatic Formaldehyde Oxidation on Nanostructured Pt/Glassy Carbon Model Electrodes. *ChemPhysChem* **2010**, *11*, 1405–1415.

(28)   Koper, M. T. M.; Vanmaekelbergh, D. The Origin of Oscillations during Hydrogen Peroxide Reduction on GaAs Semiconductor Electrodes. *J. Phys. Chem*. **1995**, *99*, 3687–3696.

(29)   Mukouyama, Y.; Yamamoto, S.; Nakazato, R.; Nakanishi, S.; Okamoto, H. Newly Found Electrochemical Oscillations during Reduction of Nitrate Ions. *ECS Trans*. **2013**, *50*, 61–70.

(30)   Mukouyama, Y.; Kawasaki, H.; Hara, D.; Yamada, Y.; Nakanishi, S. Appearance of New Oscillations (Named Oscillations I and J) during Reduction of H_2O_2 on Platinum Electrode. *J. Electrochem. Soc.* **2017**, *164*, 675–684.

(31)   Koper, M. T. M.; Gaspard, P. Mixed-Mode and Chaotic Oscillations in a Simple Model of an Electrochemical Oscillator. *J. Phys. Chem*. **1991**, *95*, 4945–4947.

(32)   Lee, J.; Eickes, C.; Eiswirth, M.; Ertl, G. Electrochemical Oscillations in the Methanol Oxidation on Pt. *Electrochim. Acta* **2002**, *47*, 2297–2301.

(33)   Wojtowicz, J., Marincic, N., Conway, B. E. Oscillatory Kinetics in the Electrochemical Oxidation of Formate and Ethylene. *J. Chem. Phys.* **1968**, *48*, 4333–4345.

(34)   Krischer K., Lubke M., Wolf, W., Eisworth M., Ertl, G. Oscillatory Dynamics of the Electrochemical Oxidation of H_2 in the Presence of Cu^{2+}: Structure Sensitivity and the Roles of Anions. *Electrochim. Acta* **1995**, *40*, 69–81.

(35)   Martins, A. L.; Batista, B. C.; Sitta, E.; Varela, H. Oscillatory Instabilities during the Electrocatalytic Oxidation of Methanol on Platinum. *J. Braz. Chem. Soc*. **2008**, *19*, 679–687.

(36)   Ferreira, G. C. A.; Napporn, T. W.; Kokoh, K. B.; Varela, H. Complex Oscillatory Kinetics in the Electro-Oxidation of Glucose on Gold. *J. Electrochem. Soc.* **2017**, *164*, H603–H607.

(37)   Varela, H.; Delmonde, M. V. F.; Zülke, A. A. The Oscillatory Electrooxidation of Small
Organic Molecules. In *Electrocatalysts for Low Temperature Fuel Cells: Fundamentals and Recent
Trends*; Wiley: New York, N.Y., 2017; pp 145–163.

(38)   Strasser, P.; Lübke, M.; Eickes, C.; Eiswirth, M. Modeling Galvanostatic Potential
Oscillations in the Electrocatalytic Iodate Reduction System. *J. Electroanal. Chem.* **1999**, *462*, 19–
33.

(39)   Mukouyama, Y.; Hasegawa, M.; Nakanishi, S. Electrochemical Oscillation during H_2O_2
Reduction in Basic Solutions. *Electrochem. Soc*. **2015**, *64*, 49–55.

(40)   Koper, M. T. M. Non-Linear Phenomena in Electrochemical Systems. *J. Electrochem. Soc.
Faraday Trans*. **1998**, *94*, 1369–1378.

(41)   Heylighen, F. The Science of Self-Organization and Adaptivity. *Encycl. Life Support Syst***.
2001**, *5*, 253–280.

(42)   Orlik, M. *Self-Organization in Electrochemical Systems I: General Principles of Self-
Organization. Temporal Instabilities*; Springer: Berlin, 2012.

(43)   Orlik, M. Self-Organization in Nonlinear Dynamical Systems and Its Relation to the
Materials Science. *J. Solid State Electrochem*. **2009**, *13*, 245–261.

(44)   Prigogine, I.; Lefever, R. Theory of Dissipative Structures. In *Synergetics Cooperative
Phenomena in Multi-Component Systems*; Haken, H., Ed.; Vieweg+Teubner Verlag, Wiesbaden:
Berlin, 1973; pp 124–135.

(45)   I. R. Epstein; Pojman, J. A. *An Introduction to Nonlinear Chemical Dynamics:
Oscillations, Waves, Patterns, and Chaos*; Oxford University Press: Oxford, U.K., 1998.

(46)   Krischer, K. Nonlinear Dynamics in Electrochemical Systems. In *Advances in Electrochemical Science and Engineering*; Wiley-VCH Verlag GmbH & Co. KGaA: Weinheim, Germany, 2002; pp 89-208.

 (47)   I. R. Epstein; Showalter, K. Nonlinear Chemical Dynamics: Oscillations, Patterns, and Chaos. *J. Phys. Chem.* **1996**, *100*, 13132–13147.

(48)   Guckenheimer, J.; Holmes, P. J. *Nonlinear Oscillations, Dynamical Systems, and Bifurcations of Vector Fields*; Springer: New York, N.Y., 1983.

(49)   Nakahara, H.; Doya, K. Dynamics of Attention as Near Saddle-Node Bifurcation Behavior. In *Advances in Neural Information Processing Systems*; **1996**; pp 38–44.

(50)   Ji, J. C. Local Bifurcation Control of a Forced Single-Degree-of-Freedom Nonlinear System: Saddle-Node Bifurcation. *Nonlinear Dyn.* **2001**, *25*, 369–382.

(51)   Scott, S. K. *Chemical Chaos*; Oxford University Press: Oxford, U.K., 1991.

(52)   Chen, G.; Moiola, J. An Overview of Bifurcation, Chaos, Nonlinear Dynamics in Control Systems. *J. Franklin Inst*. **1994**, *331*, 819–858.

(53)   Roussel, M. R. Introduction to Bifurcations. In *Nonlinear Dynamics a Hands-On Introductory Survey*; Morgan & Claypool Publishers: San Rafael, C.A., 2019; pp 1–19.

(54)   Baril, G.; Galicia, G.; Deslouis, C.; Pébère, N.; Tribollet, B.; Vivier, V. An Impedance Investigation of the Mechanism of Pure Magnesium Corrosion in Sodium Sulfate Solutions. *J. Electrochem. Soc*. **2007**, *154*, C108–C113.

(55)   Aoki, I. V.; Bernard, M.-C.; Cordoba de Torresi, S. I.; Deslouis, C.; de Melo, H. G.; Joiret, S.; Tribollet, B. AC-Impedance and Raman Spectroscopy Study of the Electrochemical Behaviour of Pure Aluminum in the Citric Acid Media. *Electrochim. Acta* **2001**, *46*, 1871–1878.

(56)   Pan, J.; Thierry, D.; Leygraf, C. Electrochemical Impedance Spectroscopy Study of the Passive Oxide Film on Titanium for Implant Application. *Electrochim. Acta* **1996**, *41*, 1143–1153.

(57)   García-Jareño, J. J.; Giménez-Romero, D.; Keddam, M.; Vicente, F. Graphical Analysis of Electrochemical Impedance Spectroscopy of Two Consecutive Irreversible Electron Transfers. 1. Theoretical Study of the Anodic Dissolution of Metals. *J. Phys. Chem. B* **2005**, *109*, 4584–4592.

(58)   Bard, A. J.; Faulkner, L. R. *Electrochemical Methods Fundamentals and Applications Second Edition*; John Wiley & Sons Inc.: Hoboken, N.J., 2000.

(59)   Chang, B.-Y.; Park, S.-M. Electrochemical Impedance Spectroscopy. *Annu. Rev. Anal. Chem.* **2010**, *3*, 207–229.

(60)   Strasser, P.; Eiswirth, M.; M. T. M. Koper. Mechanistic Classification of Electrochemical Oscillators - an Operational Experimental Strategy. *J. Electroanal. Chem.* **1999**, *478*, 50–66.

(61)   Koper, M. T. M. Oscillations and Complex Dynamical Bifurcations and in Electrochemical Systems. In *Advances in Chemical Physics*; John Wiley & Sons Inc.: Hoboken, N.J., 1996; pp 161–298.

(62)   Koper, M. T. M.; Sluyters, J. H. Instabilities and Oscillations in Simple Models of Electrocatalytic Surface Reactions. *J. Electroanal. Chem.* **1994**, *371*, 149–159.

(63)   Koper, M. T. M.; Gaspard, P.; Sluyters, J. H. Mixed-Mode Oscillations and Incomplete Homoclinic Scenarios to a Saddle Focus in the Indium/Thiocyante Electrochemical Oscillator. *J. Chem. Phys.* **1992**, *97*, 8250–8260.

(64)   Fetner, N.; Hudson, J. L. Oscillations during the Electrocatalytic Reduction of Hydrogen Peroxide on a Platinum Electrode. *J. Phys. Chem.* **1990**, *94*, 6506–6509.

(65)   Podestá, J. J.; Piatti, R. C. V.; Arvia, A. J. The Potentiostatic Current Oscillations at Iron/Sulfuric Acid Solution Interfaces. *J. Electrochem. Soc*. **1979**, *126*, 1363–1367.

(66)   Koper, M. T. M. The Theory of Electrochemical Instabilities. *Electrochim. Acta* **1992**, *37*, 1771–1778.

(67)   Sitta, E.; Nascimento, M. A.; Varela, H. Complex Kinetics, High Frequency Oscillations and Temperature Compensation in the Electro-Oxidation of Ethylene Glycol on Platinum. *Phys. Chem. Chem. Phys*. **2010**, *12*, 15195–15206.

(68)   Gojuki, T.; Numata, Y.; Mukouyama, Y.; Okamoto, H. Hidden Negative Differential Resistance in the Oxidation of Formic Acid on Platinum. *Electrochim. Acta* **2014**, *129*, 142–151.

(69)   Feng, J.; Gao, Q.; Xu, L.; Wang, J. Nonlinear Phenomena in the Electrochemical Oxidation of Sulfite. *Electrochem. commun*. **2005**, *7*, 1471–1476.

(70)   Krischer, K.; Mazouz, N.; Flätgen, G. Pattern Formation in Globally Coupled Electrochemical Systems with an S-Shaped Current-Potential Curve. *J. Phys. Chem. B* **2000**, *104*, 7545–7553.

(71)   Zensen, C.; Schönleber, K.; Kemeth, F.; Krischer, K. A Capacitance Mediated Positive Differential Resistance Oscillator Model for Electrochemical Systems Involving a Surface Layer. *J. Phys. Chem. C* **2014**, *118*, 24407–24414.

(72)   Kirsch, S.; Hanke-Rauschenbach, R.; El-Sibai, A.; Flockerzi, D.; Krischer, K. The S-Shaped Negative Differential Resistance during the Electrooxidation of H_2/CO in Polymer Electrolyte Membrane Fuel Cells: Modeling and Experimental Proof. *J. Phys. Chem. C* **2011**, *115*, 25315–25329.

(73)   Kiss, I. Z.; Kazsu, Z.; Gáspár, V. Experimental Strategy for Characterization of Essential Dynamical Variables in Oscillatory Systems: Effect of Double-Layer Capacitance on the Stability of Electrochemical Oscillators. *J. Phys. Chem. A* **2005**, *109*, 9521–9527.

(74)   Li, Z.; Cai, J.; Zhou, S. Current Oscillations in the Reduction or Oxidation of Some Anions Involving Convection Mass Transfer. *J. Electroanal. Chem*. **1997**, *436*, 195–201.

(75)   Langa, S.; Carstensen, J.; Tiginyanu, I. M.; Christophersen, M.; Föll, H. Self-Induced Voltage Oscillations during Anodic Etching of n-InP and Possible Applications for Three-Dimensional Microstructures. *Electrochem. Solid-State Lett*. **2001**, *4*, G50–G52.

(76)   Wloka, J.; Lockwood, D. J.; Schmuki, P. High Intensity and Oscillatory Electroluminescence Observed during Porous Etching of GaP in HBr and HF Electrolytes. *Chem. Phys. Lett*. **2005**, *414*, 47–50.

(77)   Ozanam, F.; Chazalviel, J. Anodic Dissolution of Si: Electrochemical Oscillations and Porous Silica Formation. *ECS Trans*. **2013**, *50*, 15–24.

(78)   Schönleber, K.; Patzauer, M.; Krischer, K. A Comparison of Modeling Frameworks for the Oscillatory Silicon Electrodissolution. *Electrochim. Acta* **2016**, *210*, 346–351.

(79)   Cattarin, S.; M. M. Musiani. Electrodissolution and Passivation of Silicon in Aqueous Alkaline Media: A Voltammetric and Impedance Investigation. *J. Phys. Chem. B* **1999**, *103*, 3162–3169.

(80)   Geraldo, A. B.; Barcia, O. E.; Mattos, O. R.; Huet, F.; Tribollet, B. New Results Concerning the Oscillations Observed for the System Iron-Sulphuric Acid. *Electrochim. Acta* **1998**, *44*, 455–465.

(81)   Russell, P.; J. Newman. Anodic Dissolution of Iron in Acidic Sulfate Electrolytes I. Formation and Growth of a Porous Salt Film. *J. Electrochem. Soc*. **1986**, *133*, 59–69.

(82)   Ferreira, J. R. R. M.; Barcia, O. E.; Mattos, O. R.; Tribollet, B. Iron Dissolution under Mass Transport Control: The Effect of Viscosity on the Current Oscillation. *Electrochim. Acta* **1994**, *39*, 933–938.

(83)   Bi, W.; He, Y.; Cabral, M. F.; Varela, H.; Yang, J.; Jiang, R.; Gao, Q. Oscillatory Electro-Oxidation of Thiosulfate on Gold. *Electrochim. Acta* **2014**, *133*, 308–315.

(84)   Bell, J. G.; Wang, J. Nonlinear Instabilities during the Electrochemical Oxidation of Hydroxymethanesulfinate. *Electrochim. Acta* **2016**, *222*, 678–684.

(85)   Xu, L.; Gao, Q.; Feng, J.; Wang, J. Oscillations and Period-Doubling Bifurcations in the Electrochemical Oxidation of Thiourea. *Chem. Phys. Lett.* **2004**, *397*, 265–270.

(86)   Feng, J.; Gao, Q.; Li, J.; Liu, L.; Mao, S. Current Oscillations during the Electrochemical Oxidation of Sulfide in the Presence of an External Resistor. *Sci. China Ser. B Chem.* **2008**, *51*, 333–340.

(87)   Chen, A.; Miller, B. Potential Oscillations during the Electrocatalytic Oxidation of Sulfide on a Microstructured Ti/Ta$_2$O$_5$IrO$_2$ Electrode. *J. Phys. Chem. B* **2004**, 108, 2245–2251.

(88)   Bell, J. G.; Dao, M.; Wang, J. Qualitative Dependence of the Electro-Oxidation Behavior of Sulfite on Solution pH. *J. Electroanal. Chem*. **2018**, *816*, 1–6.

CHAPTER 2 – THE ELECTRO-OXIDATION OF BISULFITE IN ACIDIC MEDIA

2.1 Introduction

Driven by the scarcity and high cost of noble metal electrocatalysts, in recent years there have been increasing interests and demands in studying electrochemical reactions with carbon-based materials. In this study, the low-cost glassy carbon was selected as the working electrode to mediate the electrochemical oxidation of bisulfite, an oxidation process known to have important connections to the hybrid sulfur cycle, which is an efficient energy source that leads to the renewable and clean production of H_2.[1,2] Electrochemical impedance spectra show that the oxidation of bisulfite at the glassy carbon surface involves two reaction time scales and the existence of an inductive loop, similar to the behavior frequently seen in metal corrosion. Interestingly, the studied system does not only exhibit nonlinear instabilities, but also show qualitative dependence on the size of the deployed working electrode, offering a new model for the investigation of dynamic quorum sensing phenomena.

Dynamic quorum sensing, known as the onset of synchronization of oscillatory behavior in many biological systems, has attracted a great deal of attention from scientists working in different fields.[3-10] In the Belousov-Zhabotinsky (BZ) reaction,[11] Showalter and co-workers reported that the global interactions between the beads oscillators could induce coordinated activity as a function of beads population.[3,12] More recently, Kiss and his coworkers reported a population-dependent emergence of current oscillations in an electrochemical system during the dissolution of nickel, in which the number of anode wires acts like a control parameter similar to population density and ultimately determines the dynamical transition to coherence.[13] Herein, we report the critical surface area size-dependent emergence of current and potential oscillations during the electro-oxidation of bisulfite on glassy carbon electrodes. The importance of surface area in electrochemical reactions, through its influence on the ohmic drop, has been well-documented in literature.[14-16] However, we

are not aware of any experimental report that the electrode surface could act as a bifurcation parameter leading to consecutive transitions from a steady state to complex oscillations.

In addition to the dynamic quorum sensing behavior, the study of chemical and electrochemical oscillators have made significant contributions towards the understanding of various complex phenomena encountered in nature.[17] In recent years, considerable efforts have been made to the study of nonlinear instabilities in sulfur compounds due to their unique chemical properties and broad range of applications.[18] The emergence of nonlinear instabilities was able to provide a new set of parameters to gain significant insights into the mechanistic pathway undertaken by these sulfur compounds reactions.[19-21] Oscillations in the potential and current have recently been reported during the electrochemical oxidation of sulfur dioxide, sulfite, and other several sulfur-containing compounds, such as thiosulfate, sulfide, and thiourea.[22-26]

Autocatalytic or autoinhibition reactions have been known to be the essential processes in the homogeneous chemical oscillators.[11] In the heterogeneous electrochemical reactions, on the other hand, mechanistic studies suggest that the presence of a negative differential resistance is critical. Based on that, Strasser and coworkers proposed a classification scheme for the electrochemical oscillations.[27] Many reported electrochemical oscillators are recognized as N-shaped Negative Differential Resistance (N-NDR) or Hidden N-shaped Negative Differential Resistance (HN-NDR) types, in which the double layer potential (φ) is an essential variable providing the fast necessary positive feedback loop, while the concentration of the electroactive species assumes the role of an inhibitor and supplies the slow negative feedback loop.[17,27] It has also been demonstrated that oscillatory behavior could arise in systems with convection mass transfer or capacitance mediated positive differential resistance.[28-31]

2.2 Experimental Procedures

All experiments were conducted on a CHI 760E electrochemical workstation (CHI Instruments, Texas, US) using a conventional three-electrode figuration. A silver/silver chloride (Ag/AgCl, 4 M KCl) was employed as the reference electrode, and a Pt film (Shanghai Ruosull Technology) served as the counter electrode. The surface area of glassy carbon electrodes (GCE) was controlled by either partially covering up a 3.0 mm diameter GCE or combining various 1.0 mm and 3.0 mm diameter GCEs. All potentials reported in this study is versus Ag/AgCl. The GCE working electrodes were polished with fine alumina powder (0.3 um, and 0.05 um), and were sonicated to remove any particle residues on the surface. The electrode was thoroughly rinsed before use. All solutions were prepared with double distilled water and was used immediately for experiments. Sodium bisulfite ($NaHSO_3$) was purchased from Sigma Aldrich. These chemicals were used as received without further purification. The solution volume was held constant at 80.0 mL and reactions were conducted at room temperature of $20°C \pm 1°C$. H_2SO_4 and HNO_3 stock solutions were purchased from ACP Chemicals Inc., and HCl was purchased from EMD Millipore.

2.3 Results and Discussion

2.3.1   pH Dependence of the Reaction Behavior

The behavior and mechanism of the electrochemical reaction is determined by the electroactive S(IV) species in solution. In acidic conditions (pH < 1.85) the dominant species is H_2SO_3, which is present in solution as dissolved sulfur dioxide, $SO_{2(aq)}$. When the solution pH is maintained between 1.85 and 7.20, bisulfite ions (HSO_3^-) is dominant. In alkaline solutions, (pH > 7.20) the major active species is the sulfite ion, SO_3^{2-}. The dissociation reaction and the equilibrium constants are described below:

(1) $SO_{2(gas)} + H_2O \rightarrow H_2SO_3 \rightarrow SO_{2(aq)}$

(2) $SO_{2(aq)} + H_2O \leftrightarrow HSO_3^- + H^+$ $K = \dfrac{[H^+][HSO_3^-]}{[SO_{2(aq)}][H_2O]} = 1.4125 \times 10^{-2}$ [32-33]

(3) $HSO_3^- \leftrightarrow SO_3^{2-} + H^+$ $K = \dfrac{[H^+][SO_3^{2-}]}{[HSO_3^-]} = 6.300 \times 10^{-8}$ [32-33]
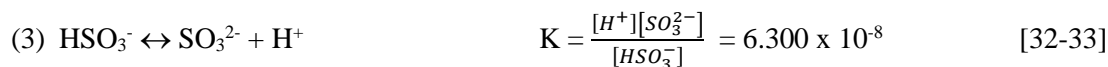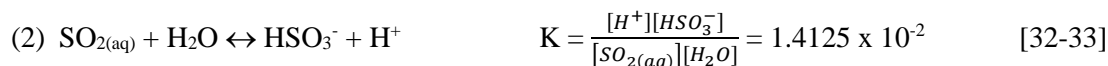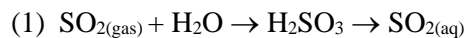
Changes in the solution pH and the active species ultimately changes the standard redox potential and rate of the observed reaction. The formation and participation of the acidic and basic surface oxides results in potential differences for the S(VI) oxidation and the oxygen evolution reaction.[34] The standard potential values for the oxidation of dissolved sulfur dioxide, bisulfite, and sulfite are given in Table 2.1. The general trend of the decrease of standard potentials with increasing pH can also be explained by relating to the Gibb's free energy.

$$\Delta G^0 = -nFE^0 \quad (1)$$

Here, n is the number of electrons involved in the charge-transfer process, and the other variables retain their usual meanings. The standard cell potential is proportional to the free energy associated with the electro-oxidation reaction and is different for each of the S(IV) compounds due to its chemical structure and properties.

In this study, the solution pH was measured to be 1.66 when 0.1 M H_2SO_4 was used as the electrolyte with 0.3 M of $NaHSO_3$. According to literature, in such an acidic solution, the dominant species of $NaHSO_3$ solution is H_2SO_3. Therefore, the electrochemical reaction process and mechanism discussed in the subsequent discussions will be likely arising from the electro-oxidation of aqueous sulfur dioxide.

Reaction		E^0 vs. SHE (V)
I	$SO_{2(aq)} + 2H_2O \leftrightarrow SO_4^{2-} + 4H^+ + 2e^-$	0.158
II	$HSO_3^- + H_2O \leftrightarrow SO_4^{2-} + 3H^+ + 2e^-$	0.105
II	$SO_3^{2-} + H_2O \leftrightarrow SO_4^{2-} + 2H^+ + 2e^-$	-0.108

Table 2.1. Electrochemical oxidation reactions of S(IV) species and their standard redox potentials.[32]

2.3.2   *Critical Surface Area Dependence of the Reaction Behavior*

The linear potential sweep curve of a GCE in the above solution (0.3 M NaHSO$_3$ + 0.1 M H$_2$SO$_4$) is shown in Figure 2.1, in which the applied scan rate is 0.5 mVs^{-1}. Under such a slow voltage scanning, the obtained result provides a useful overview on what types of reaction behaviors may be obtained under potentiostatic conditions. It is particularly effective in identifying the potential window over which nonlinear instabilities may exist. Figure 2.1(a) illustrates that onset of the oxidation occurs at approximately 0.8 V, where the current density continuously increases until a current plateau is reached (1.5 V – 1.8 V). Notably, using a GCE with a larger surface area in Figure 2.1(b), oscillations in the current density emerge at 1.2 V on the positive slope of the LSV and the oscillatory behavior extends beyond the plateau. According to literature, the occurrence of oscillations at a positive LSV branch may be connected to the presence of a hidden negative differential resistance (HN-NDR).[27,35] The smooth transition from a stable steady state to an oscillatory regime seen in the voltammetric profile indicates that it is likely a supercritical Hopf bifurcation. The decrease in the current response on the negative slope reflects a strong and rapid adsorption of SO$_4^{2-}$, which ultimately hinders the oxidation of H$_2$SO$_3$ at the occupied sites of the GCE.[23] At the applied potentials above 1.8 V, bubble formation became visible and the

oscillatory behavior observed at such conditions was likely associated with the oxidation of water (i.e., the oxygen evolution reaction). Thus, these oscillations could be induced by convection-enhanced mass transfer, rather than the NDR-type nonlinear instability.
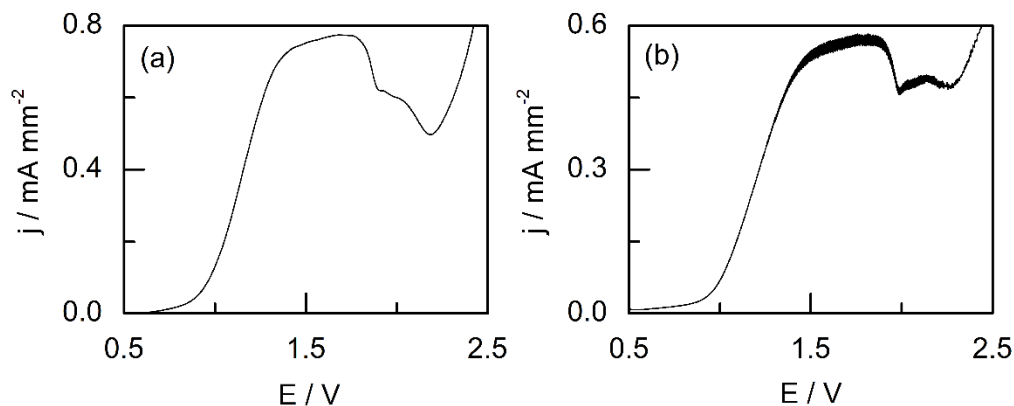
Figure 2.1. Potentiodynamic curves of 0.3 M NaHSO$_3$ in 0.1 M H$_2$SO$_4$. The scan rate was 0.5 mVs^{-1}. The surface areas of the GCE employed are (a) 0.79 mm^2 and (b) 7.07 mm^2.

LSVs in Figure 2.1 illustrates the qualitative effects of GCE surface area on the reaction behavior (i.e., stable vs. oscillatory oxidation). To further investigate such a qualitative dependence of the oxidation of H$_2$SO$_3$, potentiostatic experiments were conducted with several GCEs of different surface areas, where the applied potential of 1.5 V was selected, which was within the oscillatory domain seen in Figure 2.1(b). At a surface area size of 0.79 mm^2 (Figure 2.2(a)), the current response showed a stationary state that was observed to steadily decay over time. When the surface area was increased to 3.54 mm^2, the system exhibited an abrupt transition to an oscillatory state with small amplitudes (Figure 2.2(b)). At 7.07 mm^2, periodic oscillations emerged with large amplitudes (0.028 mA mm^{-2}), see Figure 2.2(c). More interestingly, as seen in Figure 2.2(d) and 2.2(e), the surface area size also acted as a bifurcation parameter that led to complex oscillations. A transition from simple periodic oscillations to torus oscillations was presented in Figure 2.2(d), where the surface area was slightly increased to ~ 7.85 mm^2. At 14.10 mm^2 (Figure 2(e)), the system exhibited different quasi-periodic oscillations with large amplitudes.

Considering that each active site at the GCE working electrode may be viewed as a nano-sized reactor, which are coupled through mass transportation in the solution phase as well as possible free electron migration inside the electrode, the qualitative change in the recorded reaction behavior as a result of increasing surface area (i.e., population number) resembles the dynamic quorum sensing phenomena encountered in nature.[3-10] Similar quorum behavior in chemical systems had been explored by Showalter and co-workers using chemical beads and by Kiss et. al. with coupled individual electrodes. For the system studied here, the critical population threshold is determined by the surface area size (i.e., the total number of active sites) and a minimum surface area must be exceeded for the observation of oscillatory phenomenon.

It is well-known that the surface area of a working electrode ultimately determines the size of the ohmic drop (IR). Typically, the ohmic drop increases with increasing electrode radius. While it may be true that larger electrodes provides the sufficiently large uncompensated ohmic drops necessary for the onset of electrochemical oscillations, it is solely the surface area, or the population density of the nanoreactors, that contributes to the transition to oscillatory behavior in this studied system. Time series with a 0.79 mm^2 electrode with the insertion of an external resistor to mimic the ohmic drops of a large 7.07 mm^2 electrode reveals the current response is in stable steady state and no oscillations appear. Furthermore, when IR compensation mode was applied for the time series with a 7.07 mm^2, the oscillations still appear. This shows that the emergence of oscillations during the electro-oxidation of bisulfite in acidic media occurs only when the surface area is sufficiently high.
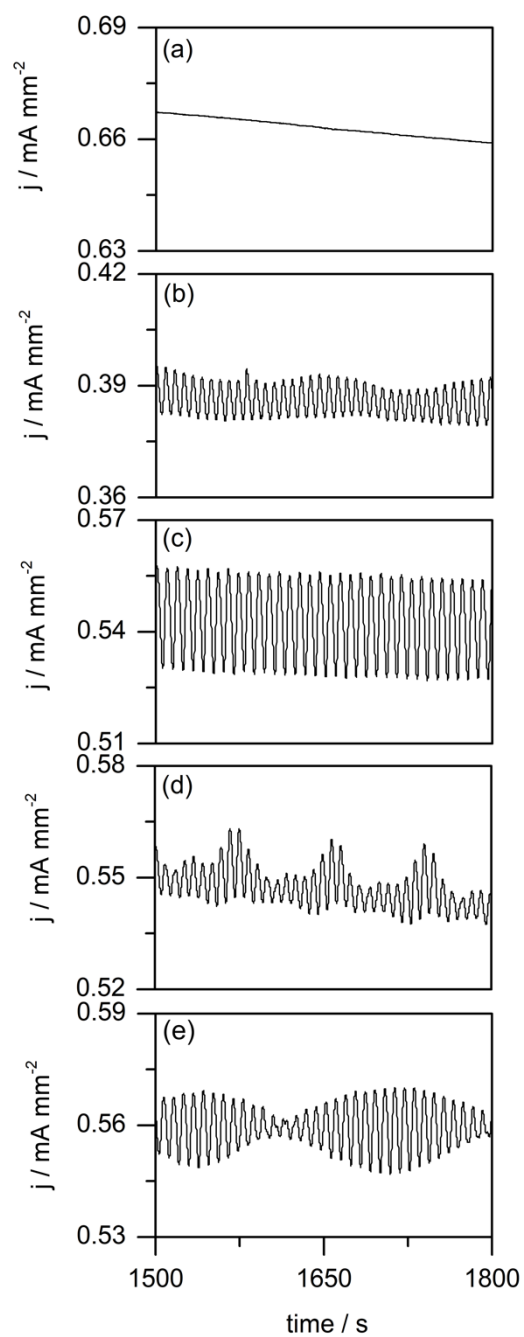
Figure 2.2. Time series under the potentiostatic control of 1.5 V with GCEs of varying surface area sizes: (a) 0.79 mm², (b) 3.54 mm², (c) 7.07 mm², (d) 7.85 mm², and (e) 14.10 mm². The solution contained 0.3 M NaHSO$_3$ and 0.1 M H$_2$SO$_4$.

2.3.3 Dependence of the Oscillatory Behavior on Reaction Conditions

At a fixed electrode surface area, effects of the applied potential on the current oscillations were examined in Figure 2.3, where the electrode surface area was 7.07 mm^2 and the solution consisted of 0.3 M NaHSO$_3$ and 0.1 M H$_2$SO$_4$. At potentials of 1.0 V or lower, no discernable oscillations could be observed (time series (d)). Dynamical instabilities emerged with periodic characteristics when the applied potential was 1.2 V (time series (c)). The frequency and the amplitude of the oscillations increased with increasing the applied potential from 1.2 to 1.6 V, as seen in time series (c) to (a). When the applied potential was further increased to 1.8 V, oscillations still existed. However, visible bubbles began to form at the working electrode.
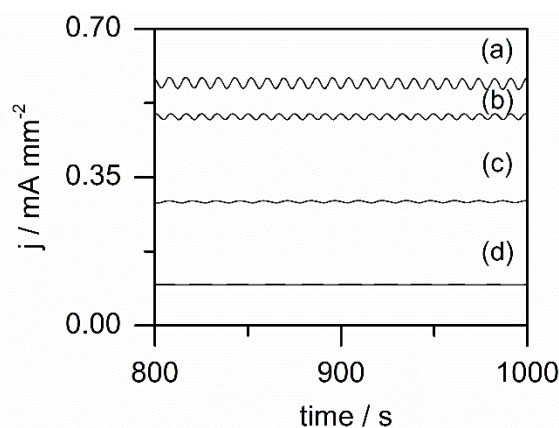
Figure 2.3. Time series under the potentiostatic control of: (a) 1.6 V, (b) 1.4 V, (c) 1.2 V, and (d) 1.0 V. The solution contained 0.3 M NaHSO$_3$ and 0.1 M H$_2$SO$_4$.

The dependence of the current oscillations on the concentration of the starting reagent NaHSO$_3$ is shown in Figure 2.4, in which the applied potential was kept constant at 1.5 V with NaHSO$_3$ concentrations ranging from 0.2 M to 0.5 M. At relatively high concentrations (0.3 M – 0.5 M), sustained oscillations with various frequencies and amplitudes were observed. Waveforms at the concentrations of 0.4 M and 0.5 M occurred with similar higher frequencies (~ 0.13 s^{-1}), as opposed to the oscillations occurring at 0.3 M with approximately 0.11 s^{-1}. However, the

40

oscillations at 0.3 M have the largest amplitude of around 0.028 mA mm^{-2}. At 0.2 M and below, the system was at a stable steady state, where no oscillations took place (Figure 2.4, time series (d)).
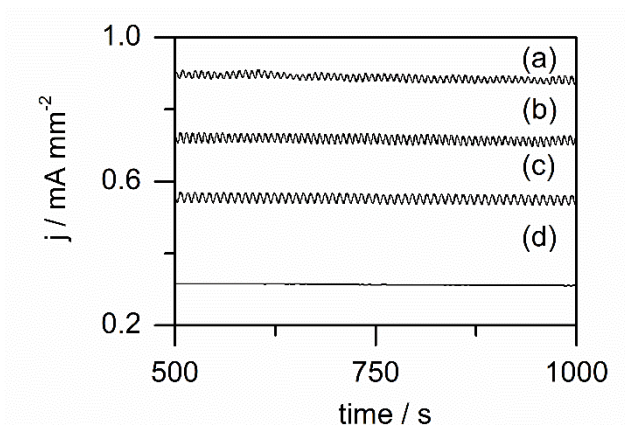
Figure 2.4. Time series under the potentiostatic control of 1.5 V with varying concentrations of NaHSO$_3$: (a) 0.5 M, (b) 0.4 M, (c) 0.3 M and (d) 0.2 M. The concentration of H$_2$SO$_4$ was 0.1 M.

In the absence of any supporting electrolyte, the electro-oxidation of HSO$_3^-$ ions were able to exhibit irregular nonlinear instabilities. The effect of the concentration of the H$_2$SO$_4$ electrolyte on the current oscillations is illustrated in Figure 2.5. Sustained periodic oscillations are observed within a small range of H$_2$SO$_4$ concentrations, between 0.05 M and 0.1 M. At 0.05 M, quasi-periodic oscillations, also known as torus oscillations emerge. As the concentration is increased to 0.1 M, large amplitude oscillations occur at high frequencies. However, when the concentration of H$_2$SO$_4$ is further increased to 0.2 M, the oscillations disappear.
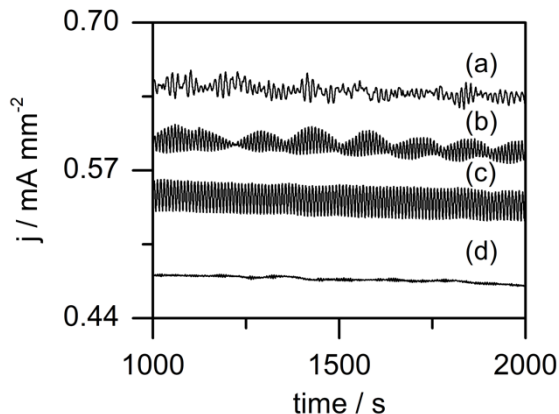
Figure 2.5. Time series under the potentiostatic control of 1.5 V with varying concentrations of H_2SO_4: (a) 0.0 M, (b) 0.05 M, (c) 0.1 M, and (d) 0.2 M. The concentration of $NaHSO_3$ was 0.3 M.

Figure 2.6 shows the effect of various types of acidic electrolytes on the reaction behaviors during the oxidation of HSO_3^-. In sulfuric acid, which is also the oxidation product, aqueous sulfur dioxide is the dominant active species and is responsible for the faraday current response. The sustained current oscillations have large and uniform amplitudes (0.015 mA mm^{-2}) and occur at a frequency of 0.11 s^{-1}. When HSO_3^- is dissolved in HCl, aperiodic oscillations emerge, see Figure 2.6(b). Within the studied potential range, chloride ions are electrochemically inactive, so $SO_{2(aq)}$ is still the major species participating in the oxidation reaction. Periodic oscillations also emerge in nitric acid, HNO_3, but the amplitudes are smaller by almost 3-fold (0.0055 mA mm^{-2}) compared to those of in H_2SO_4 solutions. Such a significant change may be partially understood based on the chemical reactions between HSO_3^- and HNO_3. It is observed during our experiment that the strong oxidant HNO_3 can chemically oxidize HSO_3^- to SO_4^{2-} upon contact. Simultaneously, HNO_3 is reduced to gaseous NO_2. The loss of some of the starting reagent prior to any electrochemical experiments may account for in Figure 2.6(c), where the average current density is lower than those measured for bisulfite in HCl and H_2SO_4.
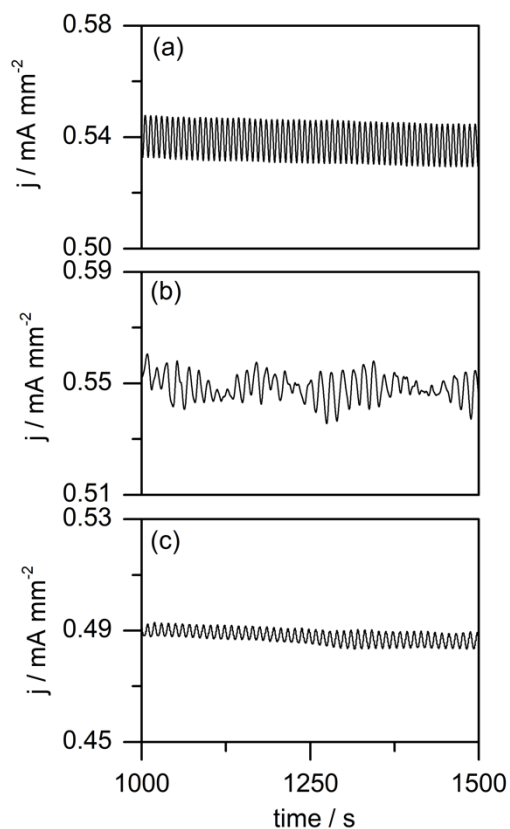
Figure 2.6. Time series under the potentiostatic control of 1.4 V with different acids as the supporting electrolyte: (a) 0.1 M H_2SO_4, (b) 0.1 M HCl, and (c) 0.1 M HNO_3. The concentration of $NaHSO_3$ was 0.3 M.

Further investigations using cyclic voltammetry (CV) reveal that when bisulfite is dissolved in equimolar HNO_3, the dominant species remains to be $SO_{2(aq)}$, as the oxidation peak overlaps the peak of a solution containing H_2SO_4, see Figure 2.7(a). In Figure 2.7(b), the oxidation peaks for $SO_{2(aq)}$ and HSO_3^- are observed at 1.58 V, and 1.45 V, respectively, see curve (ii) and (i). The above experimental potentials for the oxidation of $SO_{2(aq)}$ and HSO_3^- agree well with the trend reported in Table 2.1. The oxidation peak for the solution of 0.3 M $NaHSO_3$ in 0.1 M HNO_3 occur at 1.7 V (iii), which suggests that the oxidation process is likely a combination of $SO_{2(aq)}$ and, possibly, the dissolved NO_x and not of another S(IV) species, such as SO_3^{2-}, since the oxidation of SO_3^{2-} would have occurred at a lower anodic potential.
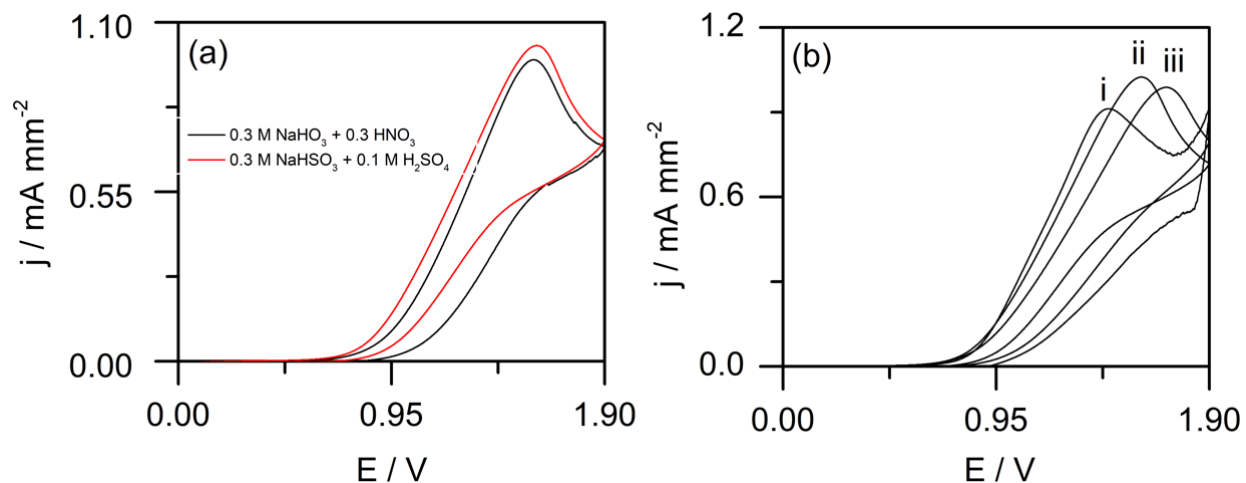
Figure 2.7. Cyclic voltammograms of (a) 0.3 M NaHSO$_3$ in 0.1 M H$_2$SO$_4$ and (b) Cyclic voltammograms of 0.3 M NaHSO$_3$ in (i) 1.0 M KCl, (ii) 0.1 M H$_2$SO$_4$, and (iii) 0.1 M HNO$_3$. The scan rate was 100 mVs^{-1}.

A further comparison of the reaction behaviors of HSO$_3^-$ in HCl electrolytes were made in Figure 2.8, which shows the current time series under the applied potentials of 1.0 – 1.6 V. At 1.0 V and below, the current is in a stable steady state as no oscillations emerges. When the applied potential increases to 1.2 V, small instabilities are observed. As the applied potential continues to increase, the amplitude of these irregular oscillations increases as well. No periodic oscillations occur within this potential window.
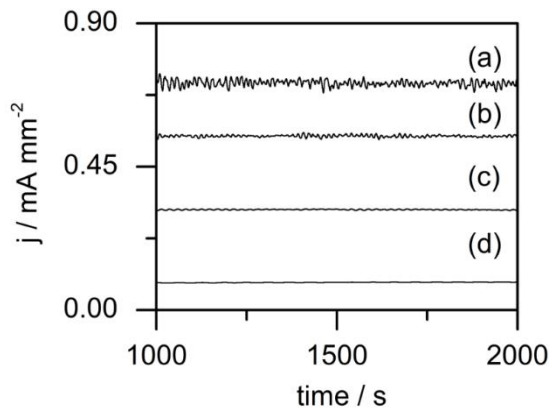
Figure 2.8. Time series under the potentiostatic control of: (a) 1.6 V, (b) 1.4 V, (c) 1.2 V, and (d) 1.0 V. The solution contained 0.3 M NaHSO$_3$ and 0.1 M HCl.

The potentiostatic time series within the same range of applied potentials in a solution containing HSO$_3^-$ and HNO$_3$ is depicted in Figure 2.9. Similarly, at low applied potentials such as 1.0 V, no dynamical instabilities occur. In contrast to the H$_2$SO$_4$ electrolytes, the oscillations are able to demonstrate higher complexity, as period-doubling phenomena are observed at 1.6 V. However, the period-2 oscillations are only transient and are viable for the first 750 seconds of the reaction time. The results obtained during the oxidation of bisulfite in H$_2$SO$_4$, HCl, and HNO$_3$ indicate that anions of the supporting acidic electrolyte also play an important role in the nonlinear reaction behaviors.
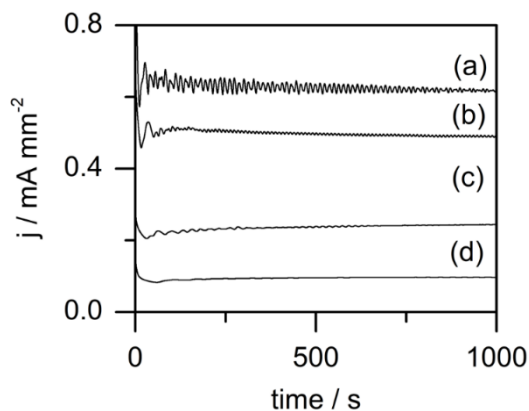
Figure 2.9. Time series under the potentiostatic control of: (a) 1.6 V, (b) 1.4 V, (c) 1.2 V, and (d) 1.0 V. The solution contained 0.3 M NaHSO$_3$ and 0.1 M HNO$_3$.

Potentiostatic experiments involving hydrodynamic effects were conducted with a glassy carbon rotating disc electrode (RDE) at various rotating speeds, as shown in Figure 2.10. A RDE provides forced convection, which increases mass transportation of the $SO_{2(aq)}$ molecules to the surface of the electrode, resulting in a higher net of the faradaic current density. At 500 rpm, 3000 rpm, and 5000 rpm, the oscillations become more complex, with substantially larger amplitudes, compared to the simple periodic oscillations observed when the electrode is stationary. Thus, the diffusion layer is not critical for the emergence of current oscillations, since the convection effectively decreases the thickness of the diffusion layer. This result is in agreeance with NDR oscillators, and also eliminate the possibility that the studied system belongs to the C-PDR oscillator.
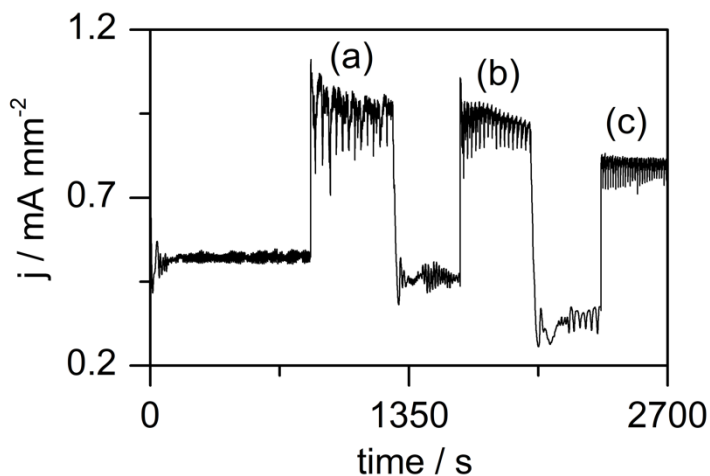
Figure 2.10. Time series under the potentiostatic control of 1.5 V using a rotating disc electrode with varying speeds: (a) 3000 rpm, (b) 5000 rpm, and (c) 500 rpm. The solution contained 0.3 M NaHSO$_3$ and 0.1 M H$_2$SO$_4$.

2.3.4 *Mechanistic Characterization*

Electrochemical impedance spectroscopy has provided an effective tool to characterize oscillations in electrochemical systems.[12,23] In this study, the impedance spectra of a GCE in the 0.3 M NaHSO$_3$ and 0.1 M H$_2$SO$_4$ solution have been measured at the applied potentials of 0.9 V,

1.0 V, 1.1 V, 1.2 V, 1.35 V and 1.4 V, which are all located on the positive branch of the LSV shown in Figure 2.1. At the potentials of 1.0 V, 1.1 V, 1.2 V, and 1.35 V, in each of the EIS spectra, two well-defined capacitive loops are present at high and intermediate frequencies, followed with an inductive loop at low frequency domains, see Figure 2.11. The presence of the first capacitance loop is associated with the charge transfer process of the oxidation of sulfur compounds and its radius decreases with the increase of the applied potential, consistent with the expectation that the rate of charge transfer is enhanced at higher potentials. The inductive loop seen at 1.0 V, 1.1 V, 1.2 V, and 1.35 V may be associated with the electrode surface relaxation of the adsorbed intermediate product species.[36-37] A dramatic change occurred in the EIS as the applied potential reached 1.4 V, where the impedance response crossed the negative impedance axis at a moderate frequency, exhibiting the feature of a hidden negative differential resistance. Note that the resistance at the intersection is around 50 Ω. The characteristics of these obtained EIS suggest that this new electrochemical oscillator likely belongs to the HN-NDR type.[23,35,38]
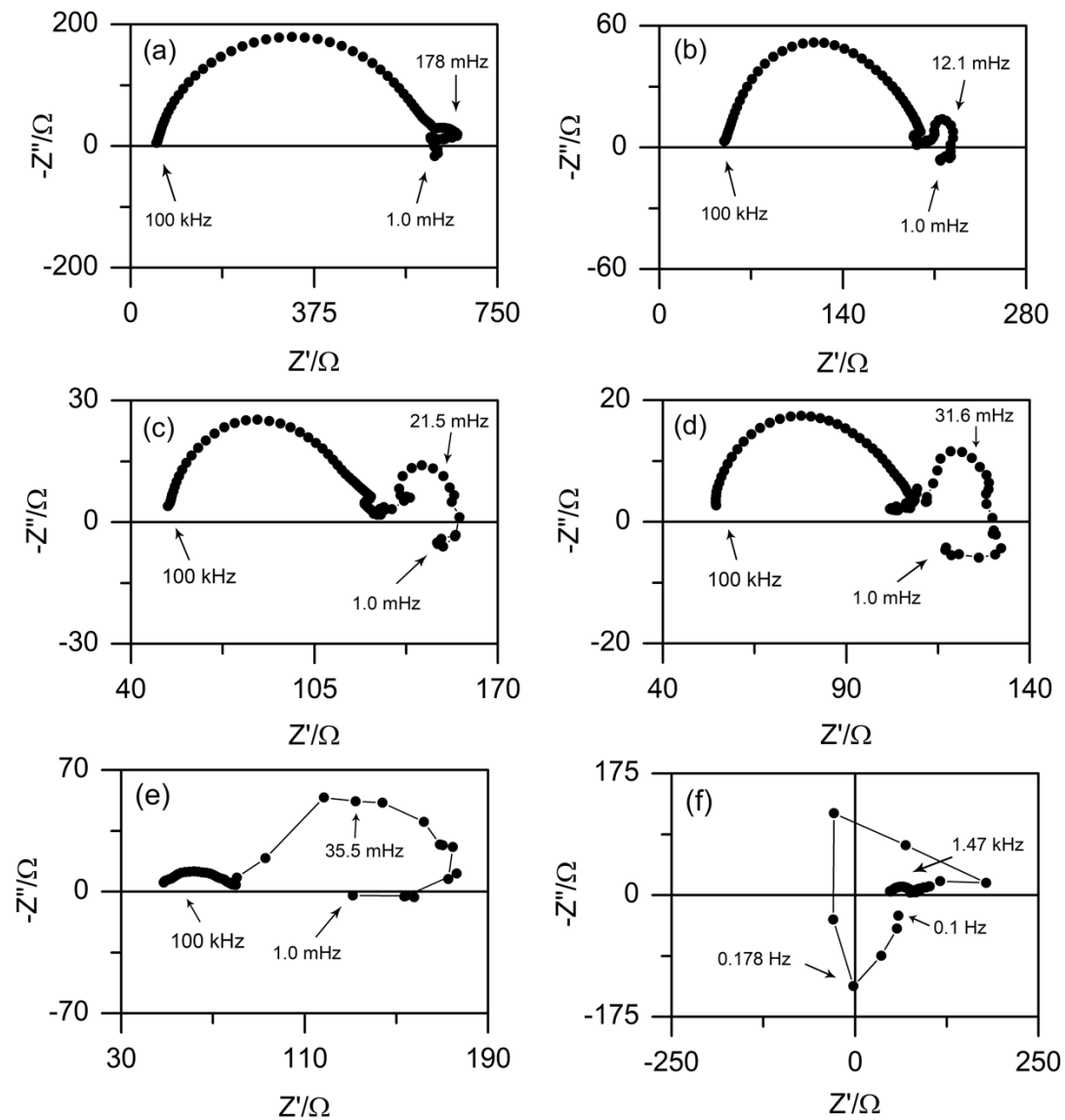
Figure 2.11. Nyquist plots during the oxidation of 0.3 NaHSO$_3$ in 0.1 H$_2$SO$_4$ at a GCE at the applied potentials of: (a) 0.90 V, (b) 1.0 V, (c) 1.1 V, (d) 1.2 V, (e) 1.35 V, and (f) 1.4 V. The frequency range was from 1.0 x 10^5 Hz to 0.001 Hz. The perturbation amplitude is 0.005 V.

To further demonstrate that the onset of electrochemical oscillations is dependent on the electrode surface area size, additional electrochemical impedance spectroscopy experiments were performed with a 0.79 mm^2 electrode at the applied potentials of 1.1 V, 1.2 V, 1.35 V, and 1.4 V, see Figure 2.12. When the potential is held at 1.1 V – 1.35 V, similar impedance spectra were produced when comparing between the two electrode surface area sizes, 7.07 mm^2 and 0.79 mm^2.

However, a noticeable difference in the impedance behavior can be discerned at 1.4 V, see Figure 2.12(d). With a smaller surface area of 0.79 mm^2, the HN-NDR characteristics, which was observed with a 7.07 mm^2 GCE, do not appear in the impedance spectrum. Instead, the Nyquist plot shows a behavior analogous to the previous applied potentials, with two-capacitance loops, and the formation of an inductive loop. The results in Figure 2.12 was found to agree with Figure 12.1(a) and Figure 12.2(a), where no dynamical instabilities such as current oscillations occur with a 0.79 mm^2 electrode.
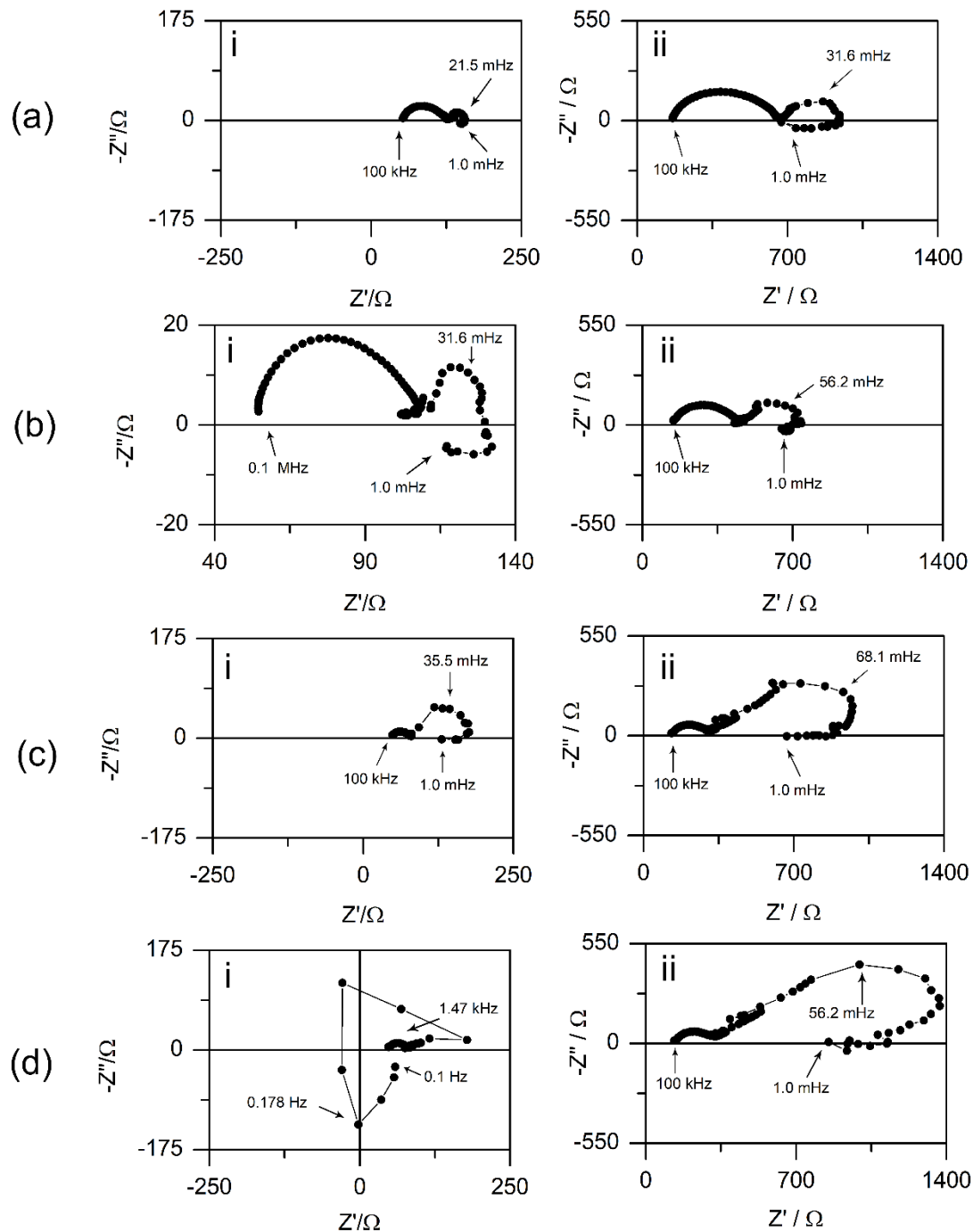
Figure 2.12. Nyquist plots during the oxidation of 0.3 M NaHSO$_3$ in 0.1 M H$_2$SO$_4$ at a GCE at the applied potentials of: (a) 1.1 V, (b) 1.2 V, (c) 1.35 V, and (d) 1.4 V. The employed GCE surface areas were: (i) 7.07 mm^2 and (ii) 0.79 mm^2. The frequency range was from 1.0 x 10^5 Hz to 0.001 Hz. The perturbation amplitude is 0.005 V.

2.3.5   Surface Characterization

The GCE was characterized by scanning electron microscopy (SEM) to gain insights into the possible surface modification accompanied with the HSO_3^- oxidation in H_2SO_4 solution. SEM images were taken of a pristine GCE and surface and after 1 hour of the oxidation of $NaHSO_3$ in H_2SO_4 at an applied potential of 1.5 V, which revealed no considerable morphological changes occurred. At a high magnification of 5000x, both images show a bare, smooth surface of the GCE, see Figure 2.13. The nanoscopic scratches observed at a 5000x magnification are caused by the polishing processes and are essentially negligible.
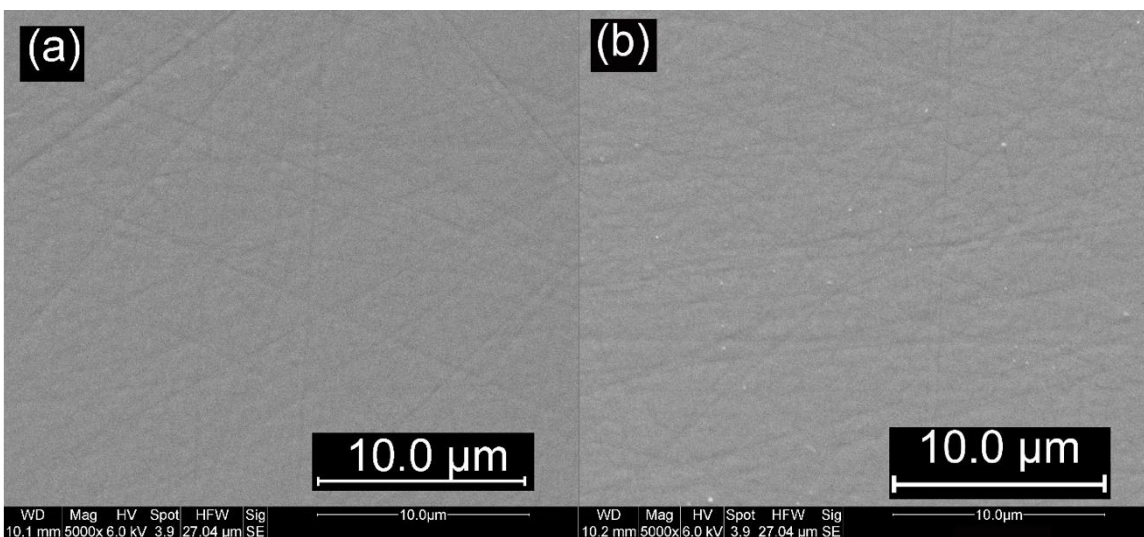
Figure 2.13. Scanning electron microscopy images of (a) a bare GCE and (b) a GCE after 1 hour of the oxidation of 0.3 M $NaHSO_3$ in 0.1 M H_2SO_4.

Energy dispersive x-ray spectroscopy (EDS) measurements were also taken of the GCE surface and is shown in Figure 2.14, which C is the major element by weight, 99.37% with trace amounts of O (0.53%). The remaining peak (F) in the spectra is not significant, as they contribute less than 0% in weight and may be from background signals picked up by the instrument.
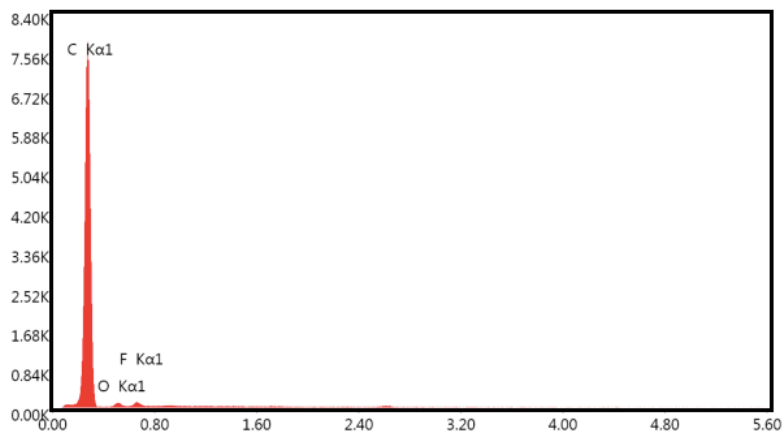
eZAF Smart Quant Results

Element	Weight %	Atomic %	Net Int.	Error %	Kratio	Z	A	F
C K	99.37	99.54	2647.87	1.87	0.9890	1.0004	0.9949	1.0000
O K	0.53	0.40	4.84	41.69	0.0010	0.9463	0.2036	1.0000
F K	0.10	0.06	1.89	74.73	0.0003	0.8756	0.3804	1.0000

Figure 2.14. EDS spectra taken at the GCE surface after 1 hour of the oxidation of 0.3 M NaHSO$_3$ in 0.1 M H$_2$SO$_4$.

2.3.6 *Potential Oscillations*

For the HN-NDR electrochemical oscillators, the system is expected to also exhibit oscillations in potential (i.e., at galvanostatic conditions). Figure 2.15 depicts a typical galvanodynamic sweep between 0 mA mm^{-2} – 0.56 mA mm^{-2} under a slow scan rate of 2.1 x 10^{-5} mA mm^{-2} s^{-1}. Small amplitude instabilities emerged around 0.26 mA mm^{-2} and gradually developed into large amplitude oscillations. As the applied current exceeded 0.51 mA mm^{-2}, the system returns to the stable steady state (past 2.0 V). This slow scan simulated galvanostatic conditions as an exploratory effort to confirm the presence of nonlinear instabilities in this system.
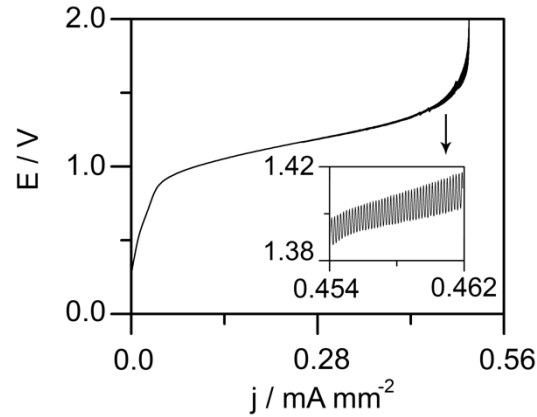
Figure 2.15. Galvanodynamic curve of 0.3 M NaHSO$_3$ in 0.1 M H$_2$SO$_4$ between 0.0 mA mm^{-2} – 0.56 mA mm^{-2}. The scan rate was 2.1 x 10^{-8} mA mm^{-2} s^{-1}.

Figure 2.16 shows the galvanostatic time series under varying applied current densities. It was found that at 0.14 mA mm^{-2}, no dynamical instabilities were observed. As the applied current increased to 0.28 mA mm^{-2}, simple oscillations with a frequency and amplitude of 3.2 mV and 0.077 s^{-1} emerges. The frequency and amplitude of the potential oscillations increased with increasing applied current densities. It is important to note that the surface area size used was 7.07 mm^2 for the current density sweep and the time series, Figure 2.15 and 2.16, respectively.
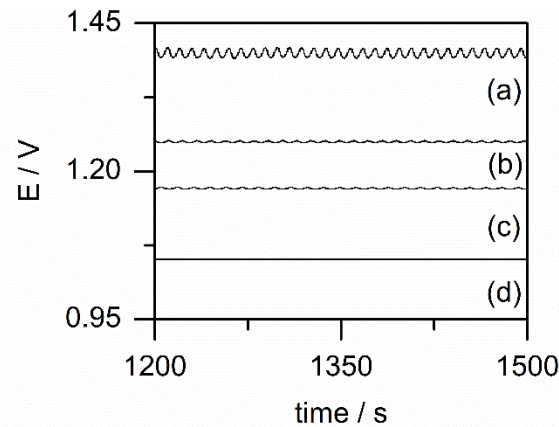
Figure 2.16. Time series under the galvanostatic control of: (a) 0.50 mA mm^{-2}, (b) 0.35 mA mm^{-2}, (c) 0.28 mA mm^{-2}, and (d) 0.14 mm^{-2}. The solution contained 0.3 M NaHSO$_3$ and 0.1 M H$_2$SO$_4$.

The population density-dependent dynamics that gave rise to global coherence in the potential was explored in Figure 2.17 at the constant current density of 0.5 mA mm^{-2}. Figure 2.17(a) presents the time series where the surface area of the working electrode was 1.57 mm^2. The potential response exhibited no dynamical instabilities. At 3.54 mm^2, the transition from a stationary state to an oscillatory state was observed. When the surface area of 7.07 mm^2 was employed in Figure 2.17(c), harmonic oscillations with large amplitudes (~ 17 mV) were obtained. At the surface area of 7.85 mm^2, a similar oscillatory pattern to that seen in Figure 2.17(c) could be seen, but with smaller amplitudes of approximately 8.0 mV (Figure 2.17(d)). A further increase of the surface area resulted in a transition from periodic oscillations to quasi-periodic torus oscillations (Figure 2.17(e)). This quorum sensing phenomenon experienced under galvanostatic conditions is comparable to what was observed earlier under potentiostatic control.
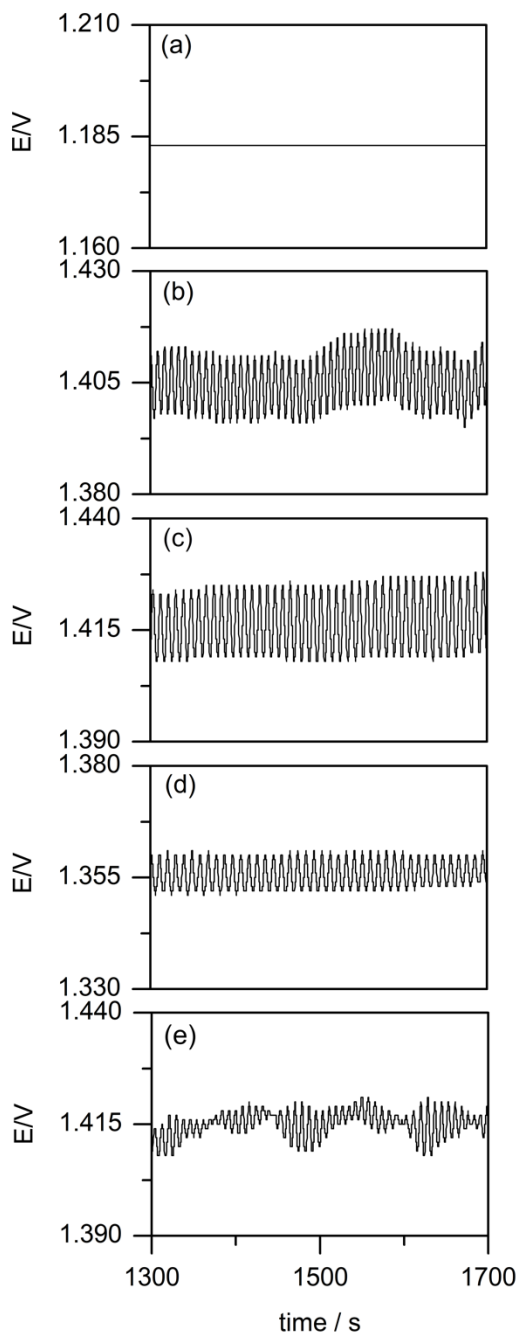
Figure 2.17. Time series under the galvanostatic control of 0.5 mA mm^{-2} with GCEs of varying surface area sizes: (a) 1.57 mm^2, (b) 3.54 mm^2, (c) 7.07 mm^2, (d) 7.85 mm^2, and (e) 14.10 mm^2. The solution contained 0.3 M NaHSO$_3$ and 0.1 M H$_2$SO$_4$.

2.3.7   Formation of Sulfur

A notable feature of this system is the accompanied formation of elemental sulfur through the reduction processes at the counter electrode (CE). Significantly, properties of the sulfur compounds products vary depending on the concentration of H_2SO_4 used. In lower concentrations, during the oxidation of $SO_{2(aq)}$ at the working electrode, yellow sulfur is formed and is evidenced with the solution turning yellow, see Figure 2.18(b). The oxidation product, SO_4^{2-}, as a cause of the solution to turn yellow can be ruled out due to the absence of color change during the oxidation of HSO_3^- in neutral media. High concentrations of H_2SO_4 produces white sulfur at the CE, as shown in Figure 2.18(a). However, the white sulfur was observed to accumulate and remain near the Pt CE for a couple hours after the reaction was completed before dissolving in the solution gradually over time. The exact form of the sulfur allotropes formed in either conditions have not been elucidated. However, according to literature, sulfur molecules typically exists as chains, rings, or both.[39] When S_n $6 < n < 12$, the configuration will likely be a ring structure in all phases.[39] S_4 and S_5 can be expected to be rings or chains, depending on the phase.[39] The ring and chain structures will vary significantly in terms of chemical and physical properties. For example, all ring structures are known to be yellow in color.[39] Therefore, in lower concentrations of H_2SO_4, the polyatom sulfur that was formed is most likely $S_6 - S_{12}$. In aqueous solutions, it is also probable that the yellow sulfur is a form of polysulfide ions of various chain lengths, since they are commonly characterized by a pale yellow color.[39] These compounds establish and participate in equilibrium where it forms complex mixtures with all members, making it difficult for separation and analysis.[39-41] However, the formation of polysulfides is less likely in this system, as the reported polysulfides are stable in alkaline or near neutral media.[40,41] For the white sulfur, as seen in higher concentrations of H_2SO_4, not many studies have been reported on sulfur with such characteristics. There is one mention, however, of a white sulfur compound, known as ω-sulfur, which is a mixture of sulfur species that are typically insoluble.[39,42]
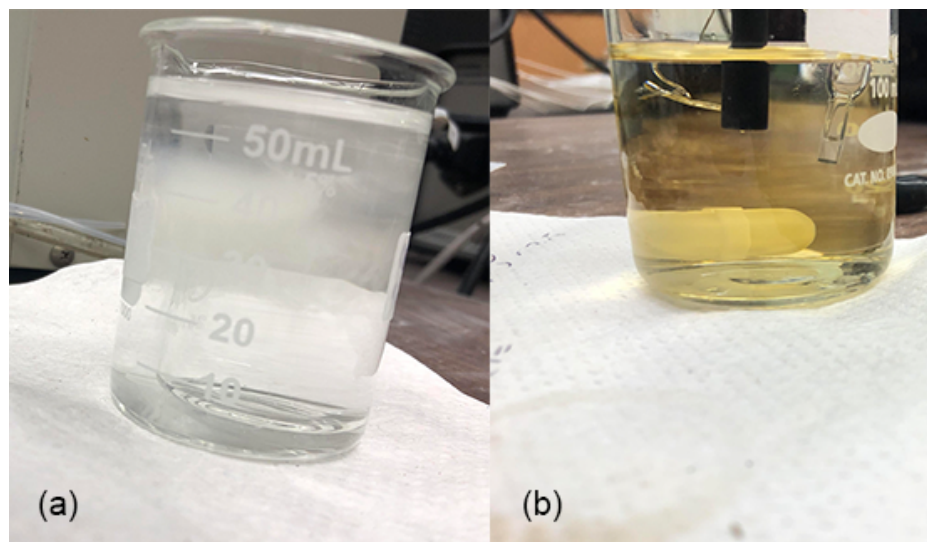
Figure 2.18. Changes to the solution after 1 hour of the oxidation reaction when it contains (a) 0.3 M NaHSO$_3$ in 0.35 M H$_2$SO$_4$ and (b) 0.3 M NaHSO$_3$ in 0.1 M H$_2$SO$_4$.

2.4 Conclusions

This study uncovers the qualitative dependence of the electro-oxidation of NaHSO$_3$ on the surface area of glassy carbon working electrode, providing a new model system for the investigation of dynamic quorum sensing phenomena. Electrochemical oxidation of HSO$_3^-$ /SO$_2$/SO$_3^{2-}$ have been widely investigated throughout the years and the general oxidation processes that lead to the formation of sulfate have been proposed to involve a two-electron transfer: HSO$_3^-$ + H$_2$O $\leftrightarrow$ 3H$^+$ + SO$_4^{2-}$ + 2e$^-$. A plot of the anodic peak current versus the square root of the scan rate showed that the R^2 was determined to be 0.97664, see Figure 2.19(a). Furthermore, a plot of the anodic peak current against the scan rate gave rise to a R^2 of 0.93219 (Figure 21.9(b)). Thus, the oxidation of bisulfite in sulfuric acid at the GCE is likely both diffusion and kinetic controlled since neither plot gave a linear proportionality. During the reaction, a number of sulfur and oxygen containing species can be formed at the interface, resulting in possible several adsorption processes at the GCE. One of the first adsorption process reported by Hunger and Lapicque involves the sulfite ion:[43] HSO$_3^-$ $\rightarrow$ SO$_3^{2-}$ $_{ads}$ + H$^+$; SO$_{2(aq)}$ $\rightarrow$ HSO$_3^-$ $_{ads}$ + H$^+$. Intermediate species such as S$_2$O$_5$

and SO_3^- are also speculated to possibly be other compounds to be adsorbed and give rise to the inductive loops observed in the impedance spectra. To account for the film capacitance (Cf) and the film resistance (Rf) arising from these soft adsorbed intermediate species layer at the GCE, an equivalent circuit of the electrode/electrolyte interface has been proposed in Figure 2.20. The circuit also consists of a solution resistance (Rs), and double layer capacitance (Cd) that is in parallel with its corresponding resistance (R_d). The overall characteristics of the simulated impedance spectrum share close similarities (two capacitance and one inductive loop) with the impedance spectrum that was obtained experimentally, confirming the importance of the adsorption of intermediate products.
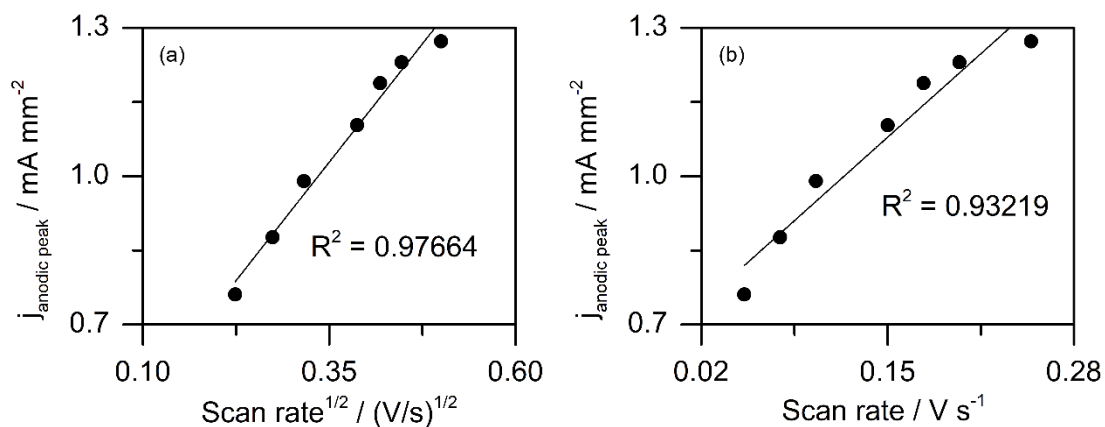
Figure 2.19. A plot showing (a) the square root of the scan rate and the anodic peak current density and (b) the scan rate and the anodic peak current density during the electro-oxidation of 0.3 M $NaHSO_3$ in 0.1 M H_2SO_4 at the GCE.

Time series obtained under constant potential or constant current conditions illustrate that the mode, frequency and amplitude of the observed oscillations are affected by various control parameters, including $NaHSO_3$ concentration and surface area of the GCE electrode. Under certain conditions, the system even showed the tendency of undergoing further bifurcations to exhibit complex oscillations. The linear potential scan and characteristics of the corresponding EIS suggest that this system belongs to the HN-NDR type oscillator. This work highlights exciting aspects of dynamic quorum sensing in a simple chemical system. It opens to further investigations to develop

a deeper understanding of the global interactions that give rise to the synchronization of oscillations and the possible implications to electrochemical detection.
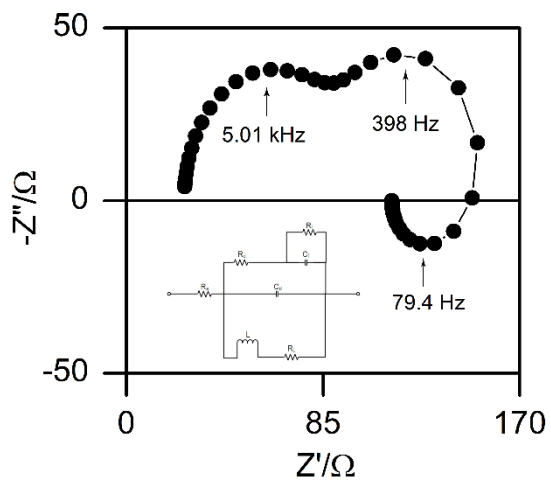
Figure 2.20. Simulated Nyquist plot based on the equivalent circuit. The frequency range was between 1.0×10^5 Hz to 0.001 Hz.

2.5 References

(1)   Corgnale, C.; Summers, W. A. Solar Hydrogen Production by the Hybrid Sulfur Process. *Int. J. Hydrogen Energy* **2011**, *36*, 11604–11619.

(2)   Allen, J. A.; Rowe, G.; Hinkley, J. T.; Donne, S. W. Electrochemical Aspects of the Hybrid Sulfur Cycle for Large Scale Hydrogen Production. *Int. J. Hydrogen Energy* **2014**, *39*, 11376–11389.

(3)   Taylor, A. F.; Tinsley, M. R.; Wang, F.; Huang, Z.; Kenneth Showalter. Dynamical Quorum Sensing and Synchronization in Large Populations of Chemical Oscillators. *Science* **2009**, *323*, 614–617.

(4)   De Monte, S.; D'Ovidio, F.; Danø, S.; P. G Sørensen. Dynamical Quorum Sensing: Population Density Encoded in Cellular Dynamics. *PNAS* **2007**, *104*, 18377–18381.

(5)   Mehta, P.; Gregor, T. Approaching the Molecular Origins of Collective Dynamics in Oscillating Cell Populations. *Curr. Opin. Genet. Dev*. **2010**, *20*, 574–580.

(6)   Danino, T.; Mondragón-Palomino, O.; Tsimring, L.; Hasty, J. A Sychronized Quorum of Genetic Clocks. *Nature* **2010**, *463*, 326–330.

(7)   Copeland, M. F.; Weibel, D. B. Bacterial Swarming: A Model System for Studying Dynamic Self-Assembly. *Soft Matter* **2009**, *5*, 1174–1187.

(8)   Cobb, S. R.; Buhl, E. H.; Halasy, K.; Paulsen, O.; Somogyi, P. Synchronization of Neuronal Activity in Hippocampus by Individual GABAergic Interneurons. *Nature* **1995**, *378*, 75–78.

(9)   Richard, P. The Rhythm of Yeast. *FEMS Microbiol. Rev*. **2003**, *27*, 547–557.

(10)   A. Goldbeter. *Biochemical Oscillations and Cellular Rhythms: The Molecular Bases of Periodic and Chaotic Behaviour*; Cambridge University Press: Cambridge, U.K., 1997.

(11)   Zaikin, A. N.; Zhabotinsky, A. M. Concentration Wave Propagation in Two-Dimensional Liquid-Phase Self-Oscillating System. *Nature* **1970**, *225*, 535–537.

(12)   Toth, R.; Taylor, A. F.; Tinsley, M. R. Collective Behavior of a Population of Chemical Coupled Oscillators. *J. Phys. Chem. B* **2006**, *110*, 10170–10176.

(13)   Hankins, M. J.; Gaspar, V.; Kiss, I. Z. Abrupt and Gradual Onset of Synchronized Oscillations Due to Dynamical Quorum Sensing in the Single-Cathode Multi-Anode Nickel Electrode. *Chaos* **2019**, *29*, 033114.

(14)   Kiss, I. Z.; Kazsu, Z.; Gáspár, V. Scaling Relationship for Oscillating Electrochemical Systems: Dependence of Phase Diagram on Electrode Size and Rotation Rate. *Phys. Chem. Chem. Phys.* **2009**, *11*, 7669–7677.

(15)   Cioffi, A. G.; Scott, M. R.; Kiss, I. Z. Electrochemical Oscillations of Nickel Electrodissolution in Epoxy-Based Microchip Flow Cell. *J. Electroanal. Chem.* **2011**, *659*, 92–100.

(16)   Wang, Y.; Hudson, J. L. Effect of Electrode Surface Area on Chaotic Attractor Dimensions. *AlChE J.* **1991**, *37*, 1833–1843.

(17)   Orlik, M. *Self-Organization in Electrochemical Systems I: General Principles of Self-Organization. Temporal Instabilities*; Springer: Berlin, 2012.

(18)   Yuan, L.; Liu, Y.; Yang, T.; Liu, H.; Gao, Q. Oscillations and Pattern Formation in Sulfur-Contained Reaction Systems. *Prog. Chem.* **2014**, *26*, 529–544.

(19)   Orbán, M.; Kurin-Csörgei, K.; Rábai, G.; Epstein, I. R. Mechanistic Studies of Oscillator Copper(II) Catalyzed Oxidation Reactions of Sulfur Compounds. *Chem. Eng. Sci.* **2000**, *55*, 267–273.

(20)   Mao, S.; Gao, Q.; Wang, H.; Zheng, J.; Epstein, I. R. Oscillations and Mechanistic Analysis of the Chlorite-Sulfide Reaction in a Continuous-Flow Stirred Tank Reactor. *J. Phys. Chem. A* **2009**, *113*, 1231–1234.

(21)   Kovács, K. M.; Rábai, G. Mechanism of the Oscillatory Decomposition of the Dithionite in a Flow Reactor. *Chem. Commun*. **2002**, *7*, 790–791.

(22)   O'Brien, J. A.; Hinkley, J. T.; Donne, S. W. Observed Electrochemical Oscillations during the Oxidation of Aqueous Sulfur Dioxide on Sulfur Modified Platinum Electrode. *Electrochim. Acta* **2011**, *56*, 4224–4230.

(23)   Bell, J. G.; Dao, M.; Wang, J. Qualitative Dependence of the Electro-Oxidation Behavior of Sulfite on Solution pH. *J. Electroanal. Chem*. **2018**, *816*, 1–6.

(24)   Bi, W.; He, Y.; Cabral, M. F.; Varela, H.; Yang, J.; Jiang, R.; Gao, Q. Oscillatory Electro-Oxidation of Thiosulfate on Gold. *Electrochim. Acta* **2014**, *133*, 308–315.

(25)   Feng, J.; Gao, Q.; Li, J.; Liu, L.; Mao, S. Current Oscillations during the Electrochemical Oxidation of Sulfide in the Presence of an External Resistor. *Sci. China Ser. B Chem.* **2008**, *51*, 333–340.

(26)   Xu, L.; Gao, Q.; Feng, J.; Wang, J. Oscillations and Period-Doubling Bifurcations in the Electrochemical Oxidation of Thiourea. *Chem. Phys. Lett*. **2004**, *397*, 265–270.

(27)   Strasser, P.; Eiswirth, M.; M. T. M. Koper. Mechanistic Classification of Electrochemical Oscillators - an Operational Experimental Strategy. *J. Electroanal. Chem.* **1999**, *478*, 50–66.

(28)   Zensen, C.; Schönleber, K.; Kemeth, F.; Krischer, K. A Capacitance Mediated Positive Differential Resistance Oscillator Model for Electrochemical Systems Involving a Surface Layer. *J. Phys. Chem. C* **2014**, *118*, 24407–24414.

(29)   Li, Z.; Cai, J.; Zhou, S. Current Oscillations in the Reduction or Oxidation of Some Anions Involving Convection Mass Transfer. *J. Electroanal. Chem*. **1997**, *436*, 195–201.

(30)   Jeffrey G. Bell, J. W. Current and Potential Oscillations during the Electro-Oxidation of Bromide Ions. *J. Electroanal. Chem*. **2015**, *754*, 133–137.

(31)   Mukouyama, Y.; Nakanishi, S.; Konishi, H.; Ikeshima, Y.; Nakato, Y. New-Type Electrochemical Oscillation Caused by Electrode-Surface Inhomogeneity and Electrical Coupling as Well as Solution Stirring through Electrochemical Gas Evolution Reaction. *J. Phys. Chem. B* **2001**, *105*, 10905–10911.

(32)   Jessica A., O.; Hinkley, J.; Donne, S.; S-E. Linquist. The Electrochemical Oxidation of Aqueous Sulfur Dioxide: A Critical Review of Work with Respect to the Hybrid Sulfur Cycle. *Electrochim. Acta* **2010**, *55*, 573–591.

(33)   Lide, D. R. *CRC Handbook of Chemistry and Physics*, 88th ed.; CRC Press/ Taylor & Francis: Boca Raton, FL., 2008.

(34)   Zelinsky, A. G.; Pirogov, B. Y. Electrochemical Oxidation of Sulfite and Sulfur Dioxide at a Renewable Graphite Electrode. *Electrochim. Acta* **2017**, *231*, 371–378.

(35)   Koper, M. T. M. Non-Linear Phenomena in Electrochemical Systems. *J. Electrochem. Soc. Faraday Trans*. **1998**, *94*, 1369–1378.

(36)   Epelboin, I.; Gabrielli, C.; Keddam, M.; H. Takenouti. A Model of the Anodic Behaviour of Iron in Sulphuric Acid Medium. *Electrochim. Acta* **1975**, *20*, 913–916.

(37)   Aoki, I. V.; Bernard, M.-C.; Cordoba de Torresi, S. I.; Deslouis, C.; de Melo, H. G.; Joiret, S.; Tribollet, B. AC-Impedance and Raman Spectroscopy Study of the Electrochemical Behaviour of Pure Aluminum in the Citric Acid Media. *Electrochim. Acta* **2001**, *46*, 1871–1878.

(38)   Krischer, K. Nonlinear Dynamics in Electrochemical Systems. *In Advances in Electrochemical Science and Engineering*; Wiley-VCH Verlag GmbH & Co. KGaA: Weinheim, Germany, 2002.

(39)   Meyer, B. Elemental Sulfur. *Chemical Reviews* **1976**, *76*, 367-388.

(40)   Giggenbach, W. F. Equilibria Involving Polysulfide Ions in Aqueous Sulfide Solutions up to 240°. *Inorganic Chemistry* **1974**, *13*, 1724-1730.

(41)   Steudel, R. Inorganic Polysulfides S_n^{2-} and Radical Anions $Sn^{\bullet-}$. *Top Curr Chem* **2003**, *231*, 127-152.

(42)   Meyer. B. Solid Allotropes of Sulfur. *Chemical Reviews* **1964**, *4*, 429-451.

(43)   Hunger, T.; Lapicque, F. Electrochemistry of the Oxidation of Sulfite and Bisulfite Ions at a Graphite Surface: An Overall Approach. *Electrochim. Acta* **1991**, *36*, 1073–1082.

CHAPTER 3 – ELECTRO-OXIDATION OF BISULFITE IN NEUTRAL MEDIA

3.1 Introduction

Studies on the electro-oxidation behavior of S(IV) species are of great importance to their

industrial applications, such as the proton exchange membrane fuel cell (PEMFC),[1–4] and the hybrid

sulfur cycle (HyS).[5–7] Over the years, investigations have found that the performance of HyS and

PEMFC are greatly affected by the aqueous S(IV) oxidation and adsorption processes.[8–11] For the

PEMFC, for example, the $SO_{2(ads)}$ poisons the cathode surface, leading to the decrease of the oxygen

reduction reaction.[1,12,13] The electro-oxidation of aqueous SO_2 and several other S(IV) species have

been pursued on a wide range of electrode substrates.[14–16] Out of the noble metals, palladium and

palladium oxide were believed to show the highest catalytic activity,[17] but this was later disproved

by Colón – Mercardo and Hobbs as Pt exhibited higher current densities at lower potentials.[18] More

recent studies demonstrated that gold had a higher performance towards the oxidation of SO_2

compared to Pd and Pt.[19,20] However, gold is generally not preferred as the electrode catalyst due

to the corrosion caused by its strong interactions with sulfur compounds.[21] Overall, the high cost

of these noble metal based electrodes has hindered the further advancements of the HyS and the

PEMFC, and the demand for cost-effective electrode materials has become increasingly important.

Carbon-based electrocatalysts such as carbide, graphite, porous catalyzed carbon, and doped

graphene has recently attracted a great deal of attention, in particular for the oxygen reduction

reactions.[22–25] In this study, the oxidation behavior of bisulfite was investigated in neutral media

using a glassy carbon electrode. Depending on the supporting electrolytes used, oscillatory

phenomena were observed here. Earlier investigations on the electrochemical oxidation of S(IV)

compounds have led to the observation of various nonlinear dynamical instabilities.[26–28] Donne and

his co-workers, for example, reported current oscillations of aqueous sulfur dioxide on modified Pt

electrodes.[27] A recent study demonstrated the qualitative pH-dependent oscillations of sulfite on a Pt electrode, in which $SO_{2(aq)}$ was the dominant electroactive species.[28]

Understanding the origins of nonlinear instabilities can provide a unique approach to the investigation of reaction kinetics and mechanisms during the oxidation of S(IV) species. Although the electrochemical oxidation of $SO_{2(aq)}$ has been extensively investigated, not many studies have been conducted towards its respective ionized counterparts, bisulfite and sulfite. To ensure bisulfite being the dominant electroactive reagent in the solution,[29] herein a neutral medium was selected in this study. Depending on the supporting electrolyte used, a slow linear potential scan (i.e., quasi-stationary voltammetric profile) revealed that the studied system might exhibit a negative differential resistance (NDR), highlighting the important changes in the migration and adsorption of intermediate products. However, despite the absence of a NDR, the system in KCl solution exhibited oscillatory phenomena under both potentiostatic and galvanostatic conditions.

3.2 Experimental Procedures

$NaHSO_3$ (a mixture of $NaHSO_3$ and $Na_2S_2O_5$) and KNO_3 were purchased from Sigma Aldrich. K_2SO_4 and KCl were obtained from Oakwood Chemicals. Solutions were prepared with double distilled water and fresh solutions were prepared for each electrochemical measurement to prevent chemical degradation over time.

All electrochemical experiments were performed with a CHI 760E electrochemical workstation (CHI Instruments) connected to cell beaker with a solution volume of 80 mL. A traditional three-electrode set up was used, in which a glassy carbon electrode (GCE) with a diameter of 3 mm (CHI Instruments) was employed as the working electrode. A saturated calomel electrode (SCE) and a platinum wire was used as the reference and the counter electrode, respectively. The distances between the electrodes were fixed for all experiments. Prior to each experiment, the GCE was polished with alumina powder with the sizes of 0.3 and 0.05 micrometer on a polishing pad. The

working electrode was thoroughly rinsed between the polishing with double distilled water, followed by sonication for approximately 5 minutes to remove any remaining particles. The electrode is finally rinsed again with double distilled water before inserting into the solution.

3.3 Results and Discussion

3.3.1 Potentiodynamic Profiles

The importance of the supporting electrolytes during the electrochemical oxidation of bisulfite is highlighted in Figure 3.1, where a typical linear sweep voltammogram (LSV) of the oxidation is presented. The used scan rate is 0.1 mVs^{-1}, which is sufficiently slow to simulate constant applied potential conditions, and therefore, is an effective way to explore the dynamical behavior in a given system. When sodium bisulfite is dissolved in KNO$_3$ (Figure 3.1(a)), or K$_2$SO$_4$ (Figure 3.1(b)), a negative differential resistance branch (NDR) developed after 1.5 V (vs. SCE), which is a noticeable contrast compared to the behavior seen in the KCl electrolyte (Figure 3.1(c)). The occurrence of a NDR is significant, as a NDR is known to be a necessary condition for the development of oscillations in electrochemical reactions.[30-33] For NDR-type electrochemical oscillators, the double-layer potential plays a crucial role in their overall dynamical behavior.[33,34] Despite the absence of a NDR branch, spontaneous oscillations emerged during the oxidation of bisulfite in KCl solutions. For all three supporting electrolytes investigated here, the onset potential of the oxidation of HSO$_3^-$ remains relatively the same, which is approximately 0.6 V. The second rapidly increasing branch, which results from the oxidation of water, began at 2.1 V for the KNO$_3$ solution, as opposed to 1.8 V for the KCl solution. It indicates that the presence of NO$_3^-$ suppressed the oxidation of water. The oxidation of water is described by the following equation, where oxygen gas is generated during the reaction.

$$2H_2O \leftrightarrow O_2 + 4H^+ + 4e^- \qquad E^0 = 1.229 \text{ V}$$
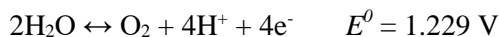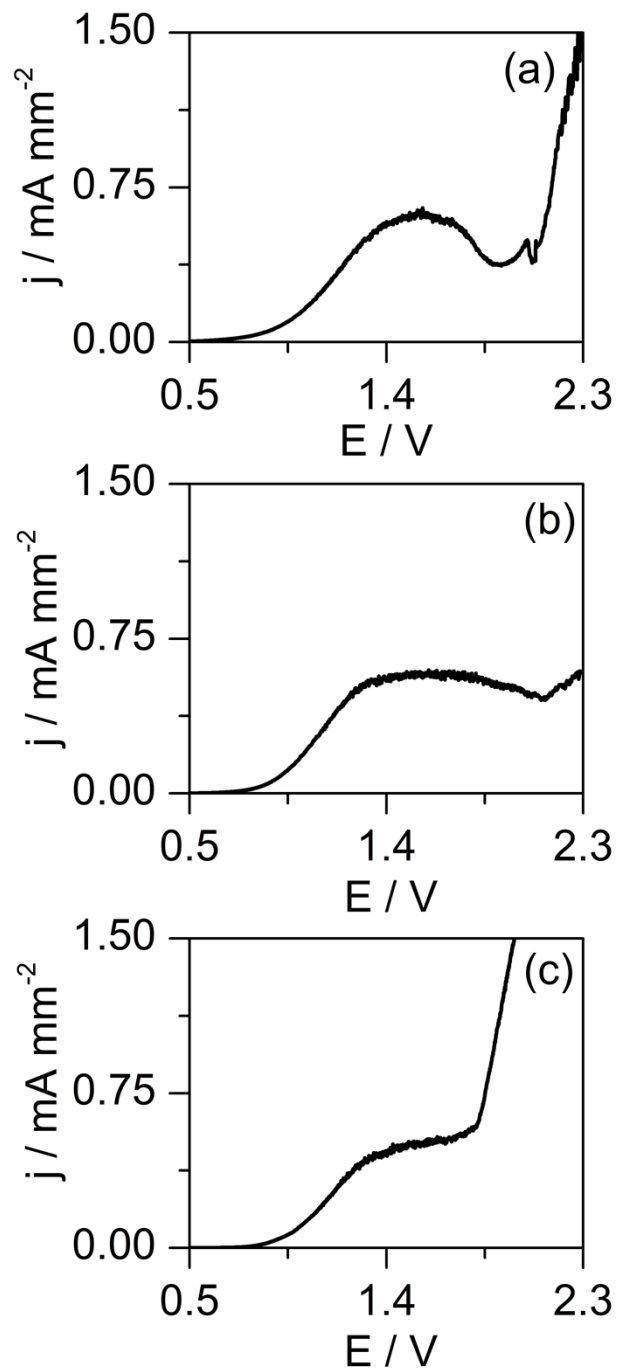
Figure 3.1. Potentiodynamic curves of 0.3 M NaHSO$_3$ in (a) 1.0 M KNO$_3$, (b) 0.35 M K$_2$SO$_4$, and (c) 1.0 M KCl. The scan rate was 0.1 mVs^{-1}.

To shed light on the origins of the observed instability in the NaHSO$_3$-KCl system, in Figure 3.2 the LSV of the oxidation of NaHSO$_3$ in a KCl solution is plotted together with the oxidation of KCl solution, suggesting that the oxidation of chloride ions begins at approximately 1.3 V (vs. SCE), before the oxidation of water occurs at approximately 1.8 V, where bubble evolution was observed at the GCE. The oxidation of Cl$^-$ ions is described by the following equation, where a two-electron transfer takes place to form chlorine.

$$2\ Cl^- \leftrightarrow Cl_2 + 2e^- \quad E^0 = 1.359\ V$$
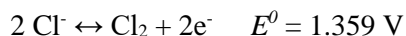
In KCl solutions, Cl$^-$ ions compete with H$_2$O molecules for the active sites at the GCE.[35] However, despite that the standard oxidation potential of water is lower than that of Cl$^-$, the oxidation of Cl$^-$ ions is the dominant process at lower anodic potentials because adsorption of Cl$^-$ ions are more favorable due to its negative charge. Oxygen evolution also occurs simultaneously, however, the reaction is almost negligible until 1.8 V, where it becomes more prevalent, evidenced by the observation of large bubbles at the GCE.

Results in Figure 3.2 also demonstrate that during the oxidation of NaHSO$_3$, the hydrodynamic transport caused by O$_2$ evolution enhances the mass transportation of Cl$^-$ and HSO$_3^-$ ions, which is indicated by the sharp response in the current density when the bubble formation occurs. Moreover, instabilities observed within the potential window between 1.3 V and 1.8 V might be affected by both the oxidation of HSO$_3^-$ and Cl$^-$ ions. In other words, it is most likely that the competition between the oxidation of HSO$_3^-$ and the oxidation of Cl$^-$ gives rise to the observed dynamical instabilities within the mentioned potential region. However, at potentials above 1.8 V, the instabilities are caused by H$_2$O oxidation that forms oxygen gas. According to literature, the convection mass transportation induced by the OER can cause the emergence of electrochemical oscillations.[36] Under these conditions, hydrodynamic convection generated by oxygen gas resulted in irregularity in the oscillations. However, it is also important to consider the oxidation of the GCE

at such high anodic potentials, resulting in the formation of carbon oxides, which may contribute to the hydrodynamic convection processes.
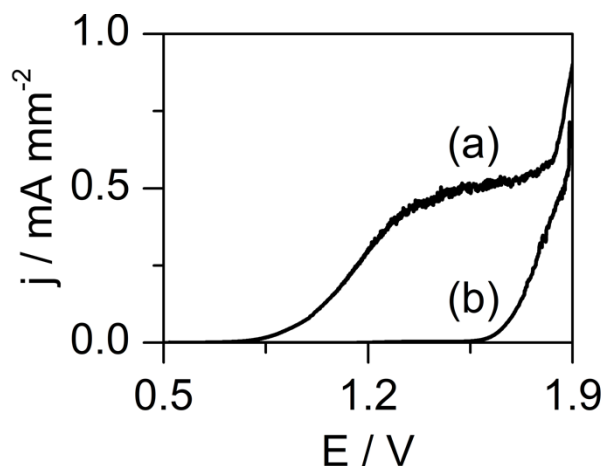
Figure 3.2. Potentiodynamic curves of (a) 0.3 M $NaHSO_3$ in 1.0 M KCl and (b) 1.0 M KCl at the GCE. The scan rate was 0.1 mVs^{-1}.

Figure 3.3 presents the slow potential sweeps in the supporting electrolytes of KCl, KNO_3 and K_2SO_4 in the absence of the electroactive species, $NaHSO_3$. The results show that a significant anodic current density can only be observed at around 1.5 V for the KNO_3 and K_2SO_4 solutions, which represents the oxidation of H_2O molecules, evidenced with rigorous bubble evolution at the GCE. However, a well-defined oxidation peak can be observed at 1.3 V in the KCl solution, suggesting the oxidation of Cl$^-$ ions, and the second positive branch indicates the H_2O oxidation. Thus, this strengthens the idea of the involvement of Cl$^-$ ions in the emergence of dynamical instabilities observed in this system. To further confirm that the oxidation of Cl$^-$ ions, the LSVs of solutions containing 0.5 M and 1.0 M KCl were plotted and is presented in Figure 3.4. Here, we see well-developed anodic peak which was observed to decrease with decreasing concentrations of KCl. However, it is important to note that the peak current density of 1.0 M KCl, is estimated to be around 200 times smaller than the peak current density for oxidation of $NaHSO_3$ in 1.0 M KCl, suggesting that the overall contributions of Cl$^-$ oxidation is minimal.

70
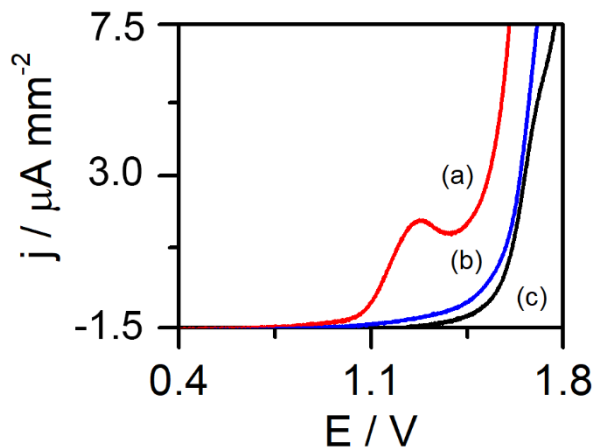
Figure 3.3. Potentiodynamic curves of (a) 1.0 M KCl, (b) 0.35 M K$_2$SO$_4$, and (c) 1.0 M KNO$_3$ at the GCE. The scan rate was 1 mVs^{-1}.
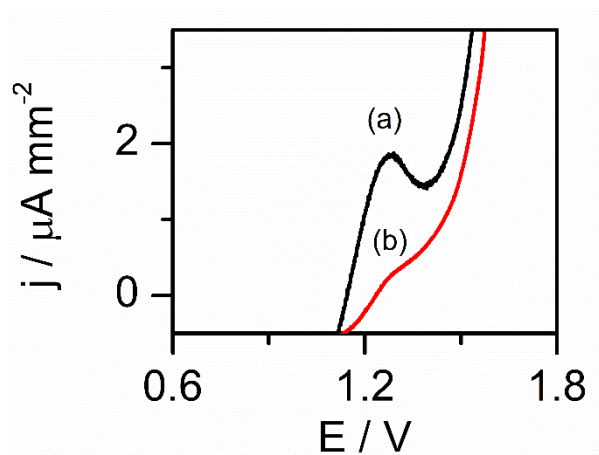
Figure 3.4. Potentiodynamic curves of (a) 1.0 M KCl and (b) 0.5 M KCl at the GCE. The scan rate was 1 mVs^{-1}.

The influence of the supporting electrolyte concentration on the electro-oxidation behavior was investigated in Figure 3.5. Notice that regardless of the amount of KCl present in solution, current oscillations occur during the oxidation process, which shows that the supporting electrolyte has no bearing on the capability of the system to oscillate. The oxidation of HSO$_3^-$ in the absence of an electrolyte gives rise to a polarization curve with a characteristic negative branch that is not observed in 1.0 M KCl electrolytes. When KCl is introduced to the system, the absence of the NDR

71

branch can be explained by the chlorine and oxygen evolution. In fact, with increasing KCl concentrations, the onset potential shift for the second rapidly increasing branch, which is presumably associated with H_2O oxidation can be observed in Figure 3.5(a) and (b), where the onset potential is clearly lower for higher concentrations of KCl compared to Figure 3.5(c), in the absence of KCl. The results suggest that in larger concentrations of KCl, there are more Cl^- ions as well as HSO_3^- ions being replenished at the GCE via hydrodynamic transport, resulting in higher current density responses at lower anodic potentials.
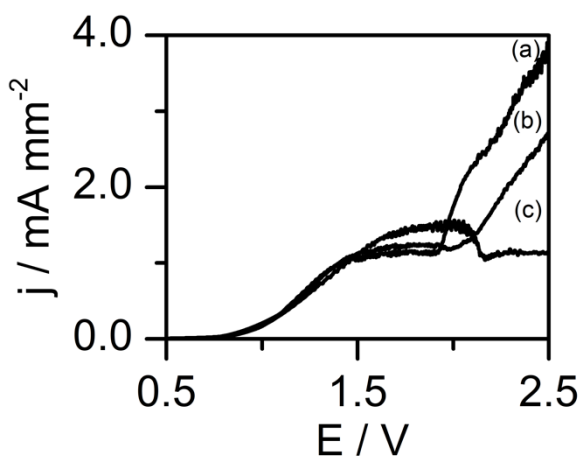
Figure 3.5. Potentiodynamic curves of 0.5 M NaHSO$_3$ in varying KCl concentrations: (a) 1.0 M, (b) 0.5 M, and (c) 0.0 M. The scan rate was 1 mVs^{-1}.

To investigate the effects of the HSO_3^- concentration on the electro-oxidation behavior, slow potential scans were conducted with varying concentrations between 0.1 and 0.8 M in 1.0 M KCl solution. Figure 3.6 shows that the current response is proportional to the initial concentrations of the HSO_3^- electroactive species. A potential shift towards higher anodic potentials was observed for the electro-oxidation of water as the HSO_3^- concentration was increased. For example, at 0.1 M HSO_3^- the OER occurs at 1.80 V, Figure 3.6(d). An increase of HSO_3^- concentration to 0.3 M results an onset potential increase of 0.03 V. When the concentration of HSO_3^- is held at 0.5 M, and 0.8 M, the oxidation potential of H_2O takes place at 1.92 V, and 1.98 V, respectively. Such a change

may be related to the variation of H_2O surface concentration, since at higher HSO_3^- concentrations more H^+ ions are dissociated in the solution, which consequently suppresses the amount of H_2O available for the oxygen evolution reaction. Another interesting change in the LSV is that at high HSO_3^- concentrations, a negative branch emerged. This is significant in terms of the emergence of nonlinear instability in an electrochemical system.
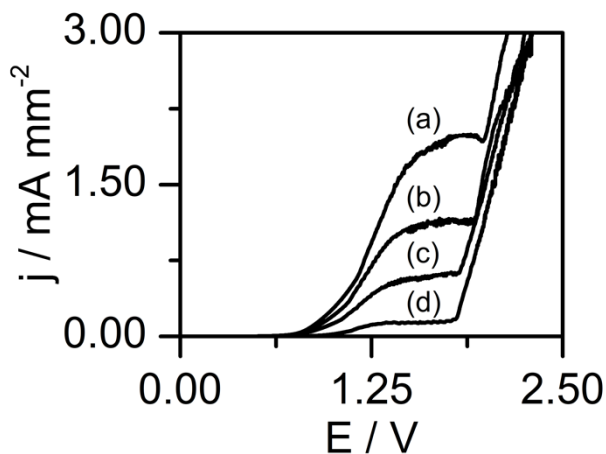
Figure 3.6. Potentiodynamic curve of varying $NaHSO_3$ concentrations: (a) 0.8 M, (b) 0.5 M, (c) 0.3 M, and (d) 0.1 M. The concentration of KCl was 1.0 M. The scan rate was 1 mVs^{-1}.

3.3.2   Effect of Reaction Parameters on the Oscillatory Dynamics

Potentiostatic experiments at various applied potentials are shown in Figure 3.7, where the current density response is in a steady stable state when the applied potential is 0.90 V or below. Small amplitude instabilities gradually emerge when the potential is 1.1 V. As the applied potential increases to 1.3 V, the oscillatory pattern began as sub-harmonic oscillations. At 1.5 V, oscillations with uniform amplitude and frequency (0.047 s^{-1}) appear and continue until the applied potential of 1.8 V is reached, where the oscillations lose regularity over time as small bubbles start to form at the working electrode (O_2 evolution).

Figure 3.7. Time series under the potentiostatic control of: (a) 0.90 V, (b) 1.1 V, (c) 1.3 V, (d) 1.5 V, and (e) 1.8 V. The solution contained 0.3 M NaHSO₃ and 1.0 M KCl.

The influence of the concentration of HSO_3^- on the current oscillations are shown in Figure 3.8, which presents a set of current time series under a constant applied potential of 1.4 V with HSO_3^- concentrations ranging from 0.02 M – 0.3 M. When the concentration of HSO_3^- is held at 0.02 M, the current density is in a stable stationary state. At 0.1 M, small amplitude oscillations were observed (time series b). The amplitude and frequency of the oscillations increases when the concentration was further increased to 0.3 M.
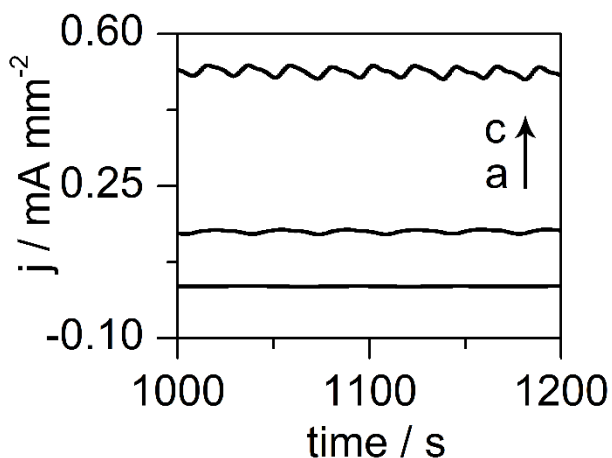
Figure 3.8. Time series under the potentiostatic control of 1.4 V with varying concentrations of NaHSO₃: (a) 0.02 M, 0.1 M, and (c) 0.3 M. The concentration of KCl was 1.0 M.

Figure 3.9 shows the effect of the KCl concentration on the oscillatory dynamics. In a solution containing just NaHSO$_3$, the system was able to exhibit small amplitude instabilities with no coherence in terms of the oscillatory pattern. In the presence of 0.5 M KCl, sustained relaxation oscillations abruptly emerged with an amplitude and frequency of 0.043 mA mm^{-2}, and 0.0563 s^{-1}, respectively. However, when the concentration of KCl was increased to 1.0 M, the frequency and the amplitude of the oscillations decreased (0.0267 mA mm^{-2} and 0.05 s^{-1}, respectively). Additionally, the oscillations become more complex as an additional shoulder peak is observed in Figure 3.9(c). The average current density decreases as the KCl concentration is increased. Such a trend is consistent with what was observed in Figure 3.5, although a different concentration of NaHSO$_3$ was used.
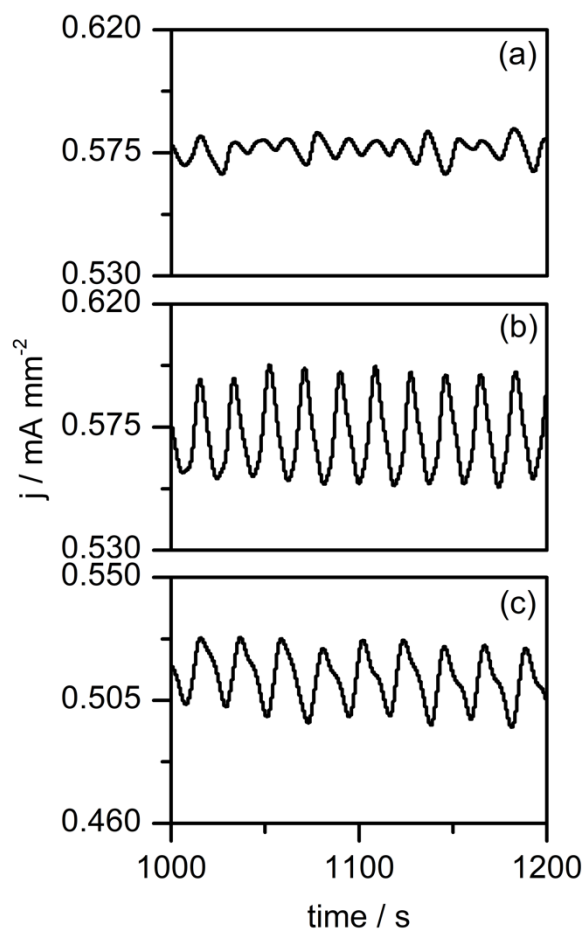
Figure 3.9. Time series under the potentiostatic control of 1.4 V with varying concentrations of KCl: (a) 0.0 M, (b) 0.5 M, and (c) 1.0 M. The concentration of NaHSO$_3$ was 0.3 M.

To extend the previous investigation on the dependence of the anions present in the electrolyte solution, potentiostatic experiments were conducted in KNO$_3$ and K$_2$SO$_4$ with applied potentials that exhibited instabilities during the potential sweep, see Figure 3.1. When bisulfite is dissolved in KNO$_3$ and K$_2$SO$_4$, aperiodic oscillations occur, but in KCl, regular oscillations emerge, Figure 3.10.
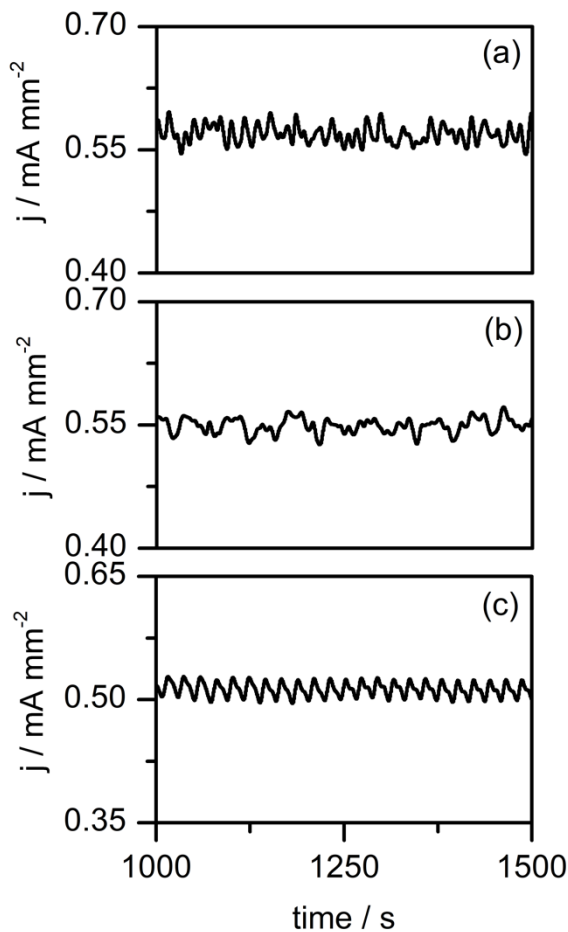
Figure 3.10. Time series under the potentiostatic control of 1.4 V with different supporting electrolytes: (a) 1.0 M KNO$_3$, (b) 0.35 M K$_2$SO$_4$, and (c) 1.0 M KCl. The concentration of NaHSO$_3$ was 0.3 M.

Figure 3.11 shows the typical oscillatory current density response under potentiostatic control of 0.9 V to 1.5 V during the electro-oxidation of HSO$_3^-$ in KNO$_3$. At low anodic potentials such as 0.9 V and below, the system remains in the stable steady state. Dynamical instabilities arise when the applied potential is held at or exceeds 1.1 V, in which its amplitude increases with increasing applied potential. However, aperiodic oscillations occur throughout the studied range of applied potentials.
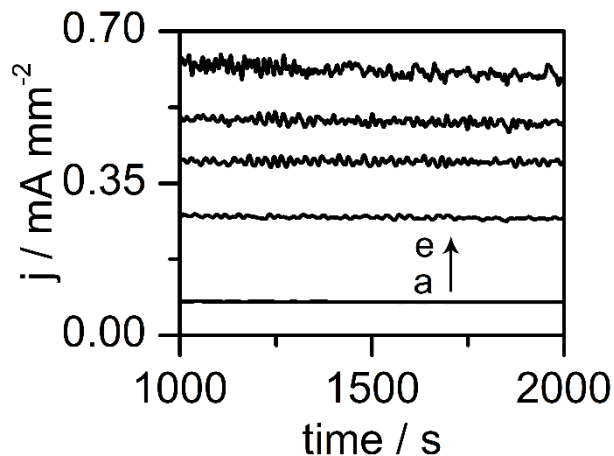
Figure 3.11. Time series under the potentiostatic control of: (a) 0.90 V, (b) 1.1 V, (c) 1.2 V, (d) 1.3 V, and (e) 1.5 V. The solution contained 0.3 M NaHSO$_3$ and 0.1 M KNO$_3$.

Figure 3.12 presents potentiostatic results for solutions containing HSO$_3^-$ and K$_2$SO$_4$, where no periodic or sustained oscillations occurred throughout the applied potentials of 0.9 V to 1.5 V. This is similar to the NaHSO$_3$-KNO$_3$ system. Results in Figure 3.12, along with the results from Figures 3.10-3.11 suggest that the Cl$^-$ ion plays a certain role in the oscillatory oxidation mechanism of HSO$_3^-$.
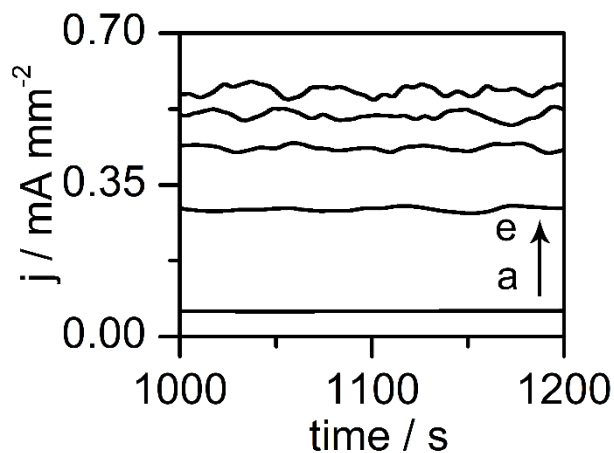
Figure 3.12. Time series under the potentiostatic control of: (a) 0.90 V, (b) 1.1 V, (c) 1.2 V, (d) 1.3 V, and (e) 1.5 V. The solution contained 0.3 M NaHSO$_3$ and 0.35 M K$_2$SO$_4$.
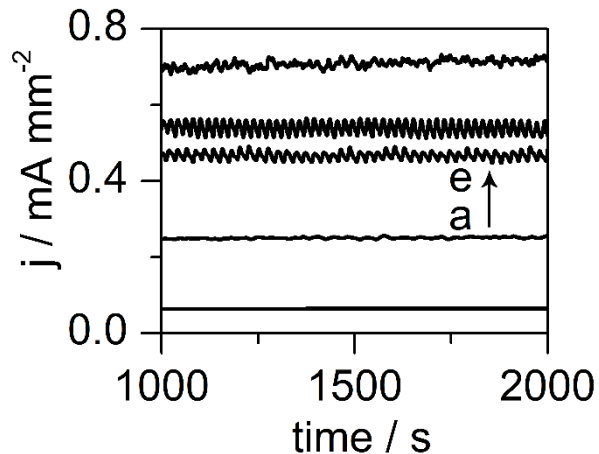
Figure 3.13 shows the current oscillations when a glassy carbon rotating disc electrode was employed with different rotating speeds, such as 500 rpm, 1000 rpm, 2000 rpm, and 3000 rpm. The RDE mimics the solution-stirring effect, which increases the mass transportation of HSO_3^- to the electrode surface. The HSO_3^- ions are then consumed via the electro-oxidation reaction. Even at large convection forces, which effectively destroys the diffusion layer, current oscillations persist, and also exhibit higher complexities and amplitudes. This result indicates that the diffusion layer is not an essential variable, which is typically true for C-PDR oscillators.[37]
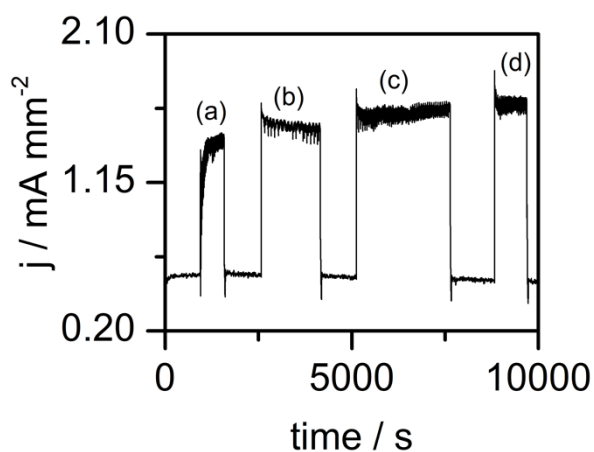
Figure 3.13. Time series under the potentiostatic control of 1.4 V using a rotating disc electrode with varying speeds: (a) 500 rpm, (b) 1000 rpm, (c) 2000 rpm, and (d) 3000 rpm. The solution contained 0.3 M $NaHSO_3$ and 0.5 M KCl.

Potenstiostatic experiments with a constant rotating speed at varying applied potentials was performed in Figure 3.14, where complex mixed mode oscillations (MMO) were observed.
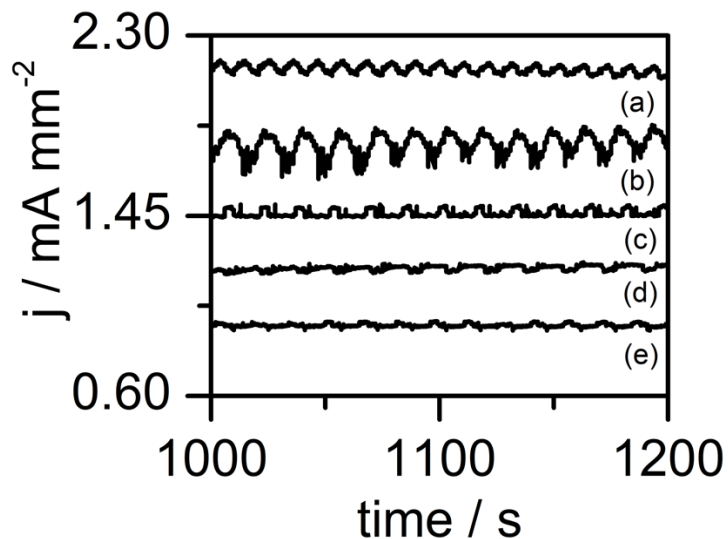
Figure 3.14. Time series under potentiostatic control of: (a) 1.6 V, (b) 1.5 V, (c) 1.4 V, (d) 1.3 V, and 1.2 V. The speed of the rotating disk electrode was 500 rpm. The solution contained 0.3 M NaHSO$_3$ and 0.5 M KCl.

The dynamic oscillatory phenomenon described above occurs in the absence of an external resistor. As mentioned earlier, for NDR oscillators, typically the presence of a sufficiently large ohmic drop is a requirement to destabilize the system. The insertion of an external resistor in series with the working electrode allows one to invoke the role of the ohmic drop in the feedback mechanism. The effect of the magnitude of the serial resistance on the dynamical behavior is summarized in Figure 3.15. The applied potential is calculated by $E = U + IR$, where U is the electrode surface potential, and IR is the potential drop caused by the serial ohmic presence (including the solution resistance). In the absence of an external resistor, large amplitude oscillations emerge, Figure 3.15(a). In this case, the only major contributing factor is the solution resistance, which was measured to be approximately 20 Ω. With the first insertion of a relatively small resistor of 100 Ω, the oscillation amplitudes decreased from 0.0428 mA mm^{-2} to 0.0289 mA mm^{-2}. The amplitude continues to decrease with increasing serial resistor size, until it becomes eventually damped when a 2200 Ω resistor was inserted, see Figure 3.15(e). This result is one of

the features belonging to the C-PDR oscillator.[37] However, this is not in agreeance with the RDE experiments shown in Figure 3.13 and 3.14. To gain a better understanding of the oscillatory mechanism, EIS investigations were performed, which will further be discussed in a subsequent section.
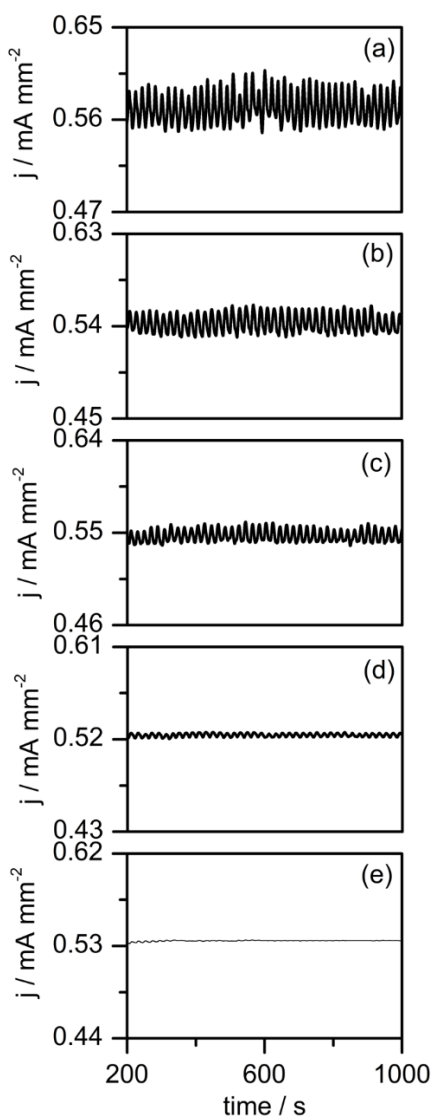
Figure 3.15. Time series under potentiostatic control with varying external resistors: (a) 100 Ω at 1.78 V, (b) 222 Ω at 2.24 V, (c) 1175 Ω at 5.86 V, and (d) 2200 Ω at 9.76 V. The estimated U is 1.4 V. The solution contained 0.3 M NaHSO$_3$ and 0.5 M KCl.

3.3.3 Potential Oscillations

Figure 3.16 depicts a typical galvanodynamic sweep between 0 mA mm^{-2} – 0.70 mA mm^{-2} under a slow scan rate of 2.1 x 10^{-5} mA mm^{-2} s^{-1}. The potential oscillatory responses can be seen when the applied current density ranged from ~ 0.33 mA mm^{-2} to 0.64 mA mm^{-2}. It takes place on the positive slope of the slow current density sweep. As the applied current density exceeds 0.64 mA mm^{-2}, the system returns to small amplitude instabilities accompanied with bubble evolution at the GCE.
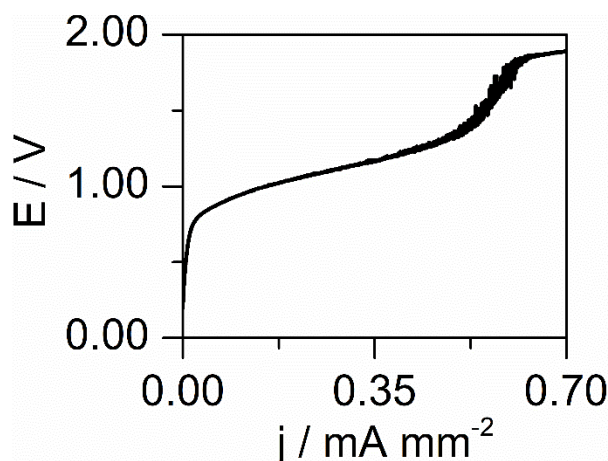
Figure 3.16. Galvanodynamic curve of 0.3 M NaHSO$_3$ in 1.0 M KCl between 0.0 mA mm^{-2} – 0.70 mA mm^{-2}. The scan rate was 2.1 x 10^{-5} mA mm^{-2} s^{-1}.

Time series at galvanostatic conditions were investigated in Figure 3.17, where at 0.13 mA mm^{-2} no dynamical instabilities were observed. As the applied current density increases to 0.35 mA mm^{-2}, relaxation oscillations with a frequency and amplitude of 23 mV and 0.03 s^{-1} suddenly emerges. The frequency and amplitude of the potential oscillations continues to increase with increasing applied current densities as seen in Figure 3.17, time series (c) and (d).
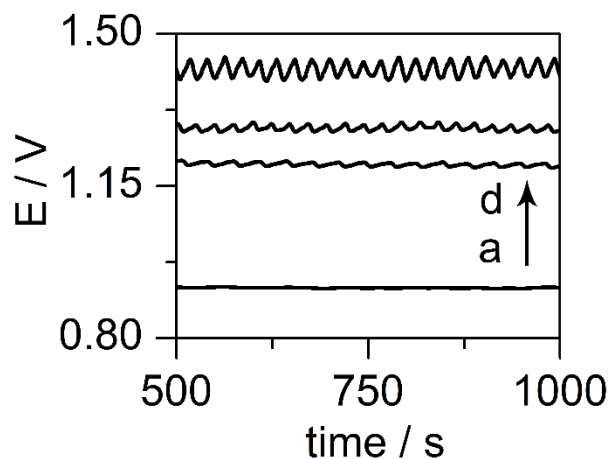
Figure 3.17. Time series under the galvanostatic control of: (a) 0.13 mA mm^{-2}, (b) 0.35 mA mm^{-2}, (c) 0.45 mA mm^{-2}, and (d) 0.50 mm^{-2}. The solution contained 0.3 M NaHSO$_3$ and 1.0 M KCl.

3.3.4   Dynamic Quorum Sensing

The dependence of the reaction behavior on the surface area size of the GCE is highlighted in Figure 3.18, where a transition from a steady state to an oscillatory behavior occurs only when the critical surface area has exceeded. Similar to the emergence of coherence observed during the electro-oxidation of SO$_{2(aq)}$, the dynamic quorum sensing phenomenon was also detected in this system. With a GCE that has surface areas less than approximately 0.0393 mm^2, the total number of oscillators, or active areas, is too low for the coupling interactions to induce collective oscillations. Thus, the system remains in a stable steady state, see Figure 3.18(a). At a surface area size of 0.0785 mm^2, the abrupt appearance of current oscillations occurs, which most likely suggests that the critical surface area is between 0.0393 mm^2 and 0.0785 mm^2, which is smaller than the one observed with the electro-oxidation of SO$_{2(aq)}$. Beyond the critical threshold, various exotic nonlinear reaction behaviors were detected. The surface area size also acts as a bifurcation parameter, leading to the formation of different oscillation modes, for example, period-2 oscillations, as seen in Figure 3.18(c) and (d) when the surface area is 0.393 mm^2 and 0.785 mm^2, respectively. With increasing GCE surface area, the oscillatory pattern changes, as period-1

oscillations were observed at 7.07 mm^2. However, the oscillations begin to lose its amplitude and frequencies when the surface area is further increased, see Figure 3.18(f) and Figure 3.18(g).
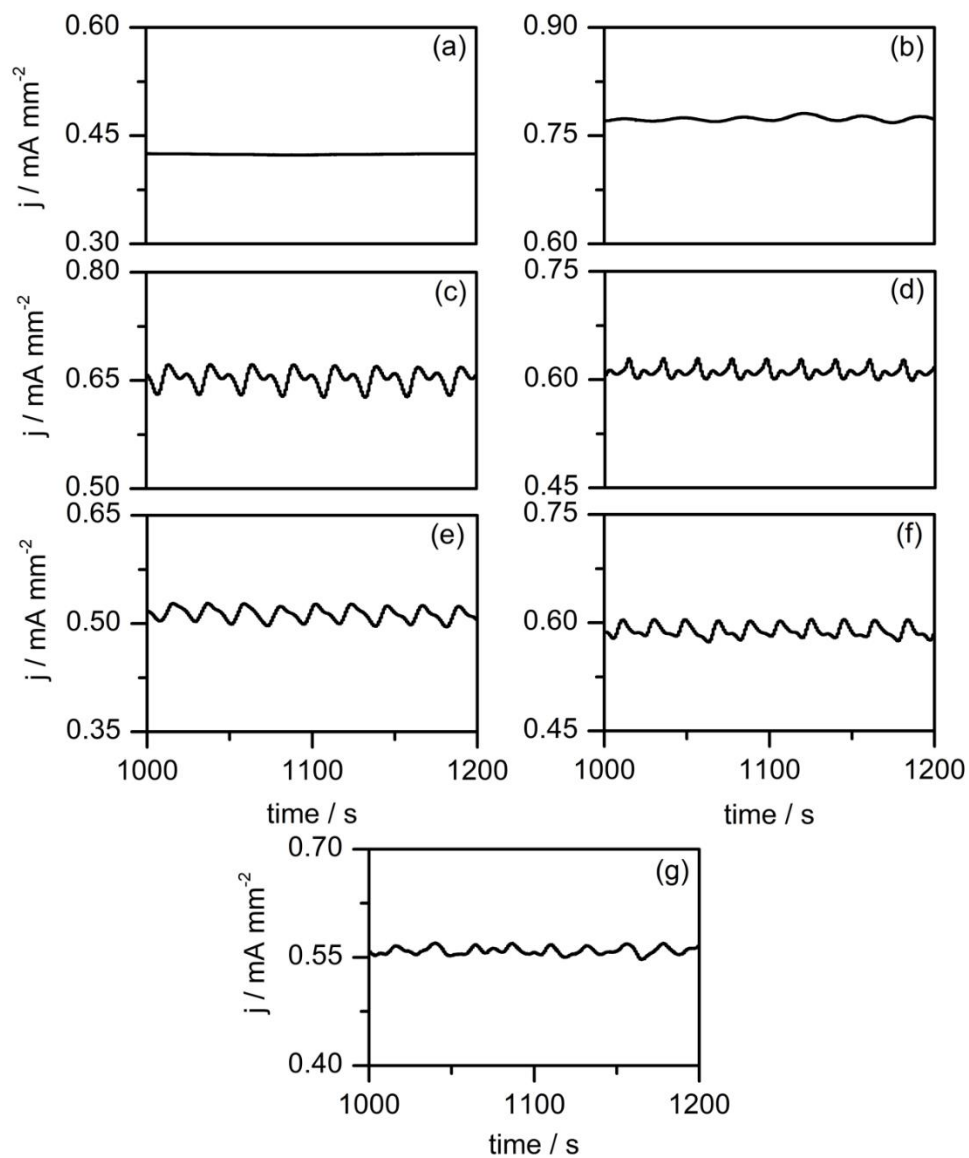
Figure 3.18. Time series under the potentiostatic control of 1.4 V with GCEs of varying surface area sizes: (a) 0.0393 mm^2, (b) 0.0785 mm^2, (c) 0.393 mm^2, (d) 0.785 mm^2, (e) 7.07 mm^2, (f) 7.85 mm^2, and (g) 14.14 mm^2. The solution contained 0.3 M NaHSO$_3$ and 1.0 M KCl.

3.3.5   Mechanistic Characterization

To examine the possible presence of NDR or hidden-NDR in the NaHSO$_3$-KCl system, electrochemical impedance spectroscopy (EIS) experiments were conducted and shown in Figure 3.19. Notably, EIS has frequently been employed to classify the electrochemical oscillator in question.[34,38] Figure 3.19 shows the Nyquist plot obtained at applied potentials prior to the instability region shown in the LSV since EIS data can only be obtained when the system is at a stable steady state. When the potential is held at 0.90 V and 1.2 V, a high-frequency (HF) capacitance loop is observed in the complex impedance spectra, correlating to the charging of the electric double layer. The capacitance loop at moderate frequencies (MF) suggests the diffusion through a porous current-limiting film layer at the surface of the GCE. The inductive loop at low frequency regimes is exhibited at 1.2 V and 1.3 V. At the potentials studied here, none of the electrochemical oscillator categories fit. Thus, the dynamical instabilities observed in this study is likely not of nonlinear nature, but simply arises from convection mass transportation caused by the oxygen bubble formation. To confirm that the characteristics seen in the above impedance spectra is not exclusive to just 0.3 M NaHSO$_3$, another set of EIS experiments were performed in solutions containing 0.5 M NaHSO$_3$, seen in Figure 3.20. The formation of the inductive loop with increasing applied potentials was observed, similar to the results in Figure 3.19.
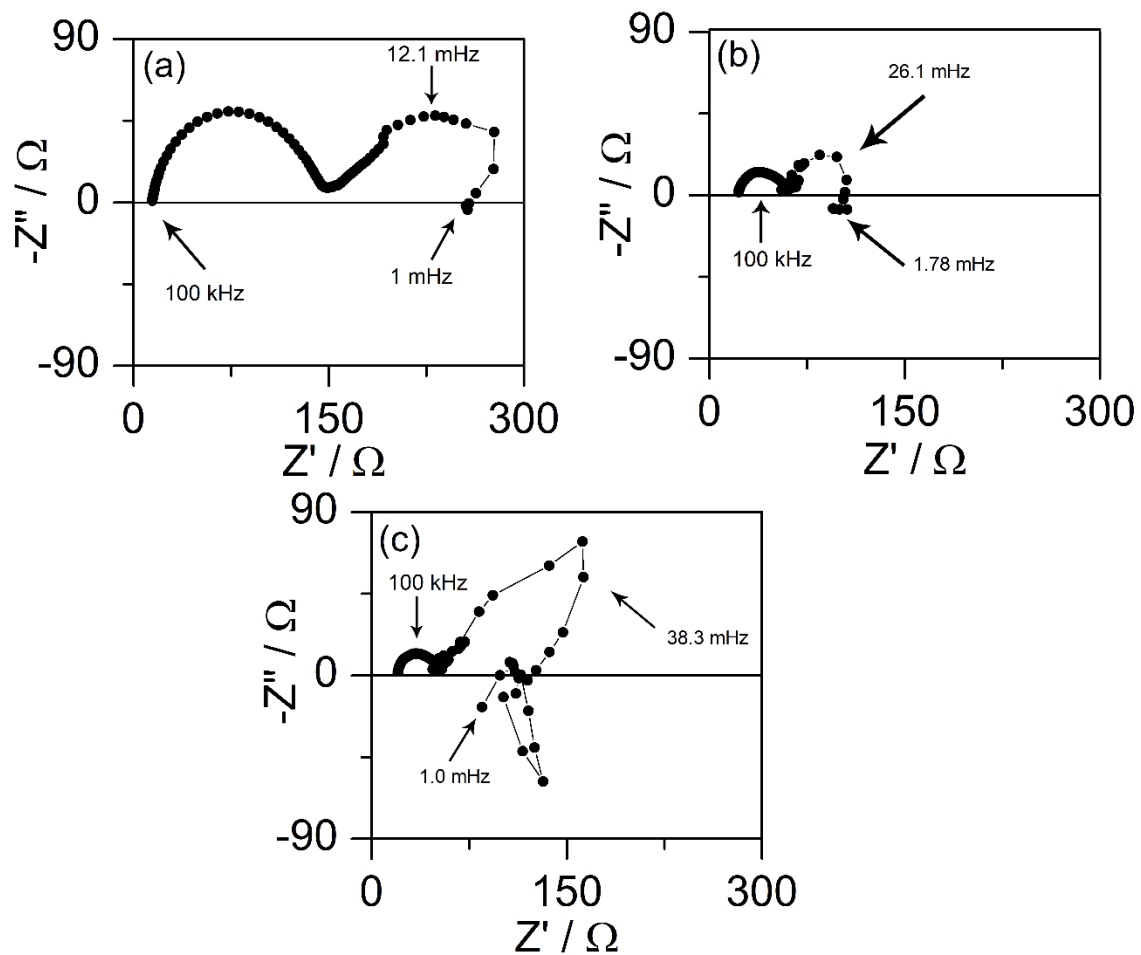
Figure 3.19. Nyquist plots during the oxidation of 0.3 NaHSO$_3$ in 1.0 M KCl at a GCE at the applied potentials of: (a) 0.90 V, (b) 1.2 V, and (c) 1.3 V. The frequency range was from 1.0 x 10^5 Hz to 0.001 Hz. The perturbation amplitude is 0.005 V.
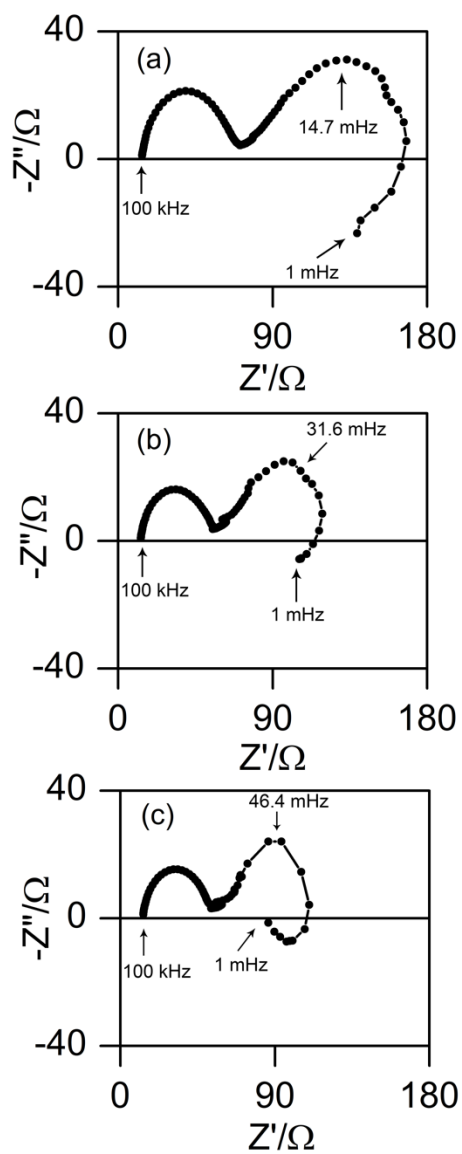
Figure 3.20. Nyquist plots during the oxidation of 0.5 NaHSO$_3$ in 1.0 M KCl at a GCE at the applied potentials of: (a) 1.0 V, (b) 1.05 V, and (c) 1.13 V. The frequency range was from 1.0 x 10^5 Hz to 0.001 Hz. The perturbation amplitude is 0.005 V.

3.3.6 Surface Characterization

The GCE surface was characterized using SEM and EDS measurements to improve the understanding of the reaction mechanism during the electro-oxidation of HSO_3^- in KCl. After one hour of the reaction (time series at 1.5 V), a SEM image at a 40x magnification reveals small amounts of deposition on the outer sides of the electrode, see Figure 3.21(b). The deposition has the resemblance of feathers or dendrites, Figure 3.21(c).
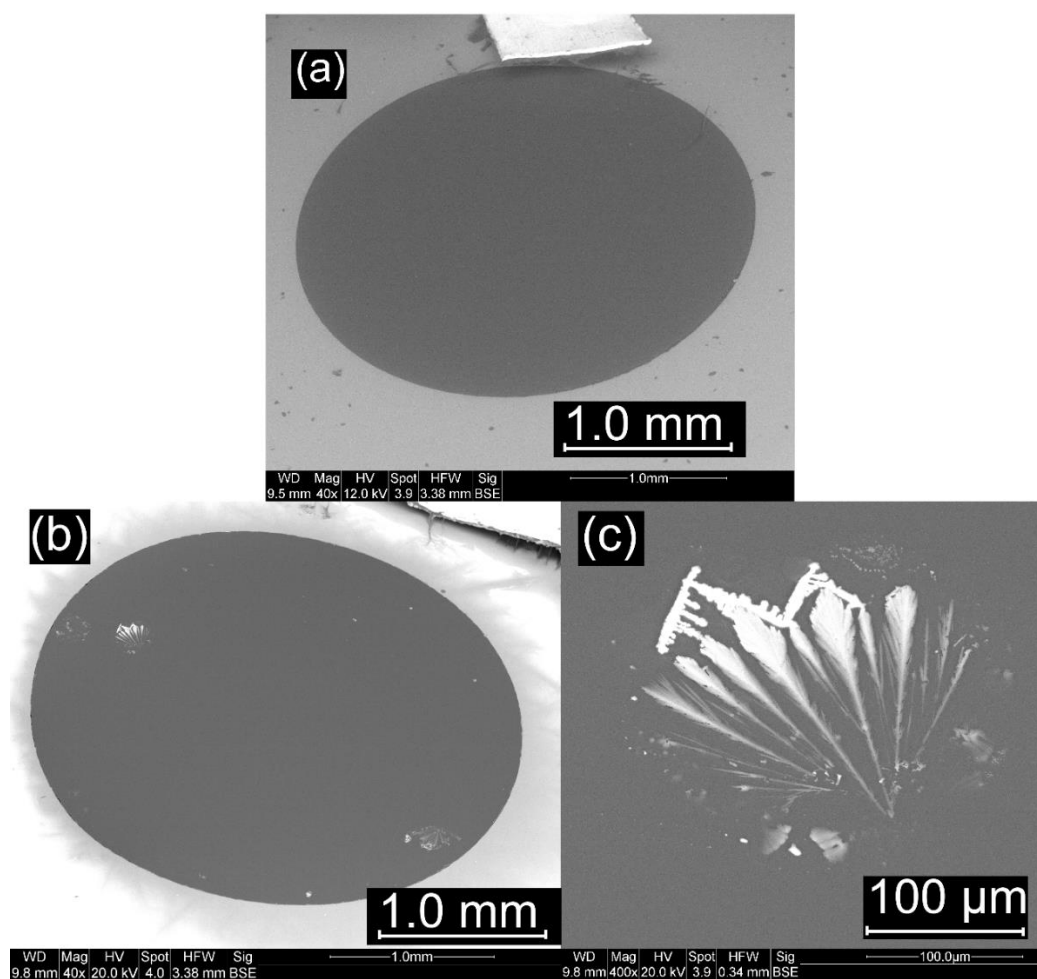
Figure 3.21. Scanning electron microscopy images of (a) a pristine GCE surface, (b) a GCE surface after 1 hour of the oxidation of 0.3 M NaHSO$_3$ in 1.0 M KCl at 40x magnification and (c) 400x magnification.

EDS measurements taken of the deposited surface of the GCE revealed that the major elemental compositions are O and K, 47.34% and 23.15% by weight, respectively, see Figure 3.22. S occurs at 13.38%, followed by Na with 10.36%, and C with 5.29%. There were trace amounts of Cl, with 0.58%. This likely suggests that the electrode surface does not undergo major changes throughout the oxidation of bisulfite. The detected elements of the deposit observed in the SEM image is likely residue from the solution (containing $NaHSO_3$ and KCl).
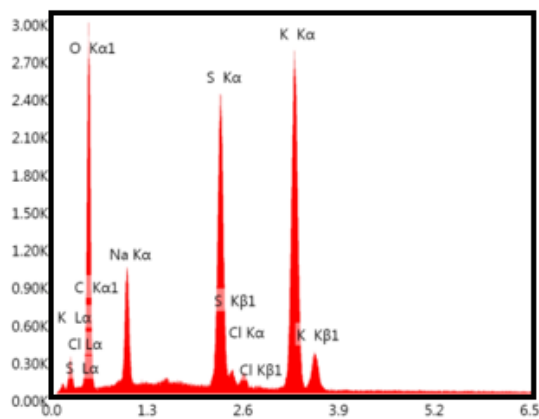
eZAF Smart Quant Results

Element	Weight %	Atomic %	Net Int.	Error %	Kratio	Z	A	F
C K	5.29	9.03	53.64	13.51	0.0113	1.1036	0.1932	1.0000
O K	47.34	60.73	1103.68	9.74	0.0936	1.0575	0.1871	1.0000
NaK	10.36	9.25	463.49	8.75	0.0344	0.9618	0.3448	1.0014
S K	13.28	8.50	1453.22	2.77	0.1134	0.9438	0.8933	1.0126
ClK	0.58	0.33	53.02	15.51	0.0045	0.8980	0.8476	1.0199
K K	23.15	12.15	1883.74	2.37	0.1940	0.8939	0.9337	1.0043

Figure 3.22. EDS spectra of the deposited species on the GCE surface after 1 hour of the oxidation of $NaHSO_3$ in KCl.

3.3.7   Electrochemical Oxidation of HSO₃⁻ on Gold

A brief investigation was done on the electro-oxidation of HSO_3^- on polycrystalline Au electrodes to study the effect of the catalyst material. Figure 3.23 shows the typical j-E dependence curve when Au is employed as the working electrode. Here, the upper potential was limited to 1.0 V to avoid irreversible damage to the electrode due to corrosion processes. It is known that sulfur containing compounds can form strong interactions with Au, leading to corrosion/dissolution of the electrode surface. One of the examples reported in literature is the oxidation of hydroxymethanesulfinate (HMS) on polycrystalline Au.[39] Oscillations spontaneously emerge on the positive branch between the potential range of 0.5 V to 1.0 V without the insertion of an external ohmic resistor, while the onset potential of the HSO_3^- oxidation occurs at approximately 0.2 V.
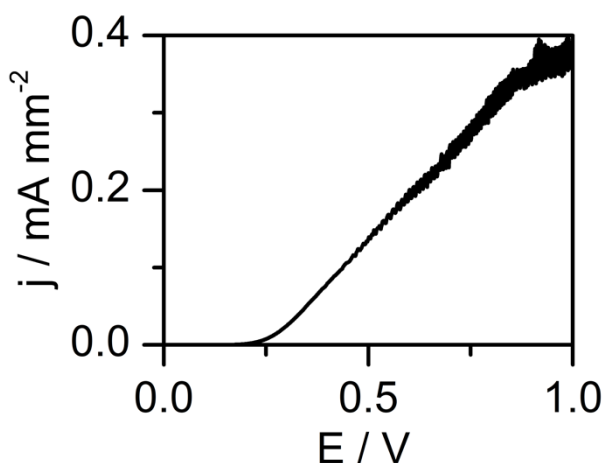
Figure 3.23. Potentiodynamic sweep of 0.2 M NaHSO₃ in 0.05 M K₂SO₄. The scan rate was 1 mVs⁻¹.

Time series under potential-controlled conditions between 0.8 V – 1.0 V are shown in Figure 3.24. At 0.8 V, transient oscillations occur for a brief 400 seconds and disappear, Figure 3.24(a). When the applied potential is held at 0.9 V, period-2 oscillations with a frequency of 0.09 s⁻¹ are observed. As the applied potential is further increased to 1.0 V, the oscillations become quasi-periodic (i.e., in the form of torus oscillations). However, through a short period of experiments,

the Au electrode was corroded and contained obvious signs of pitting that could be seen by the naked eye. Thus, the oscillations in this system was most likely involving the Au corrosion, and not simply from the oxidation of HSO_3^-. To confirm this, EIS experiments were performed to study the Au dissolution during the electro-oxidation of HSO_3^-. Figure 3.25 shows the impedance spectrum at 0.8 V, where two capacitance loops and one inductive loop is observed. Similar EIS results were reported for various types of metal dissolution processes.[40,41]
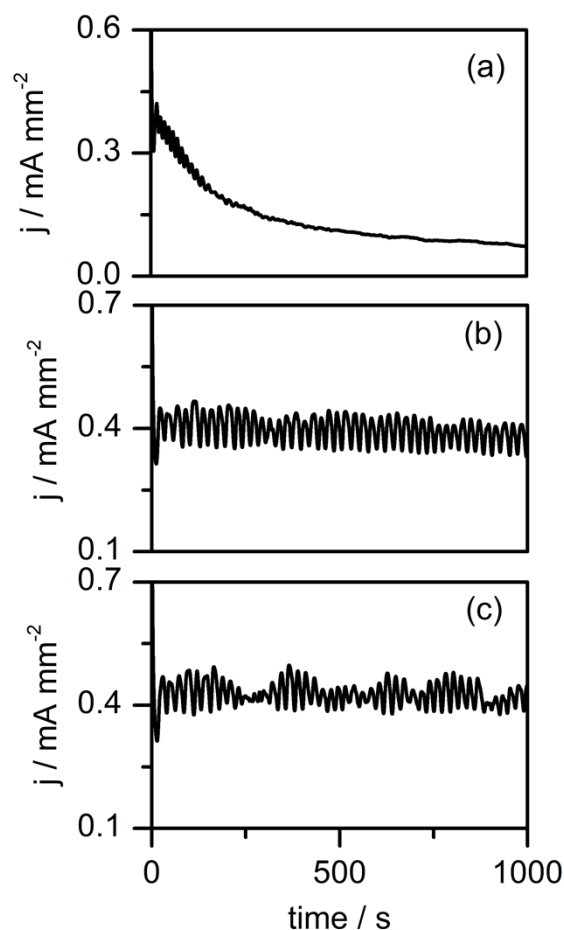
Figure 3.24. Time series under the potentiostatic control of: (a) 0.80 V, (b) 0.9V, and (c) 1.0 V. The solution contained 0.2 M $NaHSO_3$ and 0.05 K_2SO_4.
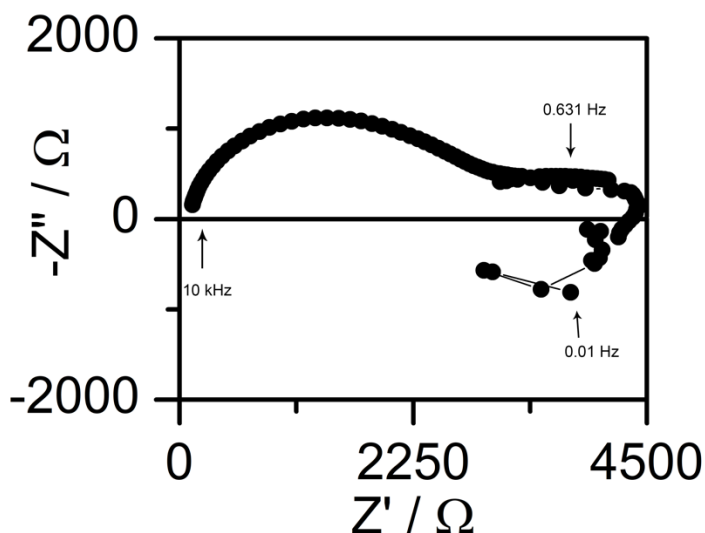
Figure 3.25. Nyquist plot during the oxidation of 0.2 NaHSO$_3$ in 0.05 M K$_2$SO$_4$ at a Au electrode at an applied potential of 0.8 V. The frequency range was from 1.0 x 10^5 Hz to 0.001 Hz. The perturbation amplitude is 0.005 V.

3.3.8 Mechanistic Pathway

The overall electrochemical oxidation of bisulfite involves a two-electron transfer process, where the final oxidation product is sulfate (SO$_4^{2-}$)· or sulfuric acid (H$_2$SO$_4$). The reaction can be described by the following reaction.

$$HSO_3^- + H_2O \leftrightarrow SO_4^{2-} + 3H^+\, 2e^- \qquad E^0 = 0.105 \text{ V}$$

Regardless of the pathway, it has been generally accepted that the fast adsorption of the starting material HSO$_{3\text{-(ads)}}$ gives rise to a reaction of an overall order of one.[42] Potential intermediates involving the pentavalent sulfur, such as pyrosulfite (S$_5$O$_4^{2-}$) and dithionate (S$_2$O$_6^{2-}$) have been proposed to be involved in the mechanistic pathway. Less commonly, various polythionates (S$_3$O$_6^{2-}$, S$_6$O$_6^{2-}$) can also be formed.[27] Dithionate has been suggested to be an intermediate for both dissolved sulfur dioxide and sulfite (in acidic and alkaline media),[43] and most likely is an intermediate for the oxidation of bisulfite (neutral media). Chang and co-workers also

proposed the disulfate ion, $S_2O_7^{2-}$ as the intermediate product of the oxidation of bisulfite by molecular oxygen.[44] Disulfate then decomposes into sulfate given by the following reaction.

$$S_2O_7^{2-} + H_2O \rightarrow 2H^+ + 2SO_4^{2-}$$
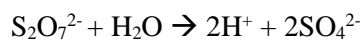
As an attempt to identify the intermediate and the final product species from the oxidation reaction, mass spectroscopy experiments were run on unreacted and reacted solutions, initially containing $NaHSO_3$ and KCl, see Figure 3.26. However, the spectra contained many background noise. Some peak values that were consistent with HSO_3^- were found in both the unreacted solution (Figure 3.26(a)) and reacted solution (Figure 3.26(b)). The final product, SO_4^{2-} was not able to be detected. A peak value of 97 m/z was present in the unreacted and reacted solutions; although this matches bisulfate (HSO_4^-), it was also found in the blank, which highly suggests the peak is due to background noise.
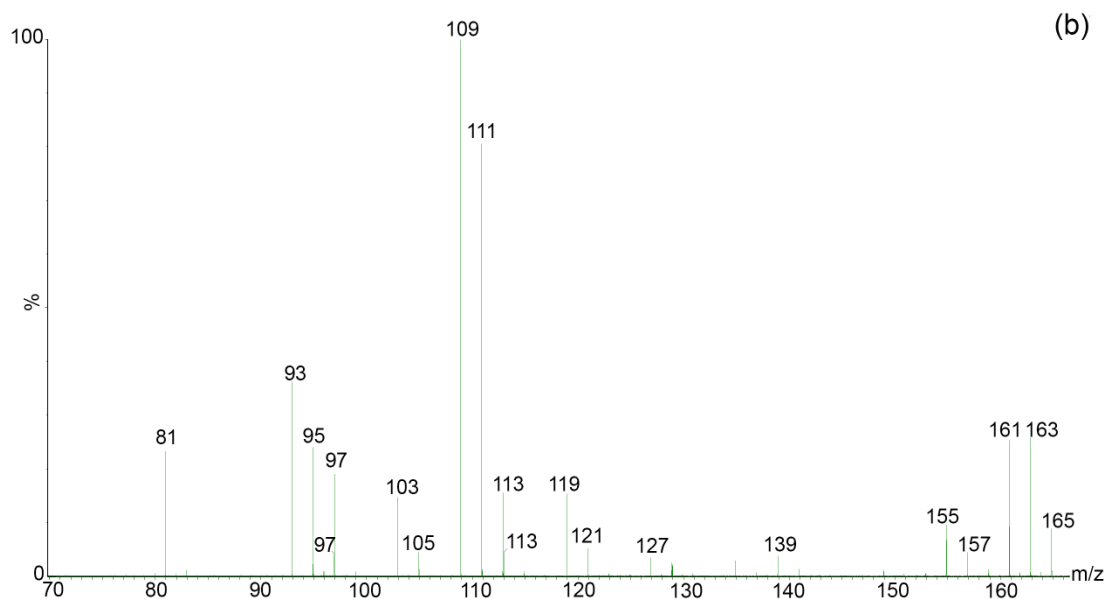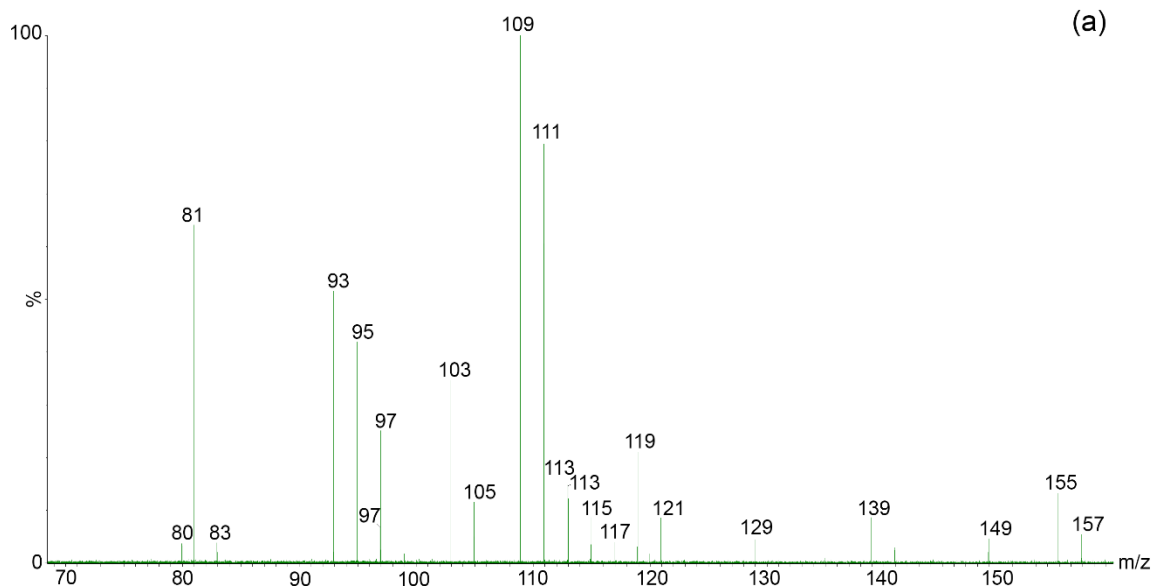
Figure 3.26. Mass (ESI TOF) spectra obtained from solutions of (a) unreacted NaHSO$_3$ and KCl, (b) NaHSO$_3$ and KCl that has been subjected to the electro-oxidation reaction by performing a potentiostatic experiment at 1.5 V for 1.5 hours.

Comparative studies involving the oxidation of bisulfite on Pt performed by Bell and Wang revealed electrochemical oscillations of the N-NDR classification.[28] In contrast, with the same dominant species (aqueous SO_2), the electrochemical oxidation on glassy carbon exhibited oscillations belonging to the HN-NDR class, as shown in the previous chapter. For the polycrystalline Pt, strong adsorption processes of SO_4^{2-} ions resulted in a NDR branch in the polarization curve. For the dominant species of HSO_3^- at the GCE in the presence of KCl, the oscillations arose from the oxidation of HSO_3^- competing with the oxidation of Cl^-. At higher potentials, the oxidation of H_2O causes hydrodynamic convection mass transportation which led to irregular oscillations.

Based on the peak current (i_p) and its relation to the square root of the scan rate, the linear proportionality reveals that the electro-oxidation of HSO_3^- on the GCE is likely diffusion controlled, see Figure 3.27.
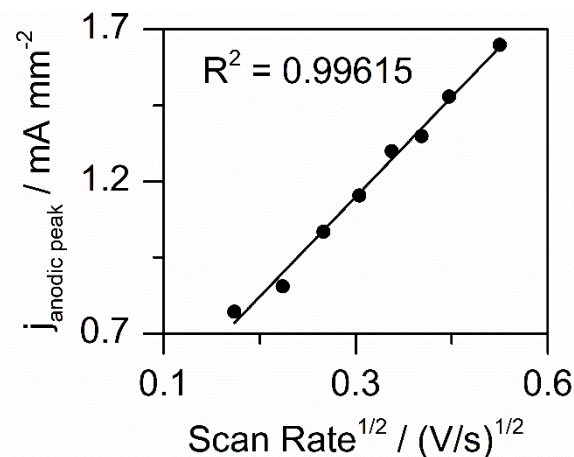
Figure 3.27. A plot showing the square root of the scan rate and the anodic peak current density during the electro-oxidation of 0.3 M NaHSO$_3$ in 1.0 M at the GCE.

3.4 Conclusions

In this study, the oxidation of bisulfite on a glassy carbon electrode in neutral media was found to depend significantly on the supporting electrolytes, where the studied system does not show a negative differential resistance in the KCl solution. However, despite the absence of a NDR, oscillations in both current and potential were observed in the bisulfite-KCl system. Notably, the instability took place in the absence of any external resistor and remained intact when using a rotating disc electrode. Considering that the oxidation of chloride begins at the potential around 1.3 V, it is plausible to suggest that the competing oxidations of bisulfite and chloride, are likely responsible for this new oscillator. The competition of H_2O can also be invoked, as this occurs at around 1.8 V. Certainly, one cannot rule out the possible chemical oxidation of bisulfite by the oxygen atom generated from the electro-oxidation of water. As the oxidation of water became more vigorous with respect to the increase of the applied potentials, erratic bubble formation due to oxygen evolution caused irregularity in the oscillation waveform. This is exactly the scenario observed at the conditions of high applied potential (i.e., potentiostatic experiments) and high applied current (i.e., galvanostatic reactions).

3.5 References

(1)   Fu, J.; Hou, M.; Du, C.; Shao, Z.; Yi, B. Potential Dependence of Sulfur Dioxide Poisoning and Oxidation at the Cathode of Proton Exchange Membrane Fuel Cells. *J. Power Sources* **2009**, *187*, 32–38.

(2)   Garsany, Y.; Baturina, O. A.; Swider-Lyons, K. E. Impact of Sulfur Dioxide on the Oxygen Reduction Reaction at Pt/Vulcan Carbon Electrocatalysts. *J. Electrochem. Soc.* **2007**, *154*, B670–B675.

(3)   Zhai, Y.; Bender, G.; Rocheleau, R. The Multiprocess Degradation of PEMFC Performance Due to Sulfur Dioxide Contamination and Its Recovery. *J. Electrochem. Soc.* **2010**, *157*, B20–B26.

(4)   Garsany, Y.; Baturina, O. A.; Pietron, J.; Swider-Lyons, K. E. Impact of Sulfur Dioxide on the Performance of the PEMFC Cathodes. *ECS Trans.* **2006**, *3*, 685–694.

(5)   Allen, J. A.; Rowe, G.; Hinkley, J. T.; Donne, S. W. Electrochemical Aspects of the Hybrid Sulfur Cycle for Large Scale Hydrogen Production. *Int. J. Hydrogen Energy* **2014**, *39*, 11376–11389.

(6)   Jessica A., O.; Hinkley, J.; Donne, S.; S.-E. Linquist. The Electrochemical Oxidation of Aqueous Sulfur Dioxide: A Critical Review of Work with Respect to the Hybrid Sulfur Cycle. *Electrochim. Acta* **2010**, *55*, 573–591.

(7)   Struck, B. D.; Junginger, R.; Boltersdorf, D.; Gehrmann, J. The Anodic Oxidation of Sulfur Dioxide in the Sulfuric Acid Hybrid Cycle. *Int. J. Hydrogen Energy* **1980**, *5*, 487–497.

(8)   Lu, P. W. T. Technological Aspects of Sulfur Dioxide Depolarized Electrolysis for Hydrogen Production. *Int. J. Hydrogen Energy* **1983**, *8*, 773–781.

(9)   Gorensek, M. B.; Summers, W. A. Hybrid Sulfur Flowsheets Using PEM Electrolysis and a Bayonet Decomposition Reactor. *Int. J. Hydrogen Energy* **2009**, *34*, 4097–4114.

(10)   Zhai, J.; Hou, M.; Zhang, H.; Zhou, Z.; Fu, J.; Shao, Z.; Yi, B. Study of Sulfur Dioxide Crossover in Proton Exchange Membrane Fuel Cells. *J. Power Sources* **2011**, *196*, 3172–3177.

(11)   Tsushima, S.; Kaneko, K.; Hirai, S. Two-Stage Degradation of PEMFC Performance Due to Sulfur Dioxide Contamination. *ECS Trans*. **2010**, *33*, 1645–1652.

(12)   Mohtadi, R.; Lee, W.-K.; Van Zee, J. W. Assessing Durability of Cathodes Exposed to Common Air Impurities. *J. Power Sources* **2004**, *138*, 216–225.

(13)   Nagahara, Y.; Sugawara, S.; Shinohara, K. The Impact of Air Contaminants on the PEMFC Performance and Durability. *J. Power Sources* **2008**, *182*, 422–428.

(14)   Moraes, I. R.; Weber, M.; Nart, F. C. On the Structure of Adsorbed Sulfur Dioxide at the Platinum Electrode. *Electrochim. Acta* 1997, *42*, 617–625.

(15)   Lee, J.; Langer, S. H. Electrochemical Sulphur Dioxide Oxidation with Platinum-Aluminum Electrocatalysts. *J. Appl. Electrochem*. **1995**, *25*, 353–357.

(16)   Scott, K.; Taama, W. M. An Investigation of Anode Materials in the Anodic Oxidation of Sulfur Dioxide in Sulfuric Acid Solutions. *Electrochim. Acta* **1999**, *44*, 3421–3427.

(17)   Lu, P. W. T.; Ammon, R. L. An Investigation of Electrode Materials for the Anodic Oxidation of Sulfur Dioxide in Concentrated Sulfuric Acid. *J. Electrochem. Soc*. **1980**, *127*, 2610–2616.

(18)   Colón-Mercado, H. R.; Hobbs, D. T. Catalyst Evaluation for a Sulfur Dioxide-Depolarized Electrolyzer. *Electrochem. commun*. **2007**, *9*, 2649–2653.

(19)   Quijada, C.; J. L. Vazquez. Electrochemical Reactivity of Aqueous Sulphur Dioxide at Polycrystalline Noble Metal Electrodes in Acidic Media. *Recent Res. Dev. Electrochem.* **2000**, *3*, 137–181.

(20)   O'Brien, J. A.; Hinkley, J. T.; Donne, S. W. Electrochemical Oxidation of Aqueous Sulfur Dioxide II. Comparative Studies on Platinum and Gold Electrodes. *J. Electrochem. Soc.* **2012**, *159*, F585–F593.

(21)   Seo, E. T.; Sawyer, D. T. Electrochemical Oxidation of Dissolved Sulphur Dioxide at Platinum and Gold Electrodes. *Electrochim. Acta* **1965**, *10*, 239–252.

(22)   Quijada, C.; J. L. Vazquez. Electrochemical Reactivity of Aqueous SO_2 on Glassy Carbon Electrodes in Acidic Media. *Electrochim. Acta* **2005**, *50*, 5449–5457.

(23)   Zhang, J.; Zhao, Z.; Xia, Z.; Dai, L. A Metal-Free Bifunctional Electrocatalyst for Oxygen Reduction and Oxygen Evolution Reactions. *Nat. Nanotechnol.* **2015**, *10*, 444–452.

(24)   Zhang, L.; Xiao, J.; Wang, H.; Shao, M. Carbon-Based Electrocatalysts for Hydrogen and Oxygen Evolution Reactions. *ACS Catal.* **2017**, *7*, 7855–7865.

(25)   Yang, C.; Jin, H.; Cui, C.; Li, J.; Wang, J.; Amine, K.; Lu, J.; Wang, S. Nitrogen and Sulfur Co-Doped Porous Carbon Sheets for Energy Storage and pH-Universal Oxygen Reduction Reaction. *Nano Energy* **2018**, *54*, 192–199.

(26)   Feng, J.; Gao, Q.; Xu, L.; Wang, J. Nonlinear Phenomena in the Electrochemical Oxidation of Sulfite. *Electrochem. commun.* **2005**, *7*, 1471–1476.

(27)   O'Brien, Jessica A., Hinkley, James T., Donne, S. W. Observed Electrochemical Oscillations during the Oxidation of Aqueous Sulfur Dioxide on a Sulfur Modified Platinum Electrode. *Electrochim. Acta* **2011**, *56*, 4224–4230.

(28)   Bell, J. G.; Dao, M.; Wang, J. Qualitative Dependence of the Electro-Oxidation Behavior of Sulfite on Solution pH. *J. Electroanal. Chem.* **2018**, *816*, 1–6.

(29)   Zelinsky, A. G.; Pirogov, B. Y. Electrochemical Oxidation of Sulfite and Sulfur Dioxide at a Renewable Graphite Electrode. *Electrochim. Acta* **2017**, *231*, 371–378.

(30)   Koper, M. T. M. Non-Linear Phenomena in Electrochemical Systems. *J. Electrochem. Soc. Faraday Trans.* **1998**, *94*, 1369–1378.

(31)   Koper, M. T. M.; Sluyters, J. H. Instabilities and Oscillations in Simple Models of Electrocatalytic Surface Reactions. *J. Electroanal. Chem.* **1994**, *371*, 149–159.

(32)   Koper, M. T. M. Oscillations and Complex Dynamical Bifurcations and in Electrochemical Systems. In *Advances in Chemical Physics*; John Wiley & Sons Inc.: Hoboken, N.J., 1996; pp 161–298.

 (33)   Krischer, K. Nonlinear Dynamics in Electrochemical Systems. In *Advances in Electrochemical Science and Engineering*; Wiley-VCH Verlag GmbH & Co. KGaA: Weinheim, Germany, 2002.

(34)   Strasser, P.; Eiswirth, M.; M. T. M. Koper. Mechanistic Classification of Electrochemical Oscillators - an Operational Experimental Strategy. *J. Electroanal. Chem.* **1999**, *478*, 50–66.

(35)   Patil, R.S.; Juvekar, V. A.; Naik, V. M. Oxidation of Chloride Ion on Platinum Electrode: Dynamics of Electrode Passivation and its Effect on Oxidation Kinetics. *Ind. Eng. Chem. Res.* **2011**, *50*, 12946-12959.

(36)   Li, Z.; Cai, J.; Zhou, S. Current Oscillations in the Reduction or Oxidation of Some Anions Involving Convection Mass Transfer. *J. Electroanal. Chem.* **1997**, *436*, 195–201.

(37)   Zensen, C.; Schönleber, K.; Kemeth, F.; Krischer, K. A Capacitance Mediated Positive Differential Resistance Oscillator Model for Electrochemical Systems Involving a Surface Layer. *J. Phys. Chem. C* **2014**, *118*, 24407–24414.

(38)   M. T. M. Koper. Stability Study and Categorization of Electrochemical Oscillators by Impedance Spectroscopy. *J. Electroanal. Chem*. **1996**, *409*, 175–182.

(39)   Bell, J. G.; Wang, J. Nonlinear Instabilities during the Electrochemical Oxidation of Hydroxymethanesulfinate. *Electrochim. Acta* **2016**, *222*, 678–684.

(40)   Baril, G.; Galicia, G.; Deslouis, C.; Pébère, N.; Tribollet, B.; Vivier, V. An Impedance Investigation of the Mechanism of Pure Magnesium Corrosion in Sodium Sulfate Solutions. *J. Electrochem. Soc*. **2007**, *154*, C108–C113.

(41)   Aoki, I. V.; Bernard, M.-C.; Cordoba de Torresi, S. I.; Deslouis, C.; de Melo, H. G.; Joiret, S.; Tribollet, B. AC-Impedance and Raman Spectroscopy Study of the Electrochemical Behaviour of Pure Aluminum in the Citric Acid Media. *Electrochim. Acta* **2001**, *46*, 1871–1878.

(42)   Hunger, T.; Lapicque, F. Electrochemistry of the Oxidation of Sulfite and Bisulfite Ions at a Graphite Surface: An Overall Approach. *Electrochim. Acta* **1991**, *36*, 1073–1082.

(43)   Skavås, E.; Hemmingsen, T. Kinetics and Mechanism of Sulphite Oxidation on a Rotating Platinum Disc Electrode in an Alkaline Solution. *Electrochim. Acta* **2007**, *52*, 3510–3517.

(44)   Littlejohn, D.; Hu, K.-Y.; Chang, S.-G. Oxidation of Bisulfite Ion by Oxygen. *Ind. Eng. Chem. Res*. **1988**, *27*, 1344–1348.

CHAPTER 4 – ELECTRO-OXIDATION OF L-CYSTEINE

4.1. Introduction

L-cysteine (CySH) plays a pivotal role in many biological systems. The sulfur amino acid is characterized by its highly reactive thiol or sulfhydryl side chain that is essential in a diverse range of cellular functions including enzyme catalysis, biosynthesis of proteins, and detoxification.[1–3] Additionally, cysteine is a key precursor for the production of glutathione (GSH), an important molecule that is responsible for various physiological phenomena.[4,5] In chemical systems, cysteine was found to modify the surface chemistry of silver nanoparticles through the formation of the monovalent silver-sulfhydryl bonds.[6] Furthermore, poly(cysteine) has recently been employed in the applications of heavy metal extraction,[7] and drug delivery.[8] Interestingly, the electrode modification by poly(cysteine) deposition was shown to increase sensitivity towards the electrochemical detections of various compounds.[9–11]

The oxidation reactions of L-cysteine are of great interest due to the unique formation of the disulfide linkages between two thiol side groups that form L-cystine. The study of the cysteine electro-oxidation on various electrode materials has been pursued in the last several decades.[12-25] For example, several authors have provided comprehensive electrochemical investigations of cysteine at mercury electrodes, which show that the reaction occurs via the adsorption of cysteine to the Hg surface to form a mercurous cysteinate film.[12–16] At noble metals, such as platinum and gold, the formation of surface oxides at high anodic potentials was found to suppress the oxidation of cysteine.[17,18] The anodic reactions of cysteine at carbon materials have attracted increasing attention in more recent studies, driven partially by the low cost and abundance of such electrocatalysts.[19–25]

Because of its multiple oxidation states, the presence of the sulfur atom provides the potential of L-cysteine to exhibit rich dynamical behaviors, such as nonlinear instabilities. For

example, Bell and Wang were able to demonstrate electrochemical oscillations during the oxidation of another sulfur amino acid, methionine, at a gold electrode.[26] However, the dissolution processes from the strong interactions of gold with the sulfur compounds was suggested to be the main driving force behind the emergence of the current oscillations. To eliminate the possible influence of electrode corrosion on the electrochemical oxidation process, Pt was selected as the working electrode in this study. Investigations using cyclic voltammetry (CV) indicated the possible existence of a negative differential resistance in the electro-oxidation of cysteine at Pt, which has been known as a necessary condition for the development of nonlinear instabilities in electrochemical systems. Experiments with multi-potential steps (MPS) method revealed the presence of complex small amplitude oscillations under certain experimental conditions. It was found that the overall characteristics of the oxidation behavior of cysteine was dependent strongly on the solution pH.

4.2 Experimental Procedures

L-cysteine (97%), sodium hydroxide, sulfuric acid (95%-98%), and potassium chloride reagents were purchased from Sigma Aldrich, EM Science, ACP Chemicals, and Oakwood Chemicals, respectively. These chemicals were weighted with an analytical balance and directly dissolved in a cell beaker with a total solution volume of 80 mL.

All electrochemical measurements were taken with a CHI 760E electrochemical workstation purchased from CHI Instruments (Texas, US). A polycrystalline platinum disc electrode with a diameter of 2.0 mm, also purchased from CHI instruments was employed as the working electrode. The reference and counter electrodes were a saturated calomel electrode (SCE) and a platinum wire, respectively. Prior to each experiment, the working electrode was polished using 0.3 µm and 0.05 µm alumina slurry and was sonicated to remove any adhered alumina particles. The electrode was then thoroughly rinsed with double distilled water.

The pH values were obtained with an Orion 410A+ pH meter, purchased from Thermo Electron Corporation. The pH meter was calibrated with 3 standard solutions prior to use.

Scanning electron microscopy (SEM) images were taken with a Quanta 200 FEG Microscope (FEI, Inc.)

4.3 Results and Discussion

4.3.1 Oxidation of L-Cysteine in Neutral Media

Figure 4.1 shows the typical voltammogram during the electrochemical oxidation of L-cysteine (0.1 M) in neutral solutions of 0.5 M KCl at a polycrystalline Pt electrode. The j-E curve revealed that the oxidation begins at the potential of 0.3 V (vs. SCE) and then rapidly reaches a maximum at 0.6 V. Clearly, such a limiting current is determined by the mass transportation process. It is useful to point out that at a very slow scan rate of 0.1 mVs^{-1}, the limiting current is expected to stay, as the mass transportation has reached its maximum. However, here a well-defined peak can be observed in the LSV, indicating that the studied system may have a negative differential resistance (NDR) within the potentials of 0.65 V – 1.1 V. The decrease in the current-density response (i.e., NDR) could be caused by the passivation of the electrode surface through the formation of surface oxides. Under the applied potential ranges undertaken in this study, Pt can undergo oxidation to form PtO. In fact, Morris was able to demonstrate that the oxide film growth begins to occur at 0.7 V vs. SCE.[27] Figure 4.2(b) depicts the j-E curve during the oxidation of L-cysteine with a PtO electrode. The modified Pt was prepared by applying a high anodic potential (1.5 V vs. SCE) for approximately 5 minutes in a 1 M NaOH solution. Such high concentrations of NaOH can facilitate the oxide film formation. The results in Figure 4.2 show that PtO exhibited a lower electrocatalytic activity towards the reaction compared to Pt electrodes since the current density response is lower and the oxidation peak occurs at a slightly higher potential. An earlier study by Davis and Bianco on the oxidation of L-cysteine on the Pt electrode suggested that the

surface oxides suppressed the reaction, which was also observed in this study.[18] However, due to the negative branch observed in Figure 4.2(b) with a PtO electrode, this suggests that the passivation of Pt was most likely not the main contributing factor that lead to the NDR branch in Figure 4.2(a) during the oxidation of L-cysteine with a Pt electrode.

It has been reported that the oxidation reaction proceeds with the initial step of cysteine adsorption. In a neutral solution, the major form of cysteine is cysteine with the protonated sulfhydryl and amino groups. When the anodic potential is increased, the adsorption of protonated cysteine becomes less favored, resulting in the NDR branch. However, this process is difficult to distinguish from the adsorption of neutral form cysteine as well as the oxidation product, cystine.[17] To recall, the presence of a NDR is crucial in the emergence of electrochemical oscillations.[28–31] To confirm that the system does indeed have a NDR, impedance investigations were performed at applied potentials that lie on the negative branch of the j-E curve.
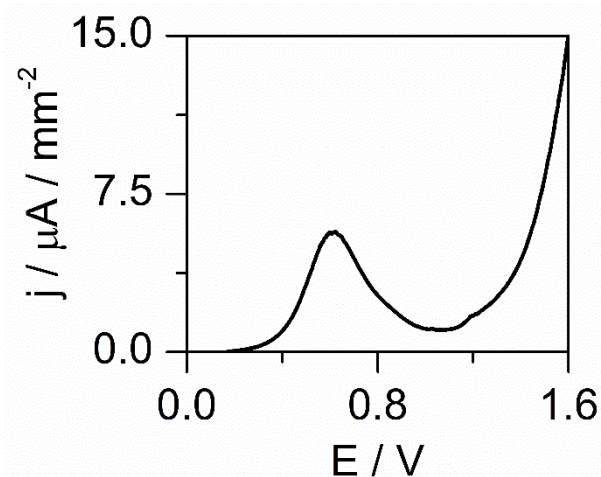
Figure 4.1. Potentiodynamic curve of 0.1 M L-cysteine in 0.5 M KCl. The scan rate was 0.1 mVs[-1].
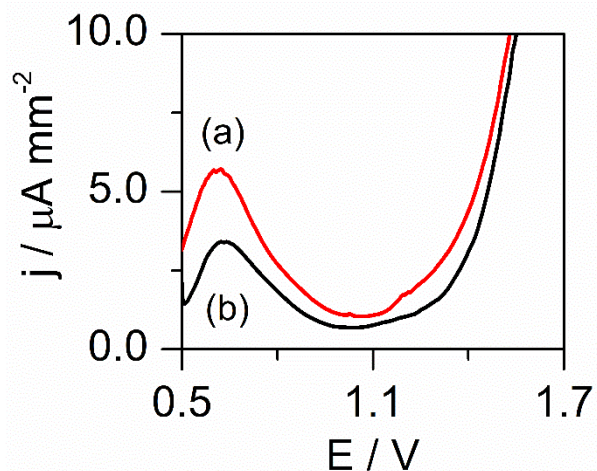
Figure 4.2. Potentiodynamic curves of 0.1 M L-cysteine in 0.5 M KCl with a (a) Pt and (b) PtO electrode. The scan rate was 0.1 mVs^{-1}.

The impedance spectra measured of a Pt electrode in a solution containing 0.1 M L-Cysteine and 0.5 M KCl at applied potentials of 0.80 V and 1.05 V are depicted in Figure 4.3. At 0.80 V, the system first crosses the real impedance axis at a positive value in the clockwise direction, and subsequently crosses the imaginary axis at an intermediate frequency. The system then intersects the real axis again at approximately -80 kΩ to -100 kΩ and terminates at around -26 kΩ. A similar behavior was observed at 1.05 V. However, the system crosses the real and imaginary axes in a counterclockwise fashion and terminates at approximately -20 kΩ, see Figure 4.3(b). The results in Figure 4.3 also contain the impedance characteristics belonging to a N-NDR oscillator, which would require the presence of a sufficiently large ohmic drop for the emergence of nonlinear instabilities such as bistability or oscillations at potentials within the NDR regime.

Figure 4.3. Nyquist plots during the oxidation of 0.1 M L-cysteine in 0.5 M KCl at a Pt electrode at the applied potentials of (a) 0.800 V and (b) 1.05 V. The frequency range was from 1.0×10^5 Hz to 0.001 Hz. The perturbation amplitude is 0.005 V.

To search for dynamical instabilities, slow potential sweeps with the insertion of a 27 kΩ, 80 kΩ, 100 kΩ, and 120 Ω external resistor are shown in Figure 4.4. The ohmic sizes were chosen according to the impedance data presented in Figure 4.3. Peak shifts were observed towards higher anodic potentials due to large ohmic drops with the increasing resistor size (E = U + IR). With a 27 kΩ resistor, the peak occurred at approximately 0.98 V, compared to 0.6 V in the absence of an external resistor. Similarly, with a 80 kΩ, 100 kΩ and 120 kΩ resistor, the anodic peaks were observed at 1.70 V, 1.85 V, and 1.98 V, respectively. However, even with such large ohmic drops, no oscillations were observed in the LSV, despite that the NDR branch persists. This is very different from what have been observed in Chapters 2 and 3 with the bisulfite system.
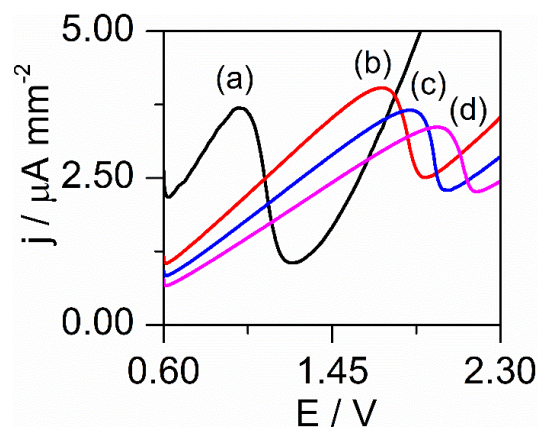
Figure 4.4. Potentiodynamic curves of 0.1 M L-cysteine in 0.5 M KCl with external resistors of (a) 27 kΩ, (b) 80 kΩ, (c) 100 kΩ, and (d) 120 kΩ connected in series with the working electrode. The scan rate was 0.1 mVs^{-1}.

Although oscillatory behavior was not observed in this system, other manifestations of nonlinear instabilities were able to be detected. A forward and reverse slow cyclic voltammogram (0.1 mVs^{-1}) obtained from a 0.1 M L-cysteine in a 0.5 M KCl solution indicates that within the potential range between 0.2 V and 1.2 V, the oxidation reaction may occur at a high current density or low current density under the same applied potential (Figure 4.5). Such a behavior is known as the bistability.

Figure 4.5. Cyclic voltammogram of 0.1 M L-cysteine in 0.5 M KCl. The scan rate was 0.1 mVs^{-1}.

4.3.2 Oxidation of L-Cysteine in Acidic Media

The results in Figure 4.6 show that the electro-oxidation of L-cysteine in acidic electrolytes produces a j-E curve that is qualitatively the same as seen in neutral solutions. Similar to the results in Figure 4.1, a negative branch was also observed in the j-E curve, between the potentials of 0.85 V – 1.20 V. An oxidation peak plateau is observed at 0.8 V, which is about 0.2 V higher than seen in neutral conditions. This indicates that a higher overpotential is needed in order to oxidize cysteine in an acidic medium.
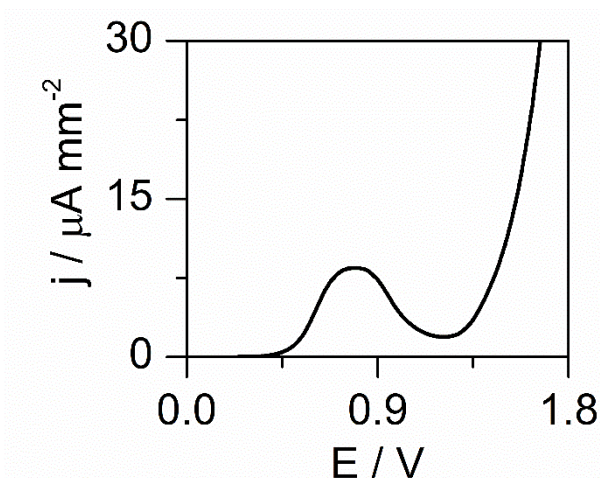
Figure 4.6. Potentiodynamic curve of 0.1 M L-cysteine in 0.1 M H_2SO_4. The scan rate was 0.1 mVs^{-1}.

Figure 4.7 presents the Nyquist plot of the Pt electrode during the electro-oxidation of L-cysteine at applied potential of 0.90 V, which lies on the NDR branch observed in the j-E curve (Figure 4.6). Similar to the L-cysteine-KCl system, the impedance response crosses the imaginary axis at an intermediate frequency and ends in quadrant II of the complex plane. Despite no intersection with the x axis (real impedance) occurs, it demonstrates a clear trend that the system will end at the negative x-axis as the frequency of the perturbation approaches to zero, which is consistent with the observation of a NDR in Figure 4.6.
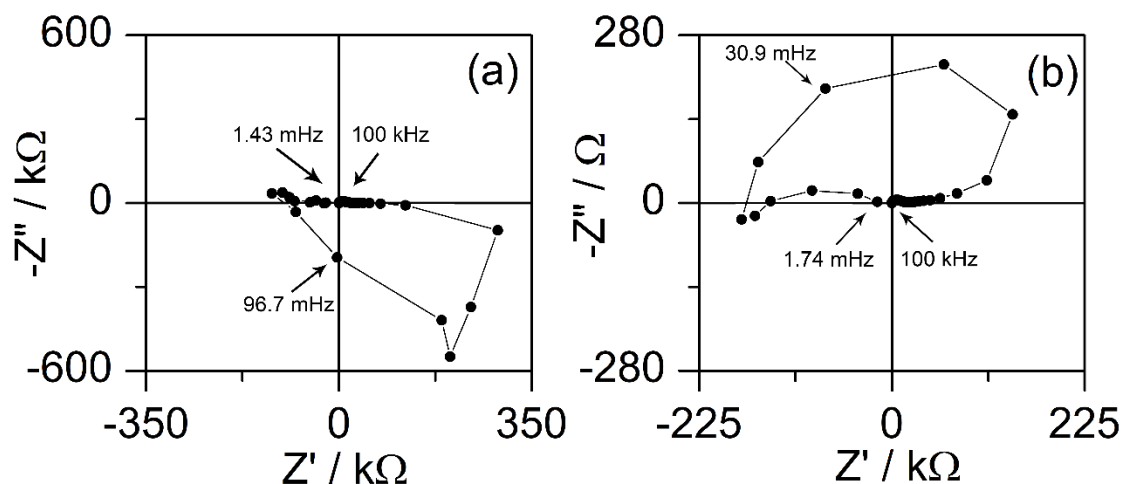
Figure 4.7. Nyquist plot during the oxidation of 0.1 M L-cysteine in 0.1 M H_2SO_4 at a Pt electrode at the applied potential of 0.90 V. The frequency range was from 1.0×10^5 Hz to 0.001 Hz. The perturbation amplitude is 0.005 V.

Another interesting feature of the L-cysteine-H_2SO_4 system is the ability to exhibit the bistability behavior, as seen in Figure 4.8. The observed phenomenon was found to be similar in the neutral system, where the system can either be in a high or low current density state between the applied potentials of 0.5 V – 1.2 V.
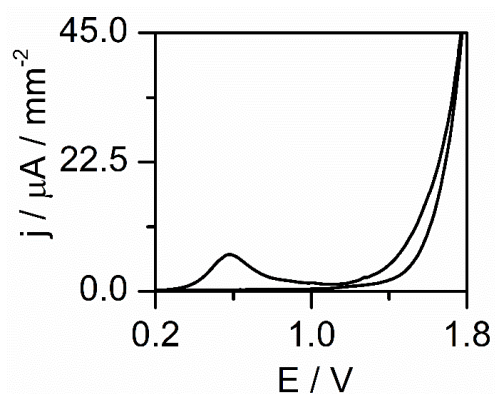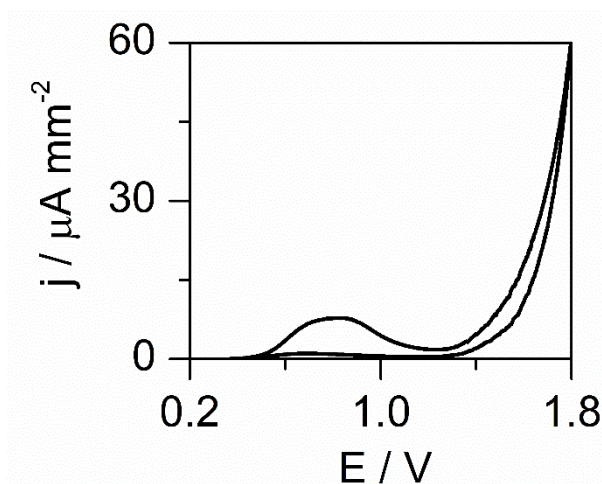

Figure 4.8. Cyclic voltammogram of 0.1 M L-cysteine in 0.5 M KCl. The scan rate was 0.1 mVs^{-1}.

4.3.3 Oxidation of L-Cysteine in Alkaline Media

The pH-dependence of the reaction behavior is especially pronounced when L-cysteine is oxidized in strong alkaline media. Figure 4.9 shows the typical polarization curve of a Pt electrode in solutions of 0.1 M L-cysteine and 0.1 M NaOH. A marked contrast can be observed in the voltammetric behavior, as Figure 4.9 presents a rather complex j-E dependence curve compared to neutral and acidic pH solutions. Firstly, a local current density maximum was observed at approximately 0.90 V, which is similar to the one seen in Figure 4.1 and Figure 4.6. However, at around 1.25 V, there is an abrupt increase in the current density, followed by the gradual decay. Such a phenomenon resembles what has been frequently seen in electrochemical oxidation of metals, where the dramatic increase in current is caused by the abrupt disruption of passivation layer at the Flade potential. Phenomenologically, a circular thin film could sometimes be seen at the bottom of the reactor, which led us to suggest that the observed spike in the current density is correlated to the fall-off of the film. A small shoulder peak is also present at a low anodic potential of 0.1 V.
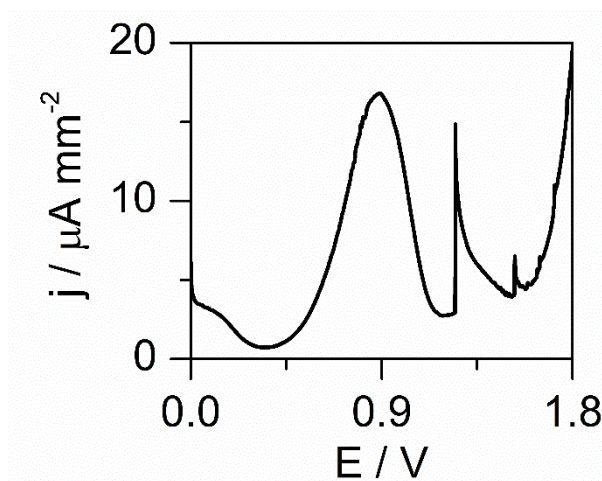
Figure 4.9. Potentiodynamic curve of 0.1 M L-cysteine in 0.1 M NaOH. The scan rate was 0.1 mVs^{-1}.

Three negative branches can be seen in the j-E curve: (1) 0.15 V to 0.35 V, (2) 0.90 V to 1.15 V, and (3) 1.25 V to 1.5 V. The impedance spectrum was taken at an applied potential in each of the above-mentioned regions and are depicted in Figure 4.10. In the first NDR, at 0.3 V, the Nyquist plot contains a semi-circle and a straight line at about a 45 degrees angle, which represents the Warburg diffusion impedance, Figure 4.10(a). As the applied potential is further changed to 0.80 V, the impedance spectrum looks similar to what was observed in the L-cysteine-H_2SO_4 system, see Figure 4.7. Please note that 0.8 V is located just outside the second negative branch, but this may be explained with a slight potential shift due to ohmic drops caused by minor differences in the solution resistance. Thus, another potential was selected within the same region. At 1.0 V, the system crosses the imaginary axis before intersecting the negative real impedance axis and continues to move away towards larger negative impedance values (Figure 4.10(c)). Comparable impedance characteristics were also observed at a potential in the third NDR regime, 1.3 V (Figure 4.10(d)). From the potentials 1.5 V and 1.65 V, which is located on the positive current-density branch, some instabilities can be noticed, shedding light on the possibility of the emergence of oscillatory behavior. The electrochemical impedance measurements were recorded at 1.5 V, which produced a Nyquist plot belonging to the HN-NDR oscillator, shown in Figure 4.11. The results from the j-E curve and the impedance spectrum indicates oscillations at higher anodic potentials that lie on the third positive branch may be feasible in this system under certain conditions.
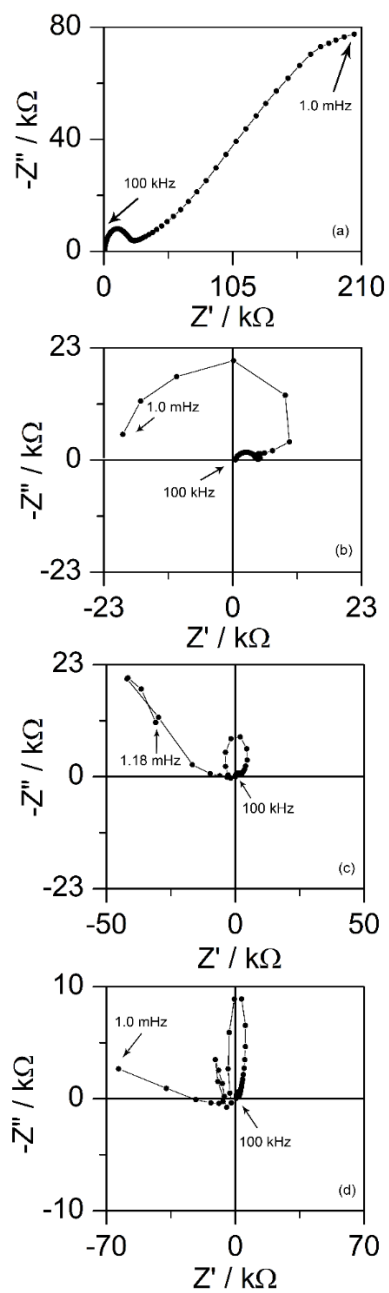
Figure 4.10. Nyquist plots during the oxidation of 0.1 M L-cysteine in 0.1 M NaOH at a Pt electrode at the applied potentials of (a) 0.3 V, (b) 0.8 V, (c) 1.0 V, and (d) 1.3 V. The frequency range was from 1.0×10^5 Hz to 0.001 Hz. The perturbation amplitude is 0.005 V.
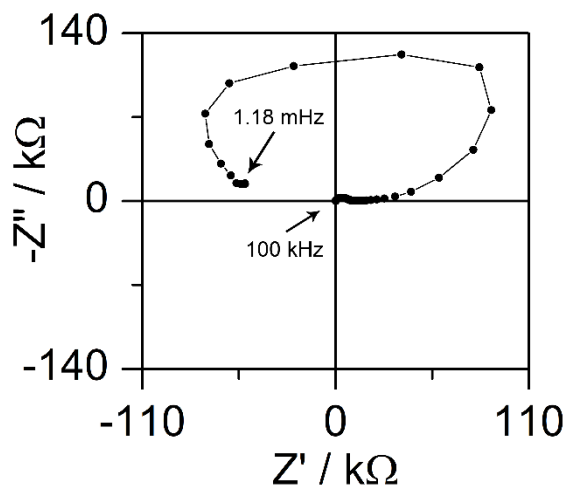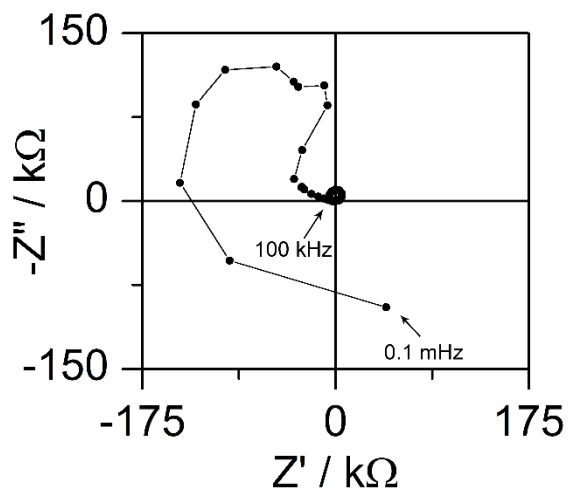
Figure 4.11. Nyquist plot during the oxidation of 0.1 M L-cysteine in 0.1 M NaOH at a Pt electrode at the applied potential of 1.5 V. The frequency range was from 1.0×10^5 Hz to 0.0001 Hz. The perturbation amplitude is 0.005 V.

In the absence of an external resistor, the L-cysteine-NaOH system was able to exhibit bistability, which is shown in Figure 4.12. A potentiodynamic curve was recorded in the forward and reverse scan in a solution containing 0.1 M L-cysteine and 0.1 M NaOH. This was followed by a separate reverse scan in the same solution with a polished bare Pt electrode. At the potential ranges of 0.6 V and 1.4 V, the system can exist at a high or low current-density. On the forward scan, the current density appears to be at 16.9 μA mm^{-2}, but in the reverse direction, no oxidation peak can be seen, and the current-density is at 2.48 μA mm^{-2}. To confirm that the passivation of the surface was not responsible for the observed behavior, a reverse potential sweep was performed beginning at a lower anodic potential, which revealed a similar behavior as Figure 4.12(b).
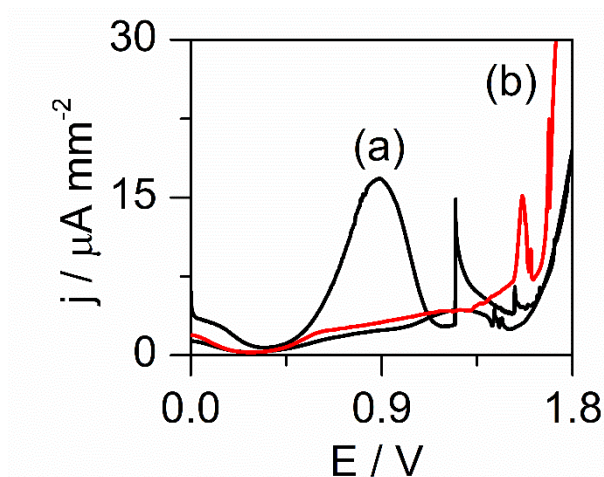
Figure 4.12. (a) Cyclic voltammogram of 0.1 M L-cysteine in 0.1 M NaOH. (b) Linear sweep voltammogram in the reverse direction. The scan rate was 0.1 mVs^{-1}.

Multi-potential steps time series were performed to investigate the bistable behavior. By applying a different potential for a short period of time, it acts as a perturbation and hopefully cause an excitation to shift the system to the neighborhood of another stable steady state. The system will then evolve to the new state and remain there even if the potential perturbation was removed (i.e., in our configuration, the potential is switched back to the prior value). For this study, the initial potential was 1.08 V, and 1.3 V and 0.4 V were also applied before reverting to 1.08 V. However, upon returning to 1.08 V, no obvious bistable behavior can be detected, as each potential step of 1.08 V has the same current density response, Figure 4.13(a), Figure 4.13(c), and Figure 4.13(e).
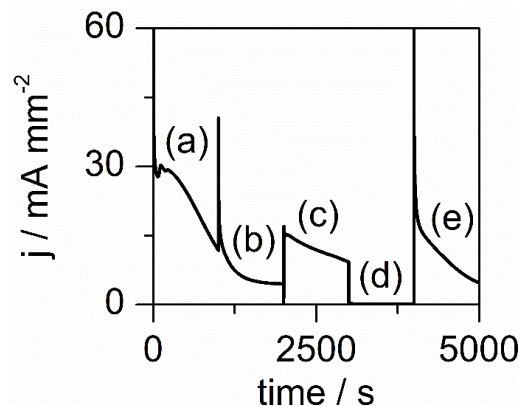
Figure 4.13. Multi-potential steps of 0.1 M L-cysteine in 0.1 M NaOH. The applied potentials were (a) 1.08 V, 1.3 V, (c) 1.08 V, (d) 0.4 V, and (e) 1.08 V.

The concentration of L-cysteine was decreased to investigate the effects on the bistability behavior. Figure 4.14 shows the multi-potential step time series in 0.05 M L-cysteine and 0.1 M NaOH. Although no discernable bistability was observed, the emergence of oscillations occurred at the potentials of 1.08 V and 1.3 V, a sharp contrast to the behavior in 0.1 M L-cysteine. The potentiostatic oscillations was unexpected, as NDR oscillators typically require the presence of an ohmic external resistor. The high solution resistance (~390 Ω) may be adequate for the onset of oscillatory behavior but was not reflected in the impedance investigations.
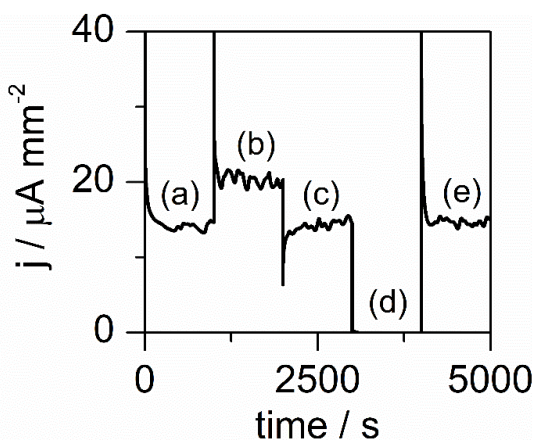
Figure 4.14. Multi-potential steps of 0.05 M L-cysteine in 0.1 M NaOH. The applied potentials were (a) 1.08 V, 1.3 V, (c) 1.08 V, (d) 0.4 V, and (e) 1.08 V.

A slow potential sweep was performed to obtain a greater level of understanding of the observed nonlinear phenomenon in the above figure. Figure 4.15 illustrates the j-E dependence curve of 0.05 M L-cysteine in 0.1 M NaOH where a dramatic change of the oxidation behavior occurs. The onset potential of L-cysteine occurs at approximately 0.4 V and continues to increase with no discernable oxidation peak or current density maximum. With a decrease of the L-cysteine concentration, the NDR that was present with 0.1 M of L-cysteine is not observed in Figure 4.15. Furthermore, the observation of spontaneous instabilities along the positive branch in the j-E curve in the absence of an external resistor is remarkably different than what was previously observed and indicates the possibility of the HN-NDR oscillator. EIS experiments were attempted to confirm the classification of the observed oscillations, however, due to the instabilities on the positive branch, the impedance spectra could not give further clarifications.
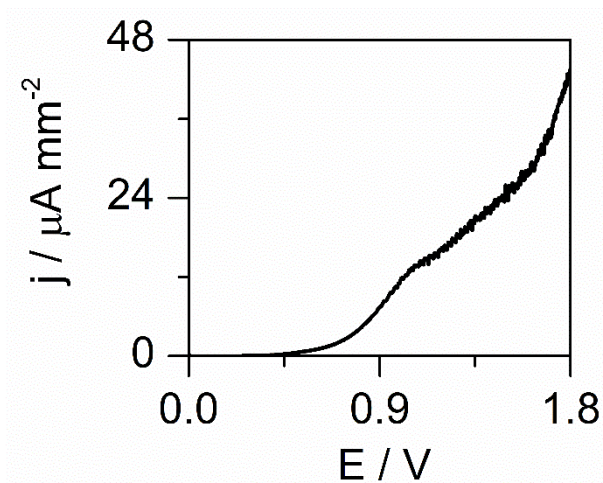
Figure 4.15. Potentiodynamic curve of 0.05 M L-cysteine in 0.1 M NaOH. The scan rate was 0.1 mVs⁻¹.

To explore the oscillatory dynamics observed in the above figures, the time series under potentiostatic control in a solution containing 0.05 M L-cysteine and 0.1 M NaOH is presented in Figure 4.16. At 1.3 V, relaxation oscillations appear with a shoulder peak with an average amplitude of approximately 1.6 μA mm^{-2}. When the applied potential is increased to 1.4 V, complex

oscillations were observed that occur with a lower frequency. It is worthy to point out that the oscillations also only occur within a narrow range of L-cysteine concentrations. Upon increasing to 0.1 M, and lowering to 0.02 M, no oscillations occur at either concentration.
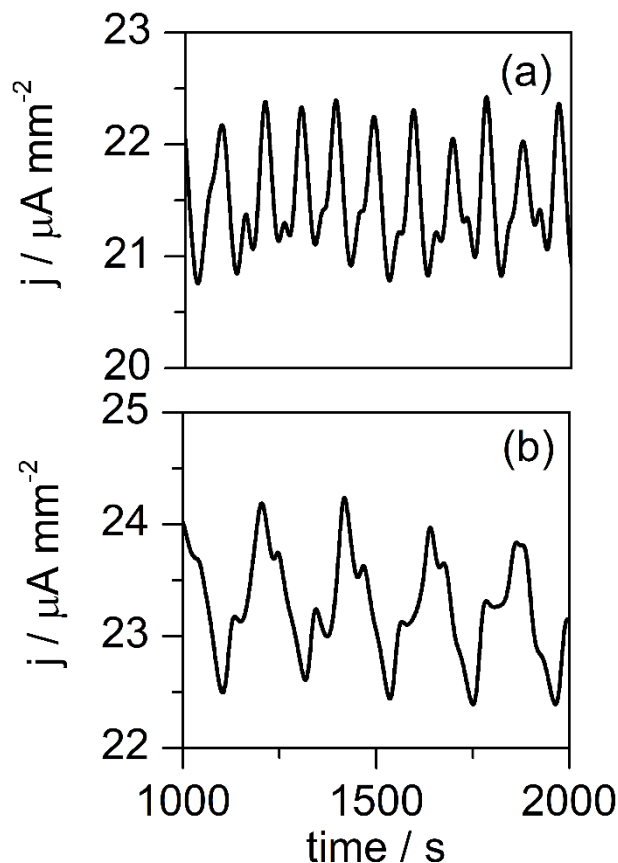
Figure 4.16. Time series under the potentiostatic control of (a) 1.3 V and (b) 1.4 V. The solution contained 0.05 M L-cysteine and 0.1 M NaOH.

The bistability phenomenon was also observed during the galvanodynamic sweeps in the forward and reverse scans, see Figure 4.17. The potential response increases monotonically with the applied current density in the forward scan. Starting with a high applied current density (19 µA mm^{-2}) in the reverse scan, the system exhibits low potentials. Upon decreasing the applied current density, the potential response increases before a sharp decrease was observed. It is suspected that the electrode surface changes have a role in the phenomenon observed in this system.
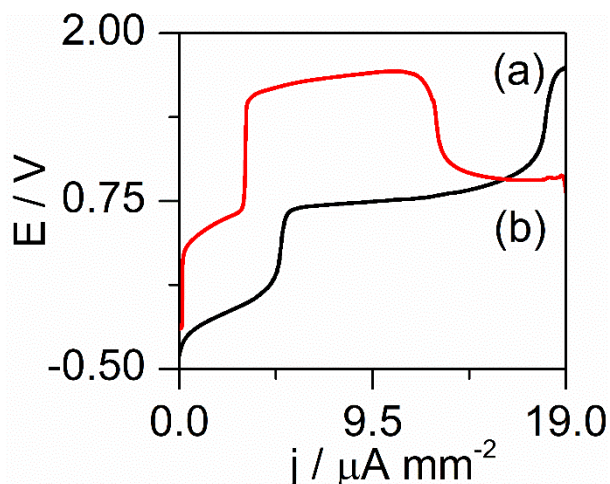
Figure 4.17. Galvanodynamic sweeps of 0.1 M L-cysteine in 0.1 M NaOH between 0 and 19 µA mm^{-2} in the (a) forward and (b) reverse scan. The scan rate was 0.00318 µA mm^{-2} s^{-1}.

4.3.4 Mechanism and Kinetic Overview

The overall oxidation reaction consists of cysteine being oxidized to cystine through the formation of the disulfide bond[32]:

$$2RSH \leftrightarrow RSSR + 2e^- + 2H^+$$

It has been previously reported that the anodic processes of cysteine are irreversible due to the slow kinetics of the reaction.[32] This was observed at the Pt electrode, as no discernable reduction peaks can be observed in the CV of L-cysteine in acidic, neutral and alkaline conditions (Figure 4.18). The results in Figure 4.18 reveal that the onset potentials for the oxidation of L-cysteine in KCl occurs at a lower anodic potential than in H$_2$SO$_4$, which is consistent with the findings of the slow LSVs presented in previous figures. However, in alkaline conditions, such as 0.1 M NaOH, no oxidation peaks can be distinguished, indicating that L-cysteine in high solution pH is possibly electrochemically inactive. Furthermore, the oxidation of L-cysteine at the Pt electrode appears to be sluggish, especially at neutral and alkaline pH.

119
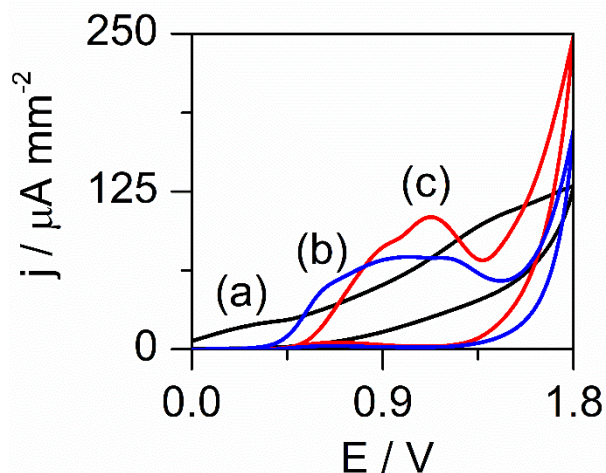
Figure 4.18. Cyclic voltammograms of 0.1 M L-cysteine in (a) 0.1 M NaOH, (b) 0.5 M KCl, and (c) 0.1 M H$_2$SO$_4$. The scan rate was 100 mVs^{-1}.

A difference in the anodic limiting current densities can be discerned in the j-E curves between the neutral, acidic, and alkaline media. In alkaline electrolytes, such as 0.1 M NaOH solution, the limiting current density for the oxidation of L-cysteine is 16.93 µA mm^{-2}, which is significantly higher than in solutions containing 0.1 M H$_2$SO$_4$ (8.56 µA mm^{-2}) and 0.5 M KCl (5.57 x µA mm^{-2}). Thus, one can assume that the kinetics, or the mass transportation characteristics of L-cysteine vary in response to changes in the solution pH. The fundamental difference between the solution pH is the relative abundance of the various forms of cysteine. The pka values of the carboxylic acid, sulfhydryl, and amine groups are given as follows: 1.92, 8.37, and 10.70, respectively.[33] In sufficiently acidic conditions, if the pH<pka$_1$, cysteine is fully protonated and contains an overall +1 charge. When L-cysteine is dissolved in 0.1 M H$_2$SO$_4$, the measured pH was 1.48, in which L-cysteine predominately exists in its fully protonated form. In 0.5 M KCl, the experimental pH was approximately 5.24, which falls in between the first and second pKa values. In these conditions, the dominant form of L-cysteine is a neutral molecule. When the electrolyte is 0.1 M NaOH, the measured pH is 9.48, surpassing the second pKa, which in turn indicates the deprotonation of the sulfhydryl group. The ionization of cysteine can be described by Figure 4.19.
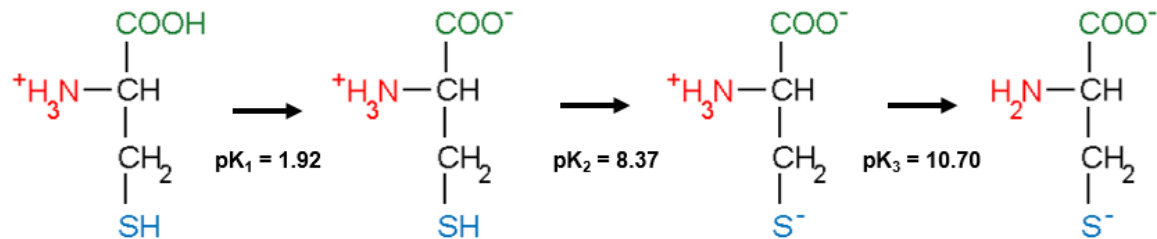
Figure 4.19. Ionization of L-cysteine in varying solution pH.

The adsorption and desorption processes at the Pt electrode vary significantly with respect to the solution pH. Dourado and co-workers have recently proposed a list of different adsorbed L-cysteine species that was confirmed with IR spectra.[34] For example, in very acidic conditions, such as a pH of 0, the strong adsorption of the carboxylic group occurs. However, it was shown that the decarboxylation of the adsorbed L-cysteine occurs when the applied potential is greater than 1.15 V vs. RHE, resulting in the formation of CO_2. The effects of the competing forces between $H_{(ads)}$ and L-cysteine cannot be ignored in acidic conditions, as in higher H^+ concentrations will result in lower L-cysteine adsorption.[34] Near neutral solution pH favors the adsorption of the amine group. Furthermore, at a solution pH of approximately 9 was reported to be the optimal condition for L-cysteine adsorption, which is mainly the adsorbed sulfone.[34] The adsorption of L-cysteine regardless of the species agrees with the findings of this study, as a well-defined negative branch was observed in the j-E curve in acidic, neutral, and alkaline media.

A sudden onset of the oscillatory behavior was observed when the concentration of L-cysteine was decreased from 0.1 M to 0.05 M in the same electrolyte solution, 0.1 M NaOH. The dynamical transition can be explained by the solution pH, which was measured to be 12.02. At such high pH, the dominant species of L-cysteine is now the fully deprotonated form, in which the amino group now only contains two protons, resulting in an overall charge of -2. To show that instabilities emerged was not due to the concentration of L-cysteine, another potentiodynamic sweep was performed with a solution containing 0.1 M L-cysteine, and 0.2 M NaOH to ensure the pH is

sufficiently high to deprotonate all groups of the amino acid. As seen in Figure 4.20, oscillations emerge on the positive branch just as in Figure 4.15, when the concentration of L-cysteine was 0.05 M in a solution of 0.1 M NaOH. It is important to highlight the absence of a NDR branch in Figure 4.20, which can be attributed by the lack of L-cysteine adsorption. According to Dourado and co-workers, at such high pH values, it facilitates unfavorable conditions for the adsorption processes of L-cysteine.[35]
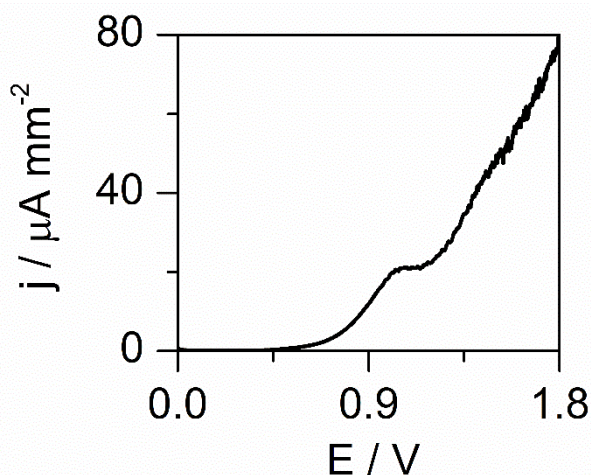
Figure 4.20. Potentiodynamic curve of 0.1 M L-cysteine in 0.2 M NaOH. The scan rate was 0.1 mVs[-1].

An interesting finding in the presented study is the formation of a thin film at the Pt electrode during the electro-oxidation of cysteine at potentials of approximately 1.2 V and above in solutions containing 0.1 M NaOH. The physisorbed layer appears to uniformly coat the electrode surface and is white in color after several hours of the reaction time. To gain a better understanding of the nature of the film, scanning electron microscopy (SEM) images were taken, and shown in Figure 4.21. At a 1500x magnification, a dense layer of the formed deposits was observed. Upon a closer examination, the film seems to be composed of many stacked layers of thin hexagonal platelets. The identity of the adsorbed species is yet to be identified but is most likely cystine due to its similarity to the hexagonal morphology of cystine crystal reported. Ward and co-workers

reported the SEM images of L-cystine crystals, which resembles the characteristics of the deposited film observed in this study.[36] The fall-off of the coating layer from Pt electrode may be related to the sudden spike seen in the j-E curve. The differences in the chemical structures of cysteine in different pH media may explain the differences of the oxidation peaks observed in the three media, i.e., H_2SO_4, KCl and NaOH.
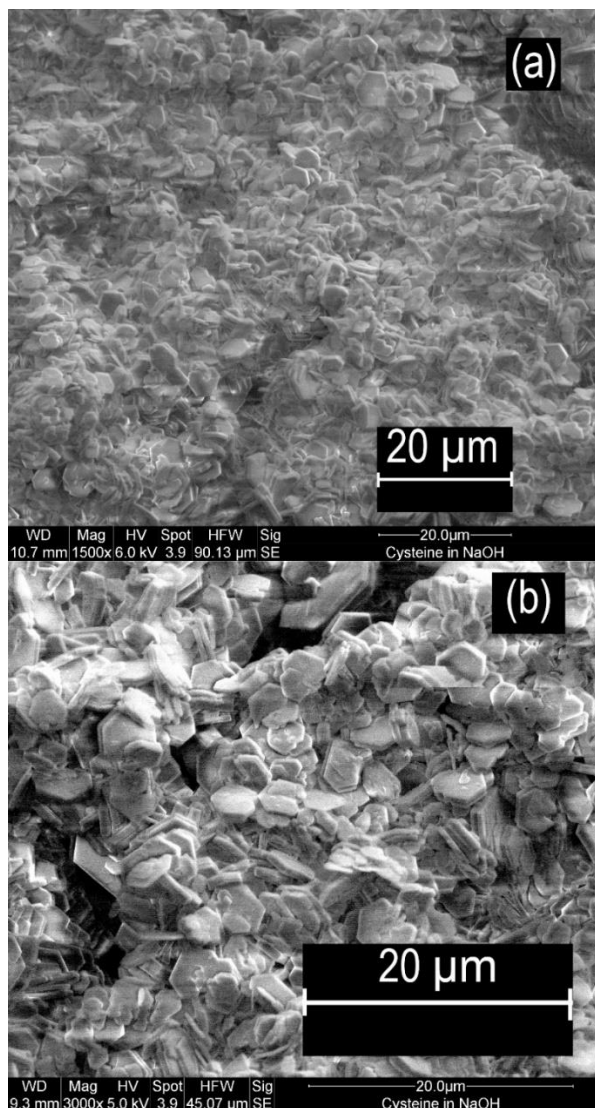
Figure 4.21. Scanning electron microscopy images of a Pt electrode after 2 hours of the oxidation of 0.1 M L-cysteine in 0.1 M NaOH at (a) 1500x magnification and (b) 3000x magnification.

4.4 Conclusions

The electrochemical oxidation of L-cysteine at the Pt electrode has been investigated in three media of different pH values, where a negative differential resistance branch was observed, providing positive support on the possibility of seeing nonlinear instabilities in this system. In alkaline conditions, the onset of oscillations occurred within a narrow range of parameters in the absence of an external resistor, which contradicts the impedance spectra that suggests an external resistor is required to bring the system from a stable steady state to the oscillatory state. The observation that the oxidation reaction kinetics of L-cysteine is dependent on the solution pH is likely due to changes of the dominant electroactive species in the solution. It was found that only in alkaline media, such as those containing NaOH, film formation on the Pt electrode is suspected to be L-cystine. The adsorption processes, formation of surface oxides, and changes of the dominant electroactive species may contribute to the differences of the oxidation behaviors in varying solution pH.

4.5 References

(1)   Claiborne, A.; Mallet, T. C.; Yeh, J. I.; Luba, J.; Parsonage, D. Structural, Redox, and Mechanistic Parameters for Cysteine-Sulfenic Acid Function in Catalysis and Regulation. *Adv. Protein Chem.* **2001**, *58*, 215–276.

(2)   Giles, N. M.; Giles, G. I.; Jacob, C. Multiple Roles of Cysteine in Biocatalysis. *Biochem. Biophys. Res. Commun.* **2003**, *300*, 1–4.

(3)   Reddie, K. G.; Carroll, K. S. Expanding the Functional Diversity of Proteins through Cysteine Oxidation. *Curr. Opin. Chem. Biol.* **2008**, *12*, 746–754.

(4)   Meister, A.; Anderson, M. E. Glutathione. *Annu. Rev. Biochem.* **1983**, *52*, 711–760.

(5)   Lu, S. C. Glutathione Synthesis. *Biochim. Biophys. Acta - Gen. Subj.* **2013**, *1830*, 3143–3153.

(6)   Gondikas, A. P.; Morris, A.; Reinsch, B. C.; Marinakos, S. M.; Lowry, G. V.; Hsu-Kim, H. Cysteine-Induced Modifications of Zero-Valent Silver Nanomaterials: Implications for Particle Surface Chemistry, Aggregation, Dissolution, and Silver Speciation. *Environ. Sci. Technol.* **2012**, *46*, 7037–7045.

(7)   Wildgoose, G. G.; Leventis, H. C.; Davies, I. J.; Crossley, A.; Lawrence, N. S.; Jiang, L.; Jones, T. G. J.; Compton, R. G. Graphite Powder Derivatised with Poly-l-Cysteine Using "Building Block" Chemistry - a Novel Material for the Extraction of Heavy Metal Ions. *J. Mater. Chem.* **2005**, *15*, 2375–2382.

(8)   Kricheldorf, H. R. Polypeptides and 100 Years of Chemistry of A-Amino Acid N-Carboxyanhydrides. *Angew. Chemie Int. Ed.* **2006**, *45*, 5752–5784.

(9)   Zheng, X.; Zhou, D.; Xiang, D.; Huang, W.; Lu, S. Electrochemical Determination of Ascorbic Acid Using the Poly-Cysteine Film-Modified Electrode. *Russ. J. Electrochem*. **2009**, *45*, 1275–1280.

(10)   Wang, L.; Huang, P.; Bai, J.; Hu, X.; Wang, H.; Zhao, Y. Simultaneous Electrochemical Detection of Hydroquinone and Catechol in Binary Mixtures Using Poly(Cysteine)-Modified Glassy Carbon Electrode. *Chem. Analityczna* **2007**, *52*, 15–24.

(11)   Ferraz, B. R. L.; Leite, F. R. F.; Malagutti, A. R. Simultaneous Determination of Ethionamide and Pyrazinamide Using Poly (l-Cysteine) Film-Modified Glassy Carbon Electrode. *Talanta* **2016**, *154*, 197–207.

(12)   Kolthoff, I. M.; Barnum, C. The Anodic Reaction and Waves of Cysteine at the Dropping Mercury Electrode and at the Platinum Micro Wire Electrode. *J. Am. Chem. Soc*. **1940**, *62*, 3061–3065.

(13)   Stankovich, M. T.; Bard, A. J. The Electrochemistry of Proteins and Related Substances I. Cystine and Cysteine at the Mercury Electrode. *J. Electroanal. Chem*. **1977**, *75*, 487–505.

(14)   Heyrovský, M.; Mader, P.; Vavřička, S.; Veselá, V.; Fedurco, M. The Anodic Reactions at Mercury Electrodes Due to Cysteine. *J. Electroanal. Chem*. **1997**, *430*, 103–117.

(15)   Monterroso-Marco, B.; López-Ruiz, B. PH Effect on Cysteine and Cystine Behaviour at Hanging Mercury Drop Electrode. *Talanta* **2003**, *61*, 733–741.

(16)   Kolthoff, I. M.; Stricks, W.; Tanaka, N. The Anodic Waves of Cysteine at the Convection and Dropping Mercury Electrodes. *J. Am. Chem. Soc*. **1955**, *77*, 5211–5215.

(17)   Koryta, J.; Pradáč, J. Electrode Processes of the Sulfhydryl-Disulfide System: III. Cysteine at Platinum and Gold Electrodes. *J. Electroanal. Chem. Interfacial Electrochem*. **1968**, *17*, 185– 189.

(18)   Davis, D. G.; Blanco, E. An Electrochemical Study of the Oxidation of L-Cysteine. *J. Electroanal. Chem*. **1966**, *12*, 254–260.

(19)   Shaidarova, L. G.; Ziganshina, S. A.; Budnikov, G. K. Electrocatalytic Oxidation of Cysteine and Cystine at a Carbon-Paste Electrode Modified with Ruthenium(IV) Oxide. *J. Anal. Chem*. **2003**, *58*, 577–582.

(20)   Gao, Z.-N.; Yao, H.-Q.; Liu, W.-Y. Study on Electrocatalytic Oxidation of L-Cysteine at Glassy Carbon Electrode by (FcM)TMA and Its Electrochemical Kinetics. *Electroanalysis* **2005**, *17*, 619–624.

(21)   Maleki, N.; Safavi, A.; Sedaghati, F.; Tajabadi, F. Efficient Electrocatalysis of L-Cysteine at Carbon Ionic Liquid Electrode. *Anal. Biochem*. **2007**, *369*, 149–153.

(22)   Zhao, Y.-D.; Zhang, W.-D.; Chen, H.; Luo, Q.-M. Electrocatalytic Oxidation of Cysteine at Carbon Nanotube Powder Microelectrode and Its Detection. *Sensors Actuators, B Chem*. **2003**, *92*, 279–285.

(23)   Tan, W. T.; Bond, A. M.; Ngooi, S. W.; Lim, E. B.; Goh, J. K. Electrochemical Oxidation of L-Cysteine Mediated by a Fullerene-C60-Modified Carbon Electrode. *Anal. Chim. Acta* **2003**, *491*, 181–191.

(24)   Zhou, M.; Ding, J.; Guo, L. -P.; Shang, Q. -K. Electrochemical Behavior of L-Cysteine and Its Detection at Ordered Mesoporous Carbon-Modified Glassy Carbon Electrode. *Anal. Chem*. **2007**, *79*, 5328–5335.

(25)   Chen, X.; Yang, Y.; Ding, M. Electrocatalytic Oxidation and Sensitive Detection of Cysteine at Layer-by-Layer Assembled Carbon Nanotube-Modified Electrode. *Anal. Chim. Acta* **2006**, *557*, 52–56.

(26)   Bell, J. G.; Wang, J. Formation of Au Nanoparticles at the Counter Electrode during the Oscillatory Oxidation of Methionine on a Gold Electrode. *J. Physcial Chem. C* **2017**, *121*, 14731–14736.

(27)   Morris, M. D. The Rate of Electrode Oxide Formation during Chronopotentiograms at a Platinum Anode. *J. Electroanal. Chem.* **1964**, *8*, 350–358.

(28)   Koper, M. T. M. Non-Linear Phenomena in Electrochemical Systems. *J. Electrochem. Soc. Faraday Trans.* **1998**, *94*, 1369–1378.

(29)   Koper, M. T. M. The Theory of Electrochemical Instabilities. *Electrochim. Acta* **1992**, *37*, 1771–1778.

(30)   Strasser, P.; Eiswirth, M.; M. T. M. Koper. Mechanistic Classification of Electrochemical Oscillators - an Operational Experimental Strategy. *J. Electroanal. Chem.* **1999**, *478*, 50–66.

(31)   Krischer, K. Nonlinear Dynamics in Electrochemical Systems. In *Advances in Electrochemical Science and Engineering*; Wiley-VCH Verlag GmbH & Co. KGaA: Weinheim, Germany, 2002.

(32)   Wang, L.-H.; Huang, W.-S. Electrochemical Oxidation of Cysteine at a Film Gold Modified Carbon Fiber Microelectrode Its Application in a Flow-through Voltammetric Sensor. *Sensors* **2012**, *12*, 3562–3577.

(33)   Voet, D.; Voet, J. G.; Pratt, C. W. *Fundamentals of Biochemistry: Life at the Molecular Level*, 4th ed.; John Wiley & Sons Inc.: Hoboken, N.J, 2016.

(34)   Dourado, A. H. B.; de Lima Batista, A. P.; Oliveira-Filho, A. G. S.; Sumodjo, P. T. A.; Cordoba de Torresi, S. I. L-Cysteine Electrooxidation in Alkaline and Acidic Media: A Combined Spectroelectrochemical and Computational Study. *RSC Advances* **2017**, *7*, 7492-7501.

(35)   Dourado, A. H. B.; Arenz, M.; Cordoba de Torresi, S. I. Mechanism of Electrochemical L-Cysteine Oxidation on Pt. *ChemElectroChem* **2019**, *6*, 1009-1013.

(36)   Mandal, T.; Shtukenberg, A. G.; Yu, A. C.; Zhong, X.; Ward, M. D. Effect of Urinary Macromolecules on L-Cystine Crystal Growth and Crystal Surface Adhesion. *Cryst. Growth Des.* **2015**, *16*, 423–431.

CHAPTER 5 – CONCLUSIONS AND FUTURE PERSPECTIVES

5.1 Conclusions

This thesis investigated the electrochemical oxidation behavior of two sulfur compounds at various conditions. The study of the oxidation of bisulfite in acidic media at a GCE demonstrated a critical surface area dependence of the onset of the current and potential oscillations, providing a useful model for the dynamical quorum sensing phenomena observed in many systems including biological media. The surface area effect is not likely related to the IR drop, as oscillations could still be obtained under the IR compensation. Further investigations involving EIS revealed that the oscillator most likely belonged to the HN-NDR class, which was consistent with the absence of a NDR branch in the LSV, and the emergence of galvanostatic oscillations. Various reaction parameters, such as the applied potential, applied current density, bisulfite concentration, the type of electrolyte and its concentrations are found to exhibit great influences on the oscillatory dynamics. Another interesting finding of this study is the production of various allotropes of sulfur at the CE during the electrochemical oxidation of bisulfite in different concentrations of sulfuric acid. In lower concentrations, yellow sulfur is produced and disperses throughout the solution over time. On the other hand, in higher concentrations of H_2SO_4, white sulfur is produced and remains near the CE. According to literature, the yellow sulfur is likely $S_6 - S_{12}$ or polysulfide anions.[1]

As the principle species of bisulfite in solution depends on the pH, Chapter 3 focused on the oxidation of bisulfite in neutral media at the GCE, where HSO_3^- is the dominant electroactive species as opposed to $SO_{2(aq)}$ in acidic media (H_2SO_4). Here, instabilities have been observed in the neutral electrolytes of KNO_3, K_2SO_4 and KCl. However, in KNO_3 and K_2SO_4 solutions, the LSV has a well-defined NDR branch, where irregular/aperiodic oscillations occur. When bisulfite is oxidized in KCl electrolytes, the LSV lacks a NDR, and is characterized with a continuous increasing positive branch, yet spontaneous oscillations appear in a wide range of reaction

parameters. The oscillations that occur in this study does not require the insertion of an external resistor, which was also the case observed in Chapter 2. Through further investigations it was revealed that the oxidation of chloride ions in KCl solutions began at 1.3 V, which is within the oscillatory regime of a LSV containing $NaHSO_3$ and KCl. Furthermore, the oxidation of HSO_3^- and Cl^- appear to suppress the oxidation of H_2O until the applied potential reaches approximately 1.8 V. At such high anodic potentials, the oxidation process of the H_2O molecules becomes significant to give rise to hydrodynamic mass transportation convection due to the oxygen bubble evolution. Therefore, within the potential range of 1.4 V – 1.8 V, the oscillations most likely are a result of the competition between the oxidation of bisulfite and chloride ions. Impedance spectra obtained at those conditions also demonstrated that the observed oscillations did not fit into the before-mentioned categories. They may represent a new class of an electrochemical oscillator.

The electrochemical oxidation of L-cysteine at the Pt electrode was investigated in Chapter 4. It was found that the reaction kinetics and oxidation behavior varied with the solution pH, which was likely due to changes of the dominant electroactive species of L-cysteine. At a pH of 1.46 (0.1 M H_2SO_4), 5.24 (0.5 M KCl), and 9.48 (0.1 M NaOH), the onset oxidation potential and peak current were different, but a negative differential branch was observed in all of the potentiodynamic curves. Electrochemical impedance spectra displayed characteristics of a N-NDR oscillator, yet no spontaneous oscillations were observed with or without a sufficiently high ohmic drop. However, the phenomenon of bistability was detected in a slow cyclic potentiodynamic sweep, where the system could exist at a high or a low current density state. With an increase of the solution pH to 12.02, spontaneous oscillations emerged along the positive branch of the LSV. Such a qualitative change in the reaction behavior can be attributed to the deprotonation of the amino group of L-cysteine. Because of the dynamical instabilities took place even in the absence of an external resistor, it was not feasible to apply the EIS technique to determine the possible existence of a hidden negative differential resistance in this system. Moreover, during the oxidation of L-cysteine

131

in an alkaline solution such as 0.1 M NaOH, a thin film was found to form on the Pt, which was observed to fall off the electrode depending on the quantity produced. Preliminary characterization with SEM illustrates that the film is composed of layers of stacked hexagonal platelets. The shape is very similar to what was reported in the study of cystine crystal. Further investigations will be needed to determine the film.

5.2 Future Perspectives

Nonlinear systems involving sulfur compounds have great potential in the applications of material fabrication and may be of great importance moving forward. With respect to the electrochemical oxidation of bisulfite in sulfuric acid at the GCE, the identification and analysis of the formed molecular sulfur species at the CE should be considered in future studies as it may elucidate their roles in the underlying mechanisms of the observed oscillatory phenomenon. In turn, this information can be useful towards the hybrid sulfur cycle. UV/vis spectroscopy can be employed to confirm the presence of the sulfur rings, where their absorption band lies in the region of 250 nm – 300 nm.[1] The H_2SO_4 concentration ranges should be further increased to examine its effect on the physical and chemical properties of elemental sulfur synthesized in this system. Moreover, the CE can be replaced with other materials to modify the electrode directly. For example, it has been observed in our group that the fabrication of copper sulfide can effortlessly be completed during the oxidation of bisulfite in H_2SO_4 at the GCE by incorporating a copper wire/sheet as the CE. By using the oscillatory dynamical approach, the morphology of the copper sulfide deposits can be manipulated due to the ease of altering various control parameters.

The results presented in Chapter 3 show that the oxidation of bisulfite in KCl at the GCE have relevance to the OER applications in part of renewable energy production. However, additional experiments are imperative to gain significant insights into this system first, such as identifying the essential variables that participates in the feedback mechanisms. For example,

repeating the experiments performed in this study with a different electrode material, such as Pt and graphite can determine whether the oscillatory behavior is exclusive to the GCE. Furthermore, additional SEM measurements need to be taken to clarify whether there are surface changes occurred during the oxidation of bisulfite and its role on the emergence of oscillations. The effect of halide ions in solution and reaction temperature can also be explored to manipulate the potential and current oscillatory behavior.

Only preliminary investigations on the electrochemical oxidation of cysteine was pursued in this research. In future investigations, to confirm that the film is indeed cystine, the film needs to be separated and purified with chromatography. UV spectroscopy can also be used to identify cystine by measuring the absorption bands, and as well as IR spectroscopy. Due to the abundance of the repeating hexagonal units, size exclusion chromatography may be used to determine the molecular weight of the film to determine whether the film is a polymer. Furthermore, another form of perturbation can be applied to manifest the bistability phenomenon. Some examples that had not been attempted in this study are the applied current densities and forced mass transportation using a rotating disc electrode.

5.3 References

(1)   Meyer, B. Elemental Sulfur. *Chemical Reviews* **1976**, *76*, 367-388.

APPENDICES

APPENDIX A. COPYRIGHT RELEASE FOR ELSEVIER

Type of Use	reuse in a thesis/dissertation
Portion	figures/tables/illustrations
Number of figures/tables/illustrations	3
Format	both print and electronic
Are you the author of this Elsevier article?	No
Will you be translating?	No
Title	Nonlinear phenomena during the electrochemical oxidation of sulfur compounds
Institution name	n/a
Expected presentation date	Jan 2020
Portions	Figure 6(g); Figure 7(d); Figure 7(h)

ELSEVIER LICENSE
TERMS AND CONDITIONS

Dec 19, 2019

This Agreement between University of Windsor -- Michelle Dao ("You") and Elsevier
("Elsevier") consists of your license details and the terms and conditions provided by
Elsevier and Copyright Clearance Center.

License Number	4726320835371
License date	Dec 12, 2019
Licensed Content Publisher	Elsevier
Licensed Content Publication	Journal of the Franklin Institute
Licensed Content Title	An overview of bifurcation, chaos and nonlinear dynamics in control systems
Licensed Content Author	Guanrong Chen,Jorge L. Moiola
Licensed Content Date	Nov 1, 1994
Licensed Content Volume	331
Licensed Content Issue	6
Licensed Content Pages	40
Start Page	819
End Page	858
Type of Use	reuse in a thesis/dissertation

Portion	figures/tables/illustrations
Number of figures/tables/illustrations	4
Format	both print and electronic
Are you the author of this Elsevier article?	No
Will you be translating?	No
Title	Nonlinear phenomena during the electrochemical oxidation of sulfur compounds
Institution name	n/a
Expected presentation date	Jan 2020
Portions	Figure 7 (a) - (d)

APPENDIX B. COPYRIGHT RELEASE FOR ROYAL SOCIETY CHEMISTRY

Copyright Clearance Center — Marketplace™

Royal Society of Chemistry - License Terms and Conditions

Order Date	04-Dec-2019
Order license ID	1007259-1
ISSN	1364-5455
Type of Use	Republish in a thesis/dissertation
Publisher	ROYAL SOCIETY OF CHEMISTRY
Portion	Chart/graph/table/figure

LICENSED CONTENT

Publication Title	Journal of the Chemical Society. Faraday transactions	Country	United Kingdom of Great Britain and Northern Ireland
Author/Editor	Royal Society of Chemistry, Chemical Society	Rightsholder	Royal Society of Chemistry
		Publication Type	e-Journal
Date	01/01/1997	URL	http://www.rsc.org/is/database/aasour.htm
Language	English		

REQUEST DETAILS

Portion Type	Chart/graph/table/figure	Distribution	Worldwide
Number of charts / graphs / tables / figures requested	3	Translation	Original language of publication
		Copies for the disabled?	No
Format (select all that apply)	Electronic	Minor editing privileges?	Yes
Who will republish the content?	Academic institution	Incidental promotional use?	No
Duration of Use	Life of current edition	Currency	CAD
Lifetime Unit Quantity	Up to 499		
Rights Requested	Main product		

NEW WORK DETAILS

Title	Nonlinear phenomena in the electrochemical oxidation of sulfur compounds	Institution name	University of Windsor
		Expected presentation date	2020-12-09
Instructor name	Dr. Jichang Wang		

ADDITIONAL DETAILS

Order reference number	N/A	The requesting person / organization to appear on the license	Michelle Dao

APPENDIX C. COPYRIGHT RELEASE FOR SPRINGER NATURE

SPRINGER NATURE LICENSE
TERMS AND CONDITIONS

Dec 19, 2019

This Agreement between University of Windsor -- Michelle Dao ("You") and Springer
Nature ("Springer Nature") consists of your license details and the terms and conditions
provided by Springer Nature and Copyright Clearance Center.

License Number	4732630195651
License date	Dec 19, 2019
Licensed Content Publisher	Springer Nature
Licensed Content Publication	Springer eBook
Licensed Content Title	Basic Principles of Nonlinear Dynamics
Licensed Content Author	Marek Orlik
Licensed Content Date	Jan 1, 2012
Type of Use	Thesis/Dissertation
Requestor type	academic/university or research institute
Format	print and electronic
Portion	figures/tables/illustrations
Number of figures/tables/illustrations	3
Will you be translating?	no

Circulation/distribution	200 - 499
Author of this Springer Nature content	no
Title	Nonlinear phenomena during the electrochemical oxidation of sulfur compounds
Institution name	n/a
Expected presentation date	Jan 2020
Portions	Figure 1.1; Figure 1.5; Figure 1.15

APPENDIX D. COPYRIGHT RELEASE FOR JOHN WILEY AND SONS

JOHN WILEY AND SONS LICENSE
TERMS AND CONDITIONS

Dec 19, 2019

This Agreement between University of Windsor -- Michelle Dao ("You") and John Wiley and Sons ("John Wiley and Sons") consists of your license details and the terms and conditions provided by John Wiley and Sons and Copyright Clearance Center.

License Number	4722710453382
License date	Dec 05, 2019
Licensed Content Publisher	John Wiley and Sons
Licensed Content Publication	Wiley Books
Licensed Content Title	Nonlinear Dynamics in Electrochemical Systems
Licensed Content Author	Katharina Krischer
Licensed Content Date	Feb 17, 2003
Licensed Content Pages	120
Type of use	Dissertation/Thesis
Requestor type	University/Academic
Format	Print and electronic
Portion	Figure/table
Number of figures/tables	3

Original Wiley figure/table number(s)	Figure 26 (a) and (b); Figure 17 (a) and (b); Figure 10 (a) and (b)
Will you be translating?	No
Title of your thesis / dissertation	Nonlinear phenomena during the electrochemical oxidation of sulfur compounds
Expected completion date	Jan 2020

VITA AUCTORIS

NAME: Michelle Dao

PLACE OF BIRTH: Toronto, ON

YEAR OF BIRTH: 1995

EDUCATION: Holy Names Secondary Catholic High School,
                    Windsor, ON, 2013

                    University of Windsor, B.Sc., Windsor, ON, 2017